NMR of Geophysical Drill Cores with a Mobile Halbach Scanner

Von der Fakultät für Mathematik, Informatik und Naturwissenschaften der Rheinisch-Westfälischen Technischen Hochschule Aachen zur Erlangung des akademischen Grades einer Doktorin der Naturwissenschaften genehmigte Dissertation

vorgelegt von

Master of Science

Elena Talnishnikh

aus Sankt Petersburg, Russland

Berichter: Univ.-Prof. Dr. rer. nat. Dr. h. c. Bernhard Blümich
Univ.-Prof. Dr. rer. nat. Christoph Clauser

Tag der mündlichen Prüfung: 21. August 2007

Foreword

Many people were involved in this interdisciplinary project. They worked together from the beginning until the end. Firstly, they designed and constructed the experimental equipment and secondly, developed measurement techniques and tested them for different geophysical applications. Then the author would like to mention personally Dr. Sophia Anferova, Prof. Vladimir Anferov, and Juliane Arnold for the teamwork.

I would like to underline the collaboration with Prof. Christoph Clauser's group from the Applied Geophysics (AG) Institute in RWTH Aachen University. All water-saturated drill cores and plugs were provided by this institute as well as their geophysical characteristics measured with independent methods: porosity with a He-gas pycnometer, and permeability with the gas flow method. Furthermore, magnetic susceptibility values of all studied cores were recorded with a Multi-Sensor Core Logger. Therefore, the NMR data were verified with independent measurements. Our partners from Applied Geophysics tested the developed mobile NMR hardware and methodologies to estimate rocks characteristics from NMR data. Juliane Arnold (AG) provided one-dimensional relaxation experiments and calibrated different mobile NMR instruments to quantify rock porosity, pore size distribution and permeability as indicated in her thesis.

The author took part in the improvement of the homogeneity of the magnetic system, the rf circuit with the 24 mm diameter coil, and the gradient system for PFG experiments. The on-line Halbach core scanner for analysis of large long drill cores was designed on the basis of an improved magnet. Dedicated software was developed for on-line measurements of porosity of long large size drill cores and for 2D correlation experiments. Standard relaxation and diffusion NMR techniques were applied with the Halbach scanner. All reported experiments were established and the results were analyzed and are reported in this thesis.

Contents

Abstract

This thesis is devoted to a mobile NMR with an improved Halbach scanner. This is a lightweight tube-shaped magnet with sensitive volume larger and a homogeneity of the magnetic field higher than the previous prototype version. The improved Halbach scanner is used for analysis of water-saturated drill cores and plugs with diameters up to 60 mm. To provide the analysis, the standard 1D technique with the CPMG sequence as well as 2D correlation experiments were successfully applied and adapted to study properties of fluid-saturated sediments. Afterwards the Halbach scanner was calibrated to fast non-destructive measurements of porosity, relaxation time distributions, and estimation of permeability. These properties can be calculated directly from the NMR data using the developed methodology. Any independent measurements of these properties with other methods are not needed. One of the main results of this work is the development of a new NMR on-line core scanner for measurements of porosity in long cylindrical and semi cylindrical drill cores. Also dedicated software was written to operate the NMR on-line core scanner.

The physical background of this work is the study of the diffusion influence on transverse relaxation. The diffusion effect in the presence of internal gradients in porous media was probed by 1D and 2D experiments. The transverse relaxation time distributions obtained from 1D and from 2D experiments are comparable but different in fine details.

Two new methodologies were developed based on the results of this study. First is the methodology quantifying the influence of diffusion in the internal gradients of water-saturated sediments on transverse relaxation from 2D correlation experiments. The second one is the correction of the permeability estimation from the NMR data taking in account the influence of the diffusion. Furthermore, PFG NMR technique was used to study restricted diffusion in the same kind of samples. Preliminary results are reported.

Zusammenfassung

Diese Arbeit widmet sich der mobilen NMR mit einem verbesserten Halbach-Scanner. Dieser ist ein leichter röhrenförmiger Magnet, der im Vergleich zum früheren Prototypen ein größeres sensitives Volumen und eine höhere Homogenität des Magnetfeldes aufweist. Der verbesserte Halbach-Scanner wird für Untersuchungen von wassergesättigten Bohrkernen und Scheiben mit einem Durchmesser bis zu 60 mm verwendet. Um die Eigenschaften von fluid-gesättigten Sedimentgesteinen zu untersuchen, wurden sowohl die standardmäßige 1D Technik mit CPMG-Sequenz, als auch 2D Korrelationsexperimente erfolgreich angewandt und angepasst. Anschließend wurde der Halbach-Scanner für schnelle zerstörungsfreie Messungen von Porosität, Relaxationszeitverteilungen und Abschätzung der Permeabilität kalibriert. Diese Eigenschaften können direkt aus den NMR-Daten unter Benutzung der entwickelten Methode errechnet werden. Es werden keine weiteren unabhängigen Messungen dieser Eigenschaften mittels anderen Methoden benötigt. Eines der Hauptergebnisse dieser Arbeit ist die Entwicklung eines neuen NMR online-core-Scanners für Messungen der Porosität in langen zylindrischen und halbzylindrischen Bohrkernen. Des weiteren wurde eine spezielle Software zur Benutzung des NMR online-core-Scanners geschrieben.

Der physikalische Hintergrund dieser Arbeit ist die Untersuchung des Diffusionseinflusses auf die transversale Relaxation. Der Diffusionseffekt in der Gegenwart von internen Gradienten in porösen Materialien wurde anhand von 1D und 2D Experimenten untersucht. Die aus 1D und 2D-Experimenten erhaltenen Verteilungen der transversalen Relaxationszeiten sind vergleichbar, unterscheiden sich aber in kleinen Details.

Zwei neue Methoden basierend auf den Ergebnissen dieser Untersuchungen wurden entwickelt. Die Erste ist die Methode zur Quantifizierung des Einflusses der Diffusion in internen Gradienten von wassergesättigtem Sedimentgestein auf die transversale Relaxation in 2D-Korrelationsexperimenten. Die Zweite ist eine Korrekturmethode bei der Abschätzung der Permeabilität aus den NMR-Daten, welche den Einfluss der Diffusion berücksichtigt. Des weiteren wurde die PFG NMR Technik benutzt, um die beschränkte Diffusion in Proben gleicher Art zu untersuchen. Vorläufige Ergebnisse werden dargestellt.

Abbreviations and Symbols

NMR	Nuclear Magnetic Resonance
MOUSE®	Mobile Universal Surface Explorer
$\boldsymbol{B}$	vector of the magnetic flux density
$\boldsymbol{B}_0$	static magnetic field vector
B_1	amplitude of the rf field
C	capacitance
CPMG	Carr, Purcell, Meiboom, Gill
$D(t)$	time-dependent diffusion coefficient
D_0	diffusion coefficient of bulk water
$\mathbf{I}$	spin operator
I	spin quantum number
f	rlative intensity
G	magnitude of the gradient vector
k	permeability
L	inductance
LT	Laplace transformation
$\boldsymbol{M}$	magnetization vector
M_0	thermodynamic equilibrium magnetization
$\mathrm{m}(\boldsymbol{r}, t)$	density of the longitudinal magnetization per unit of the volume
n	counting index
P	probability of occurrence
PFG	Pulsed field gradient
Q	quality factor
$\boldsymbol{r}$	space vector
R	correlation coefficient
$\boldsymbol{R}$	Relaxation matrix
rf	radio frequency
S	surface
SD	standard deviation
T_1	longitudinal relaxation time
T_2	transverse relaxation time

t	time
t_E	echo time
t_p	duration of an rf pulse
V	volume
ϕ	porosity
λ	regularization parameter
γ	gyromagnetic ratio
ρ	surface relaxivity
$\hbar$	the Planck's constant divided by 2π
ν	frequency
τ_1	saturation recovery time
ω_0	Larmor frequency
ω_1	precessing angular frequency in the rotating frame
1D	one dimensional experiment
2D	two-dimensional experiment

Introduction

Nuclear magnetic resonance (NMR) is a method that is widely used in medical imaging (MRI), chemical analysis (NMR spectroscopy) and in geophysics for the petroleum industry (NMR in well logging) and groundwater characterization (surface NMR) [Abr1, Blü1, Blo1, Cal1, Dun1, Dar1, Ern1, Fuk1, Pur1, Sli1, Sta1]. NMR can study molecular-scale properties of a wide range of materials. Since it was discovered that the nuclear magnetic relaxation of water in rocks is much faster than that in the bulk phase [Brown1], it was natural to use NMR to obtain information on the saturating fluids in the rocks and their transport properties to probe the structure of porous media [Coa1, Kle1, Lat1]. Therefore, the fact that the NMR signal depends on the geometry and magnetic properties of the fluid saturated porous medium was used in different relaxation and diffusion studies, for example, measurements of time-dependendent diffusion coefficient [Sen1].

Well-logging NMR is the first and most prominent example of mobile NMR, where the NMR equipment is brought to the site of interest [Fre1, Che1]. Unlike the conventional NMR apparatus, the borehole instrument is contained in a cylindrical metal pipe with the 'sample' – the earth, in fact – outside the apparatus [HNMR] and is able today to perform measurements while drilling [Coa1]. The early research work in Chevron, Schlumberger, Varian and others resulted in a number of important applications of the NMR method and led to the development of experimental logging tools and to commercial logging services [Dun1, Coa1, Coa2]. Many achievements in NMR well logging as well as developments of well logging tools are summarized in a special issue of "Concepts in Magnetic Resonance"[HNMR].

For several years the focus of mobile NMR was on inside-out NMR [Kle1] or single-sided NMR [Eid1]. Later in 2001, the unilateral sensor, the NMR-MOUSE® (Mobile Universal Surface Explorer) was successfully tested for measurements of water saturated standard IODP (Integrated Ocean Drilling Program) cores. It provides inhomogeneous static magnetic and radio frequency fields outside the magnet in the region where a sample is studied. It was shown in many applications that the NMR experiments do not always need a homogeneous magnetic field [Blü2, Blü3, Per1].

Nowadays, the use of mobile NMR moves into many new areas. Tube-shaped Halbach magnets are examples of the mobile outside-in NMR [Hal1, Rai1, Anf1]. Halbach magnets are particularly useful where the concentration or the amount of a substance have to be quantified over a larger volume, for example, the content of fluid in drill cores. Such sensors are suitable for relaxation measurements of large-size, water-saturated drill cores on drilling platforms, on board of a ship, and in laboratories.

Meanwhile a number of powerful multi-dimensional NMR concepts based on the inverse Laplace transformation have been developed in well logging to characterize porous media [Son2, Hür1]. Today, the multi-dimensional NMR experiments are an actual and popular topic. This was difficult to imagine a couple of years ago due to the absence of the software for multi-dimensional data processing. When L.Venkataramananan, Y.-Q. Song and M.D. D. Hürlimann published their paper about an efficient algorithm to solve 2 and 2.5 dimensional Fredholm integrals of the first kind [Ven1] the popularity of 2D and 3D inverse Laplace transform NMR experiments exploded. Multi-dimensional experiments provide joint probability densities of longitudinal and transverse relaxation times T_1 and T_2 with the distribution of diffusion coefficients D [Hür1-7, Son1-3]. A variety of new pulse sequences were developed with independent encoding of several quantities in the same time. The most important are $T_1 - T_2$ relaxation correlation and $D - T_2$ diffusion-relaxation correlation experiments. [Cal2, Hür3, Sel2]. Such correlation maps are most powerful for discriminating multiphase fluid properties in porous media, for example, oil and water or capillary bound and mobile water in drill cores [Son2]. While improving the measurement routine of multi-echo relaxation decays in inhomogeneous fields has been the objective for some time [Hür5], rapid measurement schemes for determining diffusion [Son1], flow [Son4], and observation of pore to pore exchange in porous media [Was1] have been developed in parallel. Multi-dimensional experiments are already used in well logging to estimate fluid production and to characterize food products [Hür5, Hür8].

This thesis is devoted to mobile NMR with a Halbach scanner to study fluid transport properties of water-saturated drill cores and plugs. The main goals of this work are the following:

- To refine measurements of porosity by the mobile Halbach scanner and extend them to non-destructive analysis of water-saturated cylindrical or semi-cylindrical drill cores and plugs with different diameters from 20 mm up to 60 mm.

- To automate and simplify measurements of porosity within a short experimental time in long, large-size cylindrical or semi-cylindrical drill cores with diameters up to 60 mm using a newly developed *on-line* core scanner. This work includes design and development of the *on-line* scanner, software for automatic scanning, and on-line study of several drill cores.
- To develop 2D correlation techniques with the Halbach scanner, pulse sequences, software for data processing, and analysis of the obtained results on water-saturated plugs with 20 mm diameter.
- To estimate permeability of water-saturated sandstone plugs with 20 mm diameter directly from transverse NMR relaxation data.
- To provide self-diffusion PFG experiments on water-saturated rocks with the Halbach scanner.

We tried to simplify the experimental routine and minimize the measurement time. The developed equipment and methodologies are not complicated for the NMR novice. This is a reason why the thesis does not require heavy mathematical or quantum mechanics. But at the same time, the thesis includes clear ideas about the general principles of measurements, modified techniques, newly developed hardware and software, detailed analysis of experimental results and their practical applications. Readers unfamiliar with NMR or interested in more details can find all additional information in the given references [Abr1, Ern1, Fuk1, Sli1, Blü1, etc].

The thesis consists of 6 chapters.

Chapter 1-'NMR in porous media'- is considered as an introduction where general ideas about NMR in rocks are presented. 'Relaxation principles' and 'Basics of NMR in water-saturated rocks' describe physical processes that constitute the NMR background of this study. Important terminology and fundamental concepts are introduced, and the studied samples are briefly characterized.

Chapter 2 - 'Halbach core scanner'- is dedicated to the hardware used in this study. There is a detailed description of the magnet, radio frequency and gradient coils, and an explanation of the reasons of all modifications of the magnet system. The benefits of the new system are pointed out.

Chapter 3 –'Advances in measurements of porosity with the Halbach scanner'- describes hardware developments such as exchangeable rf coils to determine porosity of cylindrical drill cores and plugs with different diameters. The main achievement is a new core scanner which was built for on-line measurements of porosity of long drill

cores. Its installation, construction, and developed software to operate the system are discussed. First laboratory measurement on long drill cores are reported.

Next **chapter 4 –'**Quantifying diffusion in the presence of internal gradients of porous media'-shows the effect of diffusion in internal gradients of sandstones using 1D and 2D relaxation experiments. Additionally, permeability is estimated directly from 1D and 2D NMR data with different accuracy. A new methodology to correct the permeability values in the presence of internal gradients is presented.

Chapter 5 –'Restricted diffusion study in water-saturated core plugs'- is dedicated to the PFG diffusion experiments with the Halbach scanner.

Finally, **chapter 6** contains the summary and possible new applications with the Halbach scanner.

1.NMR in porous media

The physical principle used in this study is nuclear magnetic relaxation. As Eiichi Fukushima [Fuk1] wrote: "If you go to a social gathering and announce that you an expert in relaxation, you could receive responses ranging from curious stares to hearty approvals neither of which are probably justified". This chapter gives simple description of the relaxation processes and explains the fundamentals of NMR in water-saturated rocks. The chapter is ended with brief description of the tested samples.

1.1 Relaxation principles

The key of NMR is that many nuclei possess magnetic moments and angular momenta, which are referred to as *spin*. If a nucleus is placed in a static magnetic field (let's consider the vector of the magnetic field along the z axis of the laboratory frame), the angular momentum makes the nucleus precess about the magnetic field when it experiences the torque due to the field acting on the moment [Ern1, Blü1, Cal1, Fuk1]. The classical analogue of a quantum mechanical particle with an angular momentum is a top with its angular momentum along its spinning axis, precessing about the earth's gravitational field. The precession frequency of the moment is proportional to and uniquely determined by the gyromagnetic ratio γ and the strength B_0 of the magnetic field according to the Larmor relation:

$$\omega_0=\gamma B_0, \tag{1.1.1}$$

where ω_0 is Larmor velocity, which is 2π times the Larmor frequency ν_0. γ is the proportionality constant between the moment μ and the angular momentum. Therefore, in a given magnetic field, the precession frequency is different for every distinct nucleus because each one has a uniquely defined γ. The study is based on proton ^{1}H NMR with $\gamma = 2.67522 \cdot 10^8$ (T s)$^{-1}$.

If a macroscopic NMR sample is placed in a static magnetic field, more nuclei orient in the direction of the vector of magnetic field than opposite to it according to the Boltzmann law. Hence, a macroscopic sample is characterized by the macroscopic magnetization $\boldsymbol{M}_0$, i.e. magnetic moment per volume. In thermodynamic equilibrium the

magnetization $\boldsymbol{M}_0$ established in the polarizing magnetic field $\boldsymbol{B}_0$ is given by Curie law [Blü1],

$$\boldsymbol{M}_0 = N\frac{\gamma^2\hbar^2 I(I+1)}{3k_{\mathrm{B}}T}\boldsymbol{B}_0, \tag{1.1.2}$$

where N is the number of nuclei with spin I in the sample, $\hbar$ is the Planck's constant divided by 2π, T is the temperature, k_{B} the Boltzmann constant. The magnetization is manipulated by the weak, time-dependent rf magnetic field, thus, it precesses and relaxes, that is changes direction and magnitude towards an equilibrium state, in the absence (after the finite action) of an external rf field in the laboratory magnetic field.

Applying an rf magnetic field rotating at the Larmor frequency in the plane perpendicular to the static field, the individual nuclear moments flip with the result that the entire macroscopic magnetization may be turned towards or away from the static field. If the frequency of the radiation applied to induce transitions is too high or too low, the nucleus will not undergo the transition. If somehow the magnetization is rotated away from the field, it can relax back to thermal equilibrium in a characteristic time T_1 by giving up quanta of energy to the surroundings, which are called the *lattice*. Thus, the transfer of the electromagnetic energy to the magnetic momenta of nuclei by a radio wave with frequency ν_0 is basically considered as NMR. The behavior of the magnetization is a subject of study of NMR.

The motion of the macroscopic magnetization vector has been described by Felix Bloch in 1946 [Blo1]:

$$\frac{d\boldsymbol{M}}{dt} = \gamma\boldsymbol{M}(t)\times\boldsymbol{B}(t) - \boldsymbol{R}\left[\boldsymbol{M}(t) - \boldsymbol{M}_0\right], \tag{1.1.3}$$

where $\boldsymbol{M}(t)$ is time-dependent magnetization vector. $\boldsymbol{B}$ is the magnetic field which is written as the sum of the strong static magnetic field $\boldsymbol{B}_0$ and time-dependent rf field $\boldsymbol{B}_{\mathrm{rf}}(t)$:

$$\boldsymbol{B}(\mathrm{t}) = \boldsymbol{B}_0 + \boldsymbol{B}_{\mathrm{rf}}(\mathrm{t}), \tag{1.1.4}$$

$$\boldsymbol{B}_{\mathrm{rf}} = \begin{bmatrix} B_1\cos(\omega_{\mathrm{rf}}t+\varphi) \\ B_1\cos(\omega_{\mathrm{rf}}t+\varphi) \\ 0 \end{bmatrix}, \tag{1.1.5}$$

where B_1 is the magnitude of the rotating field component.

$\boldsymbol{R}$ is the relaxation matrix,

$$\boldsymbol{R} = \begin{bmatrix} 1/T_2 & 0 & 0 \\ 0 & 1/T_2 & 0 \\ 0 & 0 & 1/T_1 \end{bmatrix}, \tag{1.1.5}$$

where the longitudinal relaxation time or, that is the same, spin-lattice relaxation time T_1. This is the energy dissipation time characteristic for building up the magnetization parallel to the magnetic field. The transverse relaxation time or spin-spin relaxation time T_2 is the time constant for disappearance of magnetization components orthogonal to the magnetic field. Therefore, during NMR experiments two relaxation processes take place. The first one is a relaxation of the macroscopic magnetization towards the equilibrium magnetization at the rate $1/T_1$. The second process is a spin-spin relaxation, when the spins re-orient without exchanging energy with the lattice at the time T_2. Generally, T_2 is shorter (in porous media) or equal to T_1 (in bulk liquids).

Additionally, it should be noted that the rotating frame which rotates with the rf frequency ω_{rf} is used to solve the Bloch equation (1.1.3). The change from the laboratory frame to the rotating frame simplifies the analysis of the motion of the magnetization. In the rotating frame the magnetic field including the rf field component appears static, but the magnitude of the B_0 field in z-direction is changed:

$$\boldsymbol{B}_{\text{in the rotating frame}} = \begin{bmatrix} B_1 \cos\varphi \\ B_1 \sin\varphi \\ B_0 + \omega_{rf}/\gamma \end{bmatrix}, \tag{1.1.6}$$

where φ describes a phase offset which can be manipulated by the transmitter electronics. Therefore, if the rf field is applied perpendicular to the z-axis parallel to the $\boldsymbol{B}_0$ and $\boldsymbol{M}_0$ directions and if $\omega_0=\omega_{rf}$, the magnetization experiences a torque and rotates about the rf field in the rotating frame [Blü1]:

$$\omega_1 = -\gamma B_1. \tag{1.1.7}$$

The angle of precession around the axis of the rf field or the flip angle is given by

$$a = \omega_1 t_p, \tag{1.1.8}$$

where t_p is the duration of the rf pulse. In this way, so-called 90° (or π/2) and 180° (or π) pulses can be applied to rotate the magnetization from its equilibrium state. Thus,

when the action of the rf field is finished, the magnetization will precess only because of the presence of the static magnetic field. This process is called free induction decay (FID) and described by the transverse relaxation time T_2.

A set of rf pulses is combined in to a pulse sequence, in order to measure a signal which has first vanished (due to free precession) with time and then reappears some time later (after applying a second rf pulse). This signal is called an echo and formally associated with a reversal of time, so that the reappearing signal can be understood in terms of time running backwards for a sufficiently isolated ensemble of molecules or spins [Blü1]. An echo will appear after a time corresponding to twice the pulse separation, which is called the echo time.

1.2 Basics of NMR in Water-Saturated Rocks

The primary information about NMR properties of fluid-saturated rocks is obtained from the study of the nuclear spin relaxation. As it is very well known, the NMR behavior of bulk water is very much different from that in porous media. Instead of one relaxation time (about a few seconds), water in the rock is characterized by a wide range of relaxation times (from microseconds up to seconds). First experiments demonstrating this effect were performed by Brown, when water in Berea sandstones and the same pure water were measured [Bro1, Dun1].

Brownstein and Tarr developed a theory which shows the importance of classical diffusion in NMR studies [Brow1]. They demonstrated that multi-exponential decay of the NMR magnetization of water in porous media arises as a consequence of an eigenvalue problem of the spin diffusion and depends on the geometry of porous media. They considered two main mechanisms of spin relaxation in the system. The first one is caused by dipole-dipole interactions with paramagnetic ions acting as relaxation centers. The second one is caused by classical diffusion of water molecules with the diffusion constant of bulk water. Since fluid molecules diffuse and eventually reach a grain surface their magnetization has a finite probability of being relaxed. As a result, either the relaxation process at the surface or the transport of the proton spins to the surface will occur (Fig. 1.1).

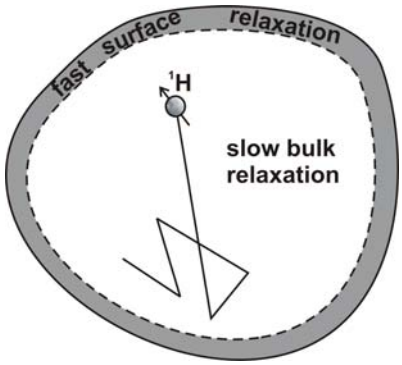

Fig. 1.1 *Basic relaxation mechanisms of a pore fluid: bulk and surface relaxation. NMR relaxation in rocks can be in the surface-limited (fast diffusion) or diffusion-limited (slow diffusion) regimes.*

The NMR properties of the water-saturated rocks are described according to the surface-limited mechanisms which are discussed in detail by Kleinberg [Klei1, Klei2]. It can be grain surface relaxation, relaxation by the molecular diffusion in the presence of magnetic field gradients or internal gradients, and bulk relaxation. Surface relaxation is the relaxation process associated with dilute paramagnetic impurities on a surface. Relaxation of fluid protons at paramagnetic ion sites on the rock grain is controlled by the dipolar-dipolar interactions between the magnetic moment of the protons and paramagnetic ions.

Relaxation by molecular diffusion in magnetic field gradients is a relaxation process, when molecular motion can cause dephasing and hence T_2 relaxation while the T_1 relaxation is not affected. In the absence of such gradients, molecular diffusion does not cause transverse relaxation. Diffusion can also take place in the presence of external and internal gradients. Internal gradients arise from susceptibility-induced gradients due to susceptibility differences between the solid matrix and the pore fluid and are proportional to the strength B_0 of the magnetic field. They depend not only on a susceptibility difference between the matrix and the fluid but also on the pore geometry.

Bulk relaxation is the relaxation that occurs in the bulk fluid itself. It is not affected by the grain space and internal field gradients. The bulk relaxation can be often neglected because it is a very slow process. Bulk relaxation is important when water is in very large pores.

According to Brownstein and Tarr, diffusion of longitudinal magnetization in porous media within the pore is described by the following equation:

$$D\nabla^2 m(\mathbf{r},t) - \frac{m(\mathbf{r},t)}{T_B} = \frac{\partial m(\mathbf{r},t)}{\partial t} \quad (1.2.1),$$

and at the interface:

$$\hat{n} \cdot D\nabla m(\mathbf{r},t) + \rho m(\mathbf{r},t)\big|_S = 0 \quad (1.2.2),$$

where D is a diffusion coefficient of fluid, $1/T_B$ is the bulk relaxation rate, $\hat{n}$ is the unit outward normal on the interface, and ρ is a surface relaxivity. $m(\mathbf{r}, t)$ is a density of the longitudinal magnetization per unit volume, which gives the total nuclear magnetization of the sample $M(t)$:

$$M(t) = \int_V m(\mathbf{r},t) d^3\mathbf{r} \quad (1.2.3),$$

The solution of these equations (Eq. 1.2.1 and Eq. 1.2.2) can be expressed as a sum of "normal modes" with a weight $A(r)$:

$$m(\mathbf{r},t) = \sum_{n=0}^{\infty} A(\mathbf{r}) e^{-t/T_n} \quad (1.2.4).$$

The eigenvalues of the time independent Eq. (1.2.1) with the boundary condition Eq. (1.2.2) are $1/T_n$. Note that the index n refers to the mode number corresponding to spin-lattice relaxation $T_{1,n}$ or spin-spin relaxation times $T_{2,n}$ in pores with different diameters.

Therefore, the magnetization in porous media based on the diffusion equation using the bulk diffusivity of water exhibits a multi exponential decay

$$M(t) = M(0) \sum_{n=0}^{\infty} f_n e^{-\frac{t}{Tn}}, \quad (1.2.5)$$

where the relative intensities f_n are normalized as

$$\sum_{n=0}^{\infty} f_n = 1. \quad (1.2.6)$$

According to Brownstein and Tarr [Brow1], the decay time T_n in Eq. (1.2.5) and its relative intensity f_n depend on the characteristics $\rho a/D$ of the porous medium, where a is a characteristic dimension of the porous medium (an average pore radius). They introduced three diffusion limits according to the value of the parameter $\rho a/D$:

$\rho a/D << 1$	- fast
$1 << \rho a/D << 10$	- intermediate
$10 << \rho a/D$	- slow

Fast diffusion takes place when the time required for the spin to diffuse to the solid/fluid interface is much shorter than the spin relaxation time. In the fast diffusion regime, the fine details of the pore geometry are not important in the magnetization decay, except for extremely short times. This is because the fast diffusion equalizes contributions from the spin density everywhere within the pore space, resulting in a uniform spin density profiles at the center of the pore and at the pore surface. In contrast, the slow diffusion mechanism yields different results for different pore shapes, and the magnetization decay has multi-exponential behavior even for a single pore. In the case of slow diffusion, the surface relaxivity is large and the diffusion is slow. Therefore the spin density provides a profile which is high at the center of the pore and close to zero at the pore surface.

Both relaxations (longitudinal and transverse) imply a simple volumetric description in the fast diffusion regime. The total longitudinal relaxation rate of the water in the pore space can be written as:

$$\frac{1}{T_1} = \frac{1}{T_{1\mathrm{B}}}\left(1 - \frac{\lambda S}{V}\right) + \frac{1}{T_{1m}}\frac{\lambda S}{V}, \tag{1.2.7}$$

where S is a surface area, V is the pore volume, λ is a surface layer thickness, $T_{1\mathrm{B}}$ is the bulk relaxation (about one second), and T_{1m} is the surface relaxation time (on the order of milliseconds). Since $T_{1\mathrm{B}} >> T_{1m}$, the relaxation rate (Eq. 1.2.7) can be written as:

$$\frac{1}{T_1} \approx \frac{1}{T_{1.B}} + \rho_1 \frac{S}{V}, \tag{1.2.8}$$

where $\rho_1 = \dfrac{V}{ST_{1m}}$ is a surface relaxivity that reflects the material properties of the rock. Equation (1.2.7) assumes that all relaxing surface sites are identical.

Since the transverse relaxation is shortened by diffusion in the internal gradients or in the inhomogeneous magnetic field, T_2 can be written as

$$\frac{1}{T_2} \approx \frac{1}{T_{2.B}} + \rho_2 \frac{S}{V} + \frac{D(\gamma G t_E)^2}{12}, \tag{1.2.9}$$

where D is the bulk self-diffusion coefficient of water, t_{E} is the echo time, γ is the proton gyromagnetic ratio, and G is a magnitude of the gradient.

If all pores are assumed to have a similar geometric shape the largest pores have lowest S/V ratio and thus the longest T_2. Therefore, the magnetization signal of rock is the sum of the relaxation rates contributed from all individual pores. Since, each pore has its own part in the relaxation time distribution, the relaxation time distribution is

used for understanding of the pore size distribution in the rock. One should mention that, in practice, it is difficult to consider each pore individually. Due to this reason, all pores with similar surface-to-volume ratios are grouped together.

1.3 Samples

The subject of this study is fluid saturated porous media. This is a very large topic that is important for environmental science (wastewater treatment), food science (food cryopreservation), polymer science (dehydration of contact lenses), well logging, etc.

There are several ways to define porous media. In general, fluid saturated porous media are defined as an immiscible mixture of a solid skeleton and fluid in pores. This can be a single fluid (gas or liquid), an immiscible fluid mixture of gas and liquids or a miscible fluid mixture of different reacting aggregates [Ehl, Bear].

The majority of samples in this study consist of sandstones, i.e. a sedimentary rock composed basically of sand-size mineral or rock grains, clastic in origin. Sandstones can have any color: white, gray, red, yellow, tan, and brown. Most sandstones are composed of quartz and/or feldspar. The formation of sandstones involves two basic steps. First, sand accumulates as a result of sedimentation, either from water (in a river, lake, or sea) or from air (in a desert). Under the pressure of overlying deposits the sand becomes sandstone and is cemented by the precipitation of minerals within the pore space between the grains. The environment where the sandstone is deposited defines the characteristics of the resulting sandstone such as grain size, sorting, composition, and even the rock geometry and the sedimentary structures.

To provide quantitative NMR measurements, these sediments must be water-saturated. Normally the saturation process is the following: the rock is dried by heating at 60° C in an oven. Once the rock has been dried, it is placed into a vacuum desiccator, where it is saturated with distilled water. The whole procedure is controlled by simple weighting of the rock from time to time. The duration of the water saturation process depends on the rock size and the rock mineralogy. All samples were always stored in distilled water to avoid drying. For the measurement, the samples were wrapped in a plastic film with a very fast decaying NMR signal and placed immediately back into the distilled water at the end of the measurements.

Fig. 1.2 *Photo of different cores and plugs used in the experiments with a Halbach sensor. The cores have diameters of 2 cm, 3 cm, 6 cm and 10 cm. A 10 eurocent coin is used as a reference scale*

A variety of mobile NMR experiments on water-saturated sediments of different lithology was performed using the Halbach sensor using cylindrical drill cores and plugs with different diameters (Fig. 1.2).

All sediments and plugs were used in a porosity study with an improved Halbach sensor except of the biggest rock in Fig. 1.2. Rocks with 10 cm diameter were measured by a specially constructed Halbach magnet built for the Institute of Applied Geophysics. The 6 cm diameter samples (core 25 in Fig. 1.2) are interesting because they are standard drill cores from the Integrated Ocean Drilling Program. *On-line* porosity measurements were tested with them. Permeability estimations and 2D correlation experiments were performed on core plugs. All plugs described below were cylinders with 2 cm diameter and 3 cm length which fit into the most homogeneous region of the magnet.

The sandstones used in this study are from different locations in Germany. Novel experimental equipment is tested on Allermöhe samples from the Northern German sediment basin near Hamburg. The Allermöhe sandstones [Arn1] have low magnetic susceptibility in the range of 0 SI – 10^{-4} SI, porosity in the range from 3 % to 11 %, and low permeability 0.05 mD – 20.7 mD. All of them belong to the same formation. This is important for the analysis, especially for the permeability estimation.

Additionally, we have studied other sandstones plugs from different outcrops located in Münsterland, Bad Bentheim, Barkhausen, Cotta, Ibbenbüren, Oberkirchen, Velpe, Züschen, Bad Karlshafen, and from other places in Germany [Arn1]. They are

from different formations and with different characteristics. Their porosity values are in the range of 1% –25%, magnetic susceptibility in the range of $(-0.75 – 24.5)\cdot10^{-5}$ SI, and permeability values in the range from 0.01 mD – 1300 mD.

A special set of samples are the ‘SCD’ plugs (sandstones from Aachen), which were cut in a special way. There are pairs cut in a vertical and parallel direction relative to the bedding of the same specimen of a sandstone. Unfortunately, there are no petrophysical measurements done for the ‘SCD’-samples. Like the core plugs, they also fit the most homogeneous region of the magnet.

More than 60 different sandstones were measured during this study plus other mineralogy sediments. The selected examples presented in the text were chosen to illustrate newly developed hardware to characterize rocks.

2. Halbach core scanner

In this study we use a new generation of a mobile Halbach sensor with improved homogeneity of the magnetic field and an enlarged sensitive volume, equipped with gradient coils for PFG diffusion NMR experiments on cylindrical objects. The new sensor is portable and weights less than 30 kg. It was designed and constructed in our group based on simulations of the magnetic field in 2004 [Vod1].

The main goal of this chapter is to show constructive and physical advantages of the Halbach magnet, which can be used for extension of the applied techniques to mobile NMR. The modification of the magnet system is explained. The benefits of the new system are pointed out.

2.1. Magnet system

Klaus Halbach invented a new design of rare earth cobalt multipole magnet that allows construction of compact quadrupoles with magnet aperture fields of at least 1.2T [Hal1]. He placed magnet material on a ring where a specified multipole field is formed. Halbach magnets offer a solution to improved homogeneity in building portable NMR tools.

Several Halbach magnets were built in our group. A first version of a Halbach magnet provided by Dr. P. Blümler was constructed from six identical “magic rings”, each of them consisting of 16 magnet blocks with dimensions of 18 × 18 × 27 mm^3 [Rai1, Anf1]. The inner diameter of this magnet is 70 mm and its total weight is less than 8 kg. It produces a static magnetic field of B_0 = 0.3 T corresponding to a resonance frequency of 12.74 MHz for protons. The estimated gradient of the magnetic field within the sensitive volume of 60 mm diameter and 60 mm height is less than 0.3 T/m. A scanner with such field homogeneity is found to be suitable for non-destructive measurements of porosity of standard drill cores with 60 mm diameter drilled from the ocean floor [Arn2].

However, the homogeneity of the magnetic field is insufficient for conventional pulsed field gradient experiments, to measure tortuosity and pore size distributions, to estimate permeability, and to investigate pore anisotropies. Also the field strength

turned out to be too high, and it is advantageous to use low magnetic fields because the internal gradients in rocks are proportional to the overall field strength of the magnet. When accepting low field strengths, the sensitive volume can be increased to accommodate cores with larger diameters.

With these considerations in mind, a new and improved Halbach magnet was built from identical cubes of NdFeB magnets with dimensions of 30 × 30 × 30 mm^3. The focus in designing the new magnet system is on high field homogeneity in the central part of the magnet in a cylindrical volume of 20 mm in diameter and 20 mm in length, where an rf coil of similar dimensions is positioned. This sensitive region is used for predictions of permeability as well as PFG and 2D experiments.

The direction of magnetization of the bar magnets in a "magic ring" rotates from magnet block to magnet block so that the resultant magnetic field is transverse to the cylinder axis of the Halbach magnet. Stacking more than six magic rings improves the field homogeneity inside the stack but increases weight and cost. On the other hand, the homogeneity of the magnetic field can also be improved by a modification of the typical Halbach geometry instead of increasing the volume of the magnet material. To investigate this, the static magnetic field of differently modified Halbach magnets was simulated with the commercial software package OPERA-3d by Vector Fields™ [Vod1]. The homogeneity of the magnet along the cylinder axis is improved by splitting the stack of six magic rings into two identical arrays, each of them consisting of three "magic rings". As follows from the simulations, the magnetic field profile along the cylinder axis becomes more homogeneous as the distance between the two arrays

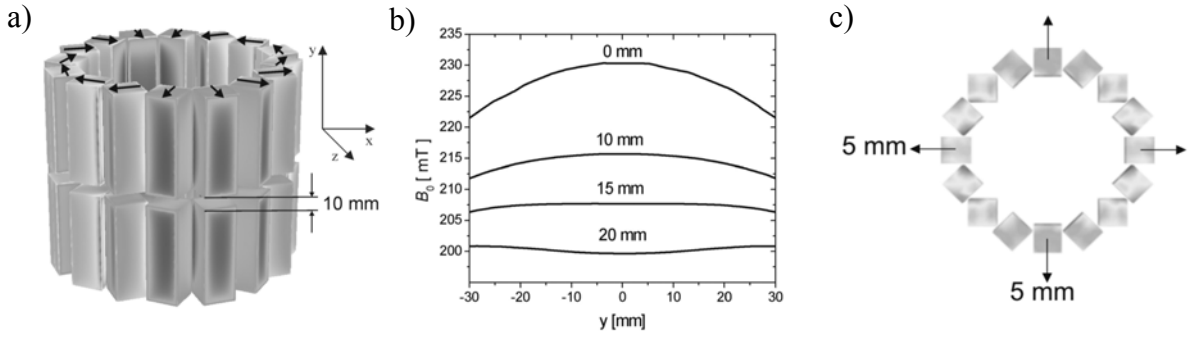

Fig. 2.1 *a) Modified Halbach magnet with improved homogeneity of the magnetic field. b) Simulations of the B_{0z} magnetic field component along the y-axis depending on the distance between Halbach arrays. c) Modified "magic ring". Every fifth bar magnet is shifted from the center by 5 mm for improving magnetic field homogeneity.*

increases. But at the same time, the overall field strength decreases. As a compromise between homogeneity and strength of the magnetic field, 10 mm was chosen as the distance between the magnet arrays (Fig. 2.1).

The homogeneity of the field in the plane transverse to the cylinder axis can be improved as well. The field simulation (Fig 2.2a) maps the field in the central transverse plane of the Halbach magnet. Within the central region with a height and diameter of 20 mm each, an ellipsoidal distribution of the field with a variation of 1 mT is obtained. If every fourth magnet block parallel and perpendicular to the main field in the "magic ring" is shifted by 5 mm along the radius from the centre, the homogeneous region becomes larger (Fig 2.2b). Additionally, the field of the modified "magic ring" is more than 10 times more homogeneous than that of the original ring.

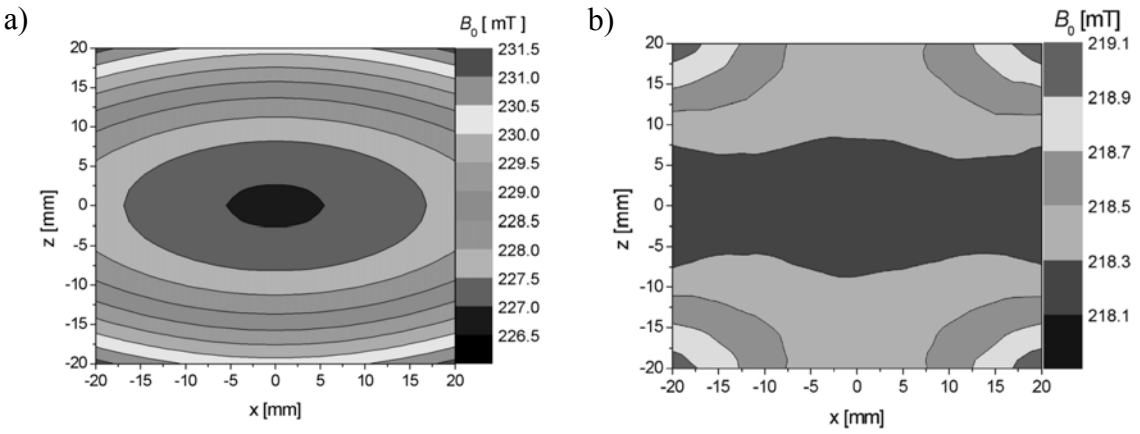

Fig. 2.2 *Simulated field maps. a) Simulated magnetic field distribution in the transverse plane of a regular Halbach magnet with six rings. b) The magnetic field of the modified Halbach magnet obtained by splitting the stack of six rings into two arrays of three rings separated by a gap of 10 mm and by shifting every fourth magnet in each magic rings radially from the center by 5 mm*

The optimum configuration of the modified Halbach magnet is designed according to these simulations. It consists of two Halbach arrays separated by an axial gap of 10 mm. Each Halbach array contains 3 stacked "magic rings" consisting of 16 magnet blocks with dimensions of 30 × 30 × 30 mm^3, arranged a circle with an inner diameter of 140 mm and an outer diameter of 260 mm. The magnet blocks are fixed with glue to an aluminum frame. The magnet hole of 140 mm diameter allows studying cylindrical samples with diameters of up to 80 mm. Also, gradient coils of corresponding

dimensions can be inserted inside the magnet for diffusion experiments. Every fourth bar magnet in the "magic rings" is shifted radially by 5 mm from the centre to improve the homogeneity. The improved magnet system produces a magnetic field of $B_0 = 0.22$ T, corresponding to a proton (^{1}H) resonance frequency of 9.6 MHz. The estimated average inhomogeneity of the magnetic field within the central sensitive volume of 20 mm × 10 mm, measured with the Hall probe is about 0.05 T/m. This means that magnetic field is sufficiently homogeneous for PFG and 2D correlation experiments on water-saturated rocks. The average field gradient of the magnetic field along the *y*-axis in the cylindrical volume of 40 mm × 80 mm is less than 0.15 T/m and sufficiently small for porosity measurements.

2.2. RF system

The modified Halbach magnet can be used for different sample geometries in combination with exchangeable rf coils of different diameters ranging from 24 mm up to 64 mm. A cylindrical rf coil with 24 mm diameter and 12 mm length which matches the region with the highest homogeneity of the magnetic field is used for the more demanding measurements in 2D T_1-T_2 correlation experiments, estimation of permeability, and pulsed field gradient (PFG) experiments. The coil is made of 0.71 mm diameter Cu wire. A glass tube supports the coil and isolates it from a water-saturated plug. The rf coil is a part of a series tuned LC circuit and is placed within a shielded box. The LC circuit is matched to the 50 Ω impedance of the spectrometer and tuned to the operating rf frequency of 9.6 MHz by variable matching and tuning capacitors, respectively. This *rf* coil can be located either in the centre of the magnet for a study that requires high magnetic field homogeneity or it can be shifted from the centre to a region with a constant gradient.

The chosen quality factor $Q=f_0/\Delta f$ of the improved rf circuit with the coil of 24 mm is 190, where f_0 is the resonance frequency, and Δf is a bandwidth at $1/\sqrt{2}$ height of the amplitude dependence on frequency. The quality factor was reduced to its current value by adding an additional resistance into the rf circuit. The reason is that the samples should be measured at the shortest possible echo spacing to detect fast decays coming from small pores. The rf circuit with lower quality factor has shorter ringing oscillations compared to the circuit with higher Q factor. With a decreased value of the

Q factor, the echo time was reduced from 0.20 ms to 0.06 ms. Therefore, the influence of diffusion on the T_2 relaxation time was minimized and decays from smaller pores can be detected. In Fig 2.3 T_2 distribution curves measured on the same sandstone with different Q factors and corresponding shortest echo time in each case are presented.

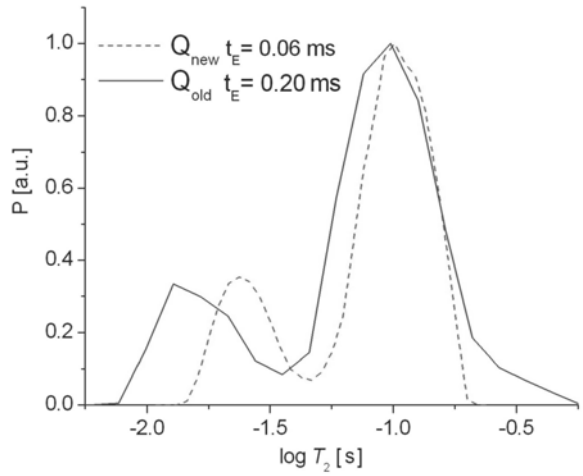

Fig. 2.3 *Dependence of the T_2 distributions of the same sandstone measured at different Q factors of the rf circuit. The modified rf circuit with a lower Q_{new} and a shortest echo time of 0.06 ms was used.*

Further cylindrical rf coils with diameters of 34 mm and 64 mm were used for porosity measurements of plugs with diameters of 30 mm and of standard drill cores with diameters of 60 mm, respectively. Also, a surface figure-8 rf coil with an outer diameter of 60 mm was used for the analysis of standard Ocean Drilling Program (ODP)/Integrated Ocean Drilling Program (IODP) cores. These cores have a diameter of 60 mm and are split along the axis after recovery. No further calibration of the sample volume is required because the sensitive volume probed by the surface coil is well defined by the geometry of the coil. Due to the large sensitive volume and the high signal-to-noise ratio for the Halbach core-scanner, a typical measurement of porosity lasts from only a few tenths of a second to a few minutes, depending on the porosity and number of scans.

2.3. Gradient coils

A gradient coil system (Fig 2.4) was designed to perform PFG experiments. A set of conventional anti-Helmholtz coils produces a linear gradient field in the direction of the field of the Halbach magnet. The anti-Helmholtz coil consists of two equal, square coils separated by a gap of 30 mm. Each coil was made of 85 turns of Cu wire (0.71 mm diameter), which results in a 2.5 mm thick coil, with inner dimensions of 40 × 40 mm^2 and outer dimensions of 65 × 65 mm^2.

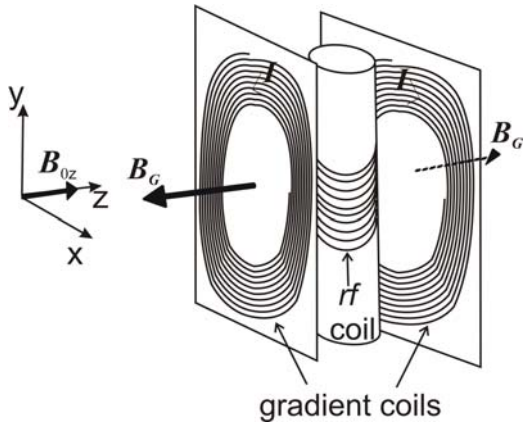

Fig. 2.4 *Gradient coil system. The cylindrical sample is placed in the rf coil between two square gradient coils.*

These coils were optimized in a way to provide a linear gradient field in the *z* direction. To check the linearity of the gradient field it was measured with a Hall probe at a constant current of 2 A and the dependence of the magnetic field generated by these coils was analyzed as a function of position. Results are presented in Fig 2.5. The field gradient is constant within 5 % over the cylindrical volume of 20 mm diameter and 12 mm length. The gradient strength is 0.11 T/m/A. As the gradient coils restrict the axial access to the magnet, only cylindrical plugs with 20 mm diameters can be analysed by PFG NMR methods.

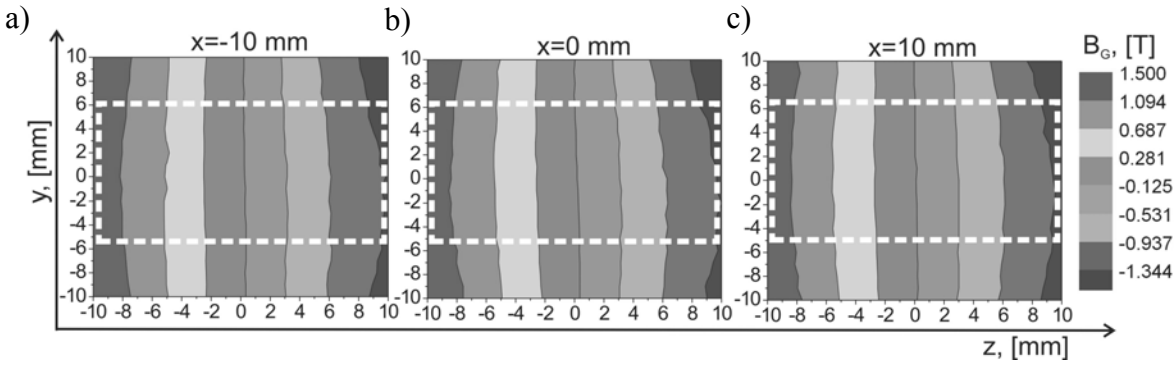

Fig. 2.5 *Scanned magnetic field produced by the gradient coils with a current of 2A. The entire space between gradient coils was measured. a) Scan in the yz plane at x=-10 mm. b) Central scan in the yz plane at x=0 mm, and c) High scan in the yz plane at x=10 mm of the entire space between the gradient coils. The dashed rectangles show the region where the rf coil is placed.*

2.4. Conclusion

The Halbach magnet has several advantages for measuring cylindrical and semi-cylindrical samples: Firstly, the Halbach magnet has the magnetic field transverse to the cylinder axis. Hence, simple solenoidal rf coils, centered around the cylinder axis, can be employed, and the magnet can be accessed to investigate long cylindrical objects. Secondly, a Halbach magnet can be constructed from small magnet blocks at light weight and low cost with a magnetic field sufficiently homogeneous and strong for various NMR applications. A further advantage is the very weak stray field of the magnet, which allows motors and other ferromagnetic and moving parts in the direct vicinity.

An improved Halbach sensor was built with characteristics shown in Fig 2.6 for analysis of water-saturated drill cores. It is equipped with exchangeable rf coils of different diameters and a special inset of the gradient coils. The most homogeneous part of the central volume of the magnet with a diameter of 20 mm is used in experiments to estimate permeability, in 2D correlation and PFG experiments. The Halbach magnet is a part of an on-line NMR core scanner.

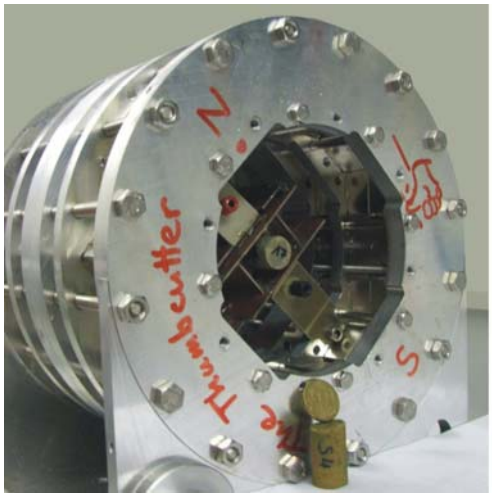

inner diameter: 14 cm
outer diameter: 26 cm
length: 20 cm
solenoidal rf coils ⌀: 2 cm - 8 cm
weight < 30 kg
frequency 9.65 MHz
G < 0.05 T/m (in the central area)

Fig. 2.6 *Photo of the Halbach sensor with improved homogeneity of the magnetic field. All experiments were done using this magnet. The rf coil with 2 cm diameter fits the most homogeneous part of the magnetic field.*

3. Advances in measurements of porosity with the Halbach scanner

Successful applications of the mobile NMR have been developed in the past for measurements of porosity of drill cores of different lithology. These measurements are fast and non-destructive. In this work we show a further development in this area using the improved Halbach scanner. The focus of this study is on fast and non-destructive measurements of porosity of different sized cylindrical drill cores and plugs with exchangeable rf coils. In this study, one of the key points is o*n-line* measurements of porosity of long drill cores with minimum human interaction and special preparation of the rocks. A newly developed experimental machine is presented here and first on-line measurements are discussed.

3.1. Porosity by mobile NMR with exchangeable rf coils

In a previous study [Blü4, Anf1] the methodology for measurements of porosity was already developed, applied, and tested with mobile NMR instrumentation, in particular the NMR-MOUSE® (21.1 MHz) and the first version of the Halbach sensor (12.7 MHz). It has been shown that mobile NMR can be used for accurate measurements of porosity of drill cores with different litholigy [Anf2, Arn1]. The NMR-MOUSE® requires samples with a flat surface while the first Halbach sensor was used to analyze cylindrical and semi-cylindrical cores with 6 cm diameters. Both mobile NMR instruments were found to be attractive for the rapid analysis of water-saturated drill cores on research vessels and drilling platforms [Arn2].

In this study measurements of porosity are performed with the improved Halbach sensor. It has two main advantages compared to the first version of the Halbach scanner: A lower magnetic field with the corresponding resonance frequency of protons at 9.6 MHz and a larger sensitive volume. A lower magnetic field minimizes the influence of

the internal gradients in water-saturated porous media. Also, the improved scanner is furnished with exchangeable rf coils and can be used to study different sized samples.

NMR methods can determine the total porosity, which is the total void space in the rock whether or not it contributes to fluid flow. This includes isolated fluid-filled pores. Also, it includes the effective porosity, which is the interconnected pore volume in a rock that contributes to the fluid flow in a reservoir. It excludes isolated, fluid-free pores. Thus, effective porosity is typically less than total porosity. Calculation of the total porosity needs an additional correction in this case.

The background of the NMR experiment is the following: The initial amplitude of the CPMG decay curve is directly proportional to the number of polarized protons in the pore fluid. The NMR porosity is given by the ratio of this amplitude to the initial amplitude of bulk water measured in the same sensitive volume which is considered to have 100% porosity. Our study shows that this porosity is independent of the lithology of the rock matrix and validated by comparing laboratory NMR measurements on cores with independent measurements in the helium-gas-pycnometer.

Thus, porosity Φ is defined as the portion of the formation that contains fluid and it can be determined directly from the signal amplitude of the fluid in the rock normalized to the signal amplitude of the bulk water in the same sensitive volume:

$$\Phi = \frac{\text{amount of protons inside the rock matrix}}{\text{amount of protons of the bulk water in the same sensitive volume}}.$$

Non-destructive NMR measurements were performed with the improved Halbach scanner using a CPMG-sequence. Fully cylindrical cores and core plugs of different lithology, porosity, pore sizes, and magnetic susceptibility with diameters ranging from 20 mm up to 60 mm were studied. Depending on the diameter of the drill core, exchangeable cylindrical rf coils with different diameters were applied. These rf coils can be easily exchanged. Typical recording times vary between a few tenths of a second to a few minutes, depending on the porosity of the core and number of scans. In all cases, porosity values from the NMR measurements with different rf coils agree well with those determined independently on core plugs in a helium gas pycnometer (Fig 3.1). There is a slight scatter in Fig 3.1 caused by averaging over different volumes from which the data were collected in the NMR experiment (sections of drill cores and plugs

with different diameters) and the pycnometer-measurements (plugs with 20 mm diameter cut from these sections).

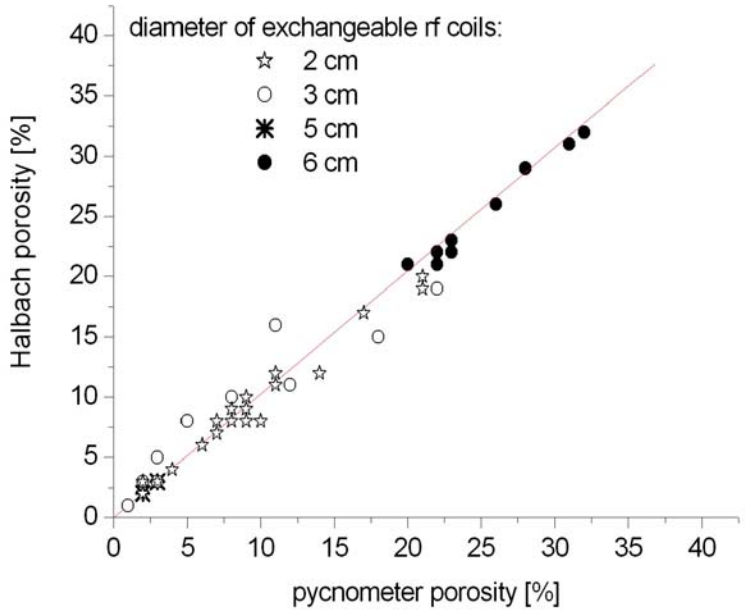

Fig. 3.1 *Correlation of porosity values of drill cores and plugs with different diameters measured by two different methods: NMR (y-axis) and He-gas pycnometer (x-axis).*

In the case of sandstones with many big pores characterized by long decays it is enough to use the normalization coefficient to calculate porosity value directly from the CPMG amplitude at experimental echo time with a good accuracy. For sediments with small pores characterized by fast decays (for example, mud) the full CPMG decay curve has to be reconstructed from the T_2 distribution and extrapolated to zero echo time using a multi-exponential fit to improve the accuracy. Due to the large sensitive volume of the Halbach core-scanner, low inhomogeniety of the magnetic field and its high signal-to-noise ratio, porosities as low as 1 % (in some cases even less) can be determined.

The results show that the NMR measurements with the improved mobile Halbach core-scanner are well suited to determine porosity of water-saturated cylindrical drill cores and plugs with diameters up to 60 mm. Drill cores can be measured in their original water-saturated state directly after recovery at the drilling platform or in the laboratory without prior preparation.

3.2. *On-line* measurements of porosity

This paragraph is about the NMR *on-line* core scanner which was built in this study. It is the object of novel achievements reached in the measurements of porosity. Special software has been developed to control the *on-line* measurement process, the CPMG sequence was improved, and all studies made on long drill cores.

Hardware

Since it has been shown that the Halbach sensor is well suited for core analysis in the laboratory, the idea evolved to automate porosity measurements. The goal was to construct equipment which can be installed, for example, on a drilling platform for *on-line* non-destructive structural analysis of long drill cores. The developed NMR *on-line* core scanner is presented in Fig 3.2.

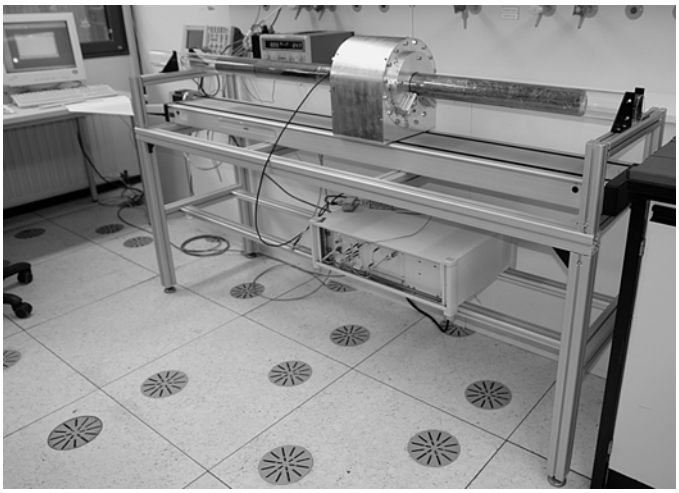

Fig. 3.2 *The NMR on-line core scanner with a sliding Halbach magnet along the tube with a cylindrical drill core inside for automatic measurements of porosity. The power supply (PS280) is on the left side of the Halbach sensor and a Minispec spectrometer is under it.*

The Halbach scanner is furnished with a sliding table. Long drill cores are placed inside a fixed plastic tube with an inner diameter of 64 mm and a length of 2.2 m. A tube with such dimensions matches different standards of drill cores. Different types of

plastic tubes were studied. A transparent Plexiglas tube was chosen (Fig 3.3) which had the fastest decaying CPMG signal, and does not contribute to the NMR signal from the drill core.

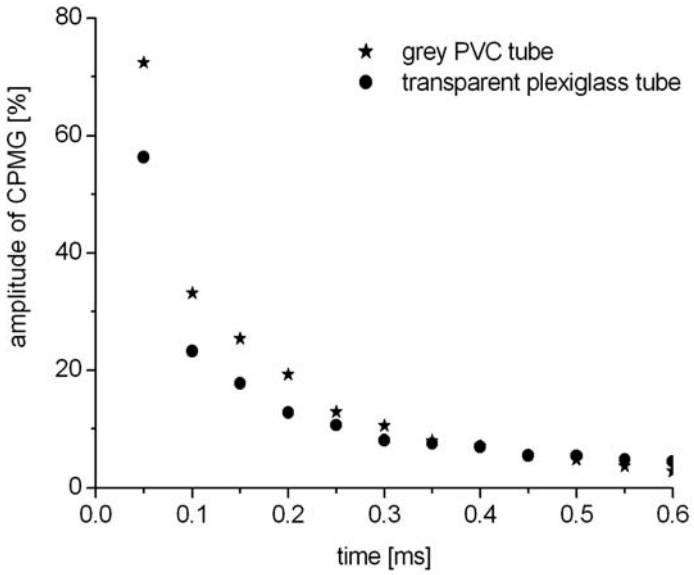

Fig. 3.3 *Analysis of CPMG decays from different tubes supposed to be used for on-line measurements of porosity*.

With the core fixed, the Halbach scanner is moved along the tube by a step motor and, hence, along the drill core up to a distance of 1.8 m. It performs measurements using a Carr-Purcell-Meiboom-Gill (CPMG) pulse sequence [Car1, Mei1]. The experiment itself does not take much time (15 – 20 seconds per point), nor does the further data processing. This sequence (Fig 3.4) is a multiple-echo sequence where an

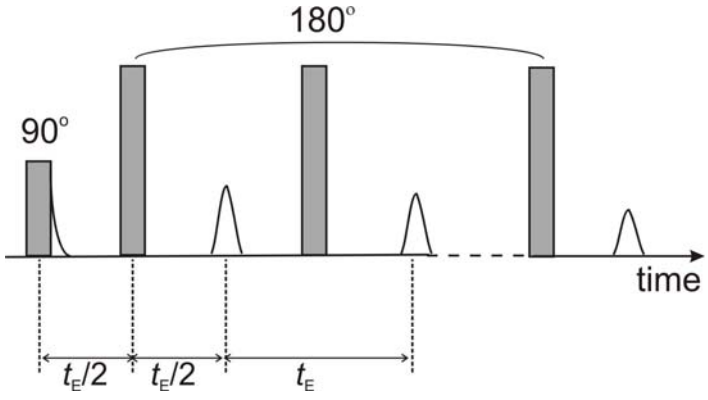

Fig. 3.4 *Schematic representation of a CPMG pulse sequence for excitation of multiple echoes to measure T_2 distribution* .

initial π/2 pulse, followed by a train of π pulses, each separated by an echo time t_E from the previous π pulse. Echoes form between π pulses.

A block diagram of the core scanner is shown in Fig 3.5. The Halbach core scanner is assembled from different commercial and home-made parts: the NMR spectrometer (Bruker Minispec), a PC, the step motor (JVL MST341, JVL Industri Elektronik), a power supply (PS280) and a step motor controller (JVL SMC35B). All these parts are chosen because of their particular characteristics. For example, the JVL SMC35B step motor controller was chosen because it is a multi-task system with the possibility to change velocity, acceleration, etc without stopping the motor. Also, it has small geometrical dimensions and can be mounted on a surface and programmed via Windows-based 'Moto Ware' software.

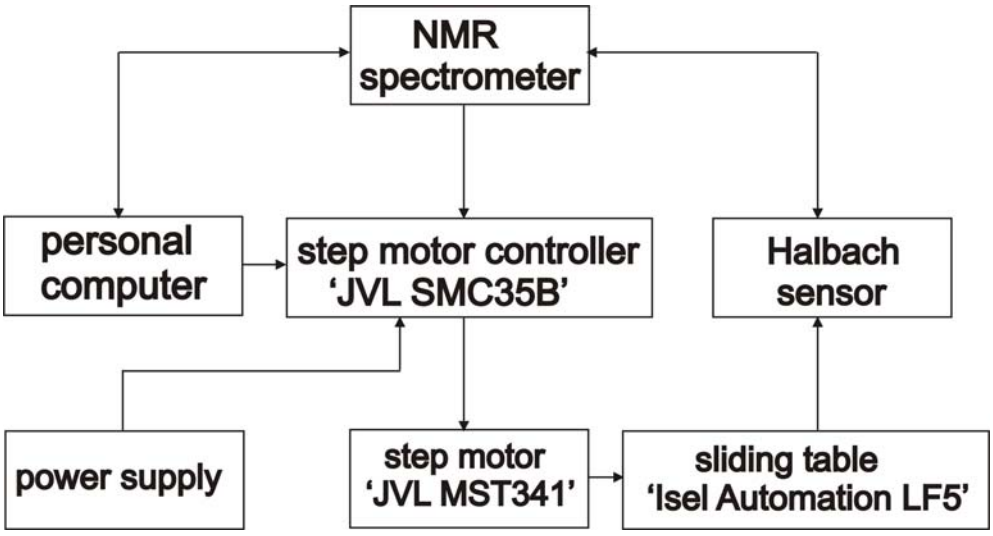

Fig. 3.5 *Block diagram of the NMR on-line core scanner. The NMR spectrometer sends pulses to the controller and to the Halbach sensor and receives the signal back from the Halbach sensor, controlled by a computer. In turn, the step motor controller obeys the spectrometer and a PC.*

The 2-phase motor has parallel connection of the phases (Fig. 3.6). This provides better performance at frequencies higher than 1 kHz compared to serially connected phases.

The Power supply is connected in a relatively simple way. Initially, a standard power supply PS280 with 24 V voltage was used for testing. Afterwards, the PS280 was changed to a homemade power supply yielding 80 V to achieve the best torque performance of the motor at high speed. This value of voltage is limited by the

Controller which operates with voltage in the range 20 V – 80 V DC. The Controller is protected against incorrect polarity connection and voltage overload.

The connection between the Controller and a PC is illustrated in Fig 3.6. All PCs and standard terminals can be connected via the COM2 port but the interface cable should not be longer than 10 m.

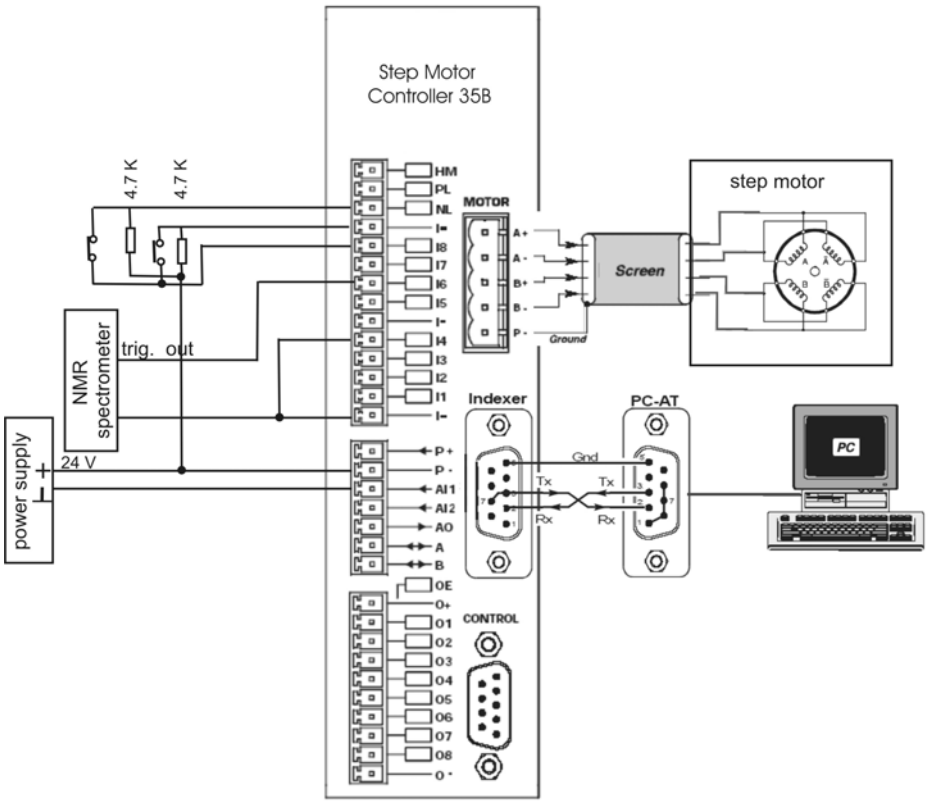

Fig. 3.6 *Connection diagram. There are analogue inputs and outputs on the left side of the controller. They are used for the NMR spectrometer and power supply connection. The right side of the controller has special slots for the motor and a PC connection.*

Software

Two different computer programs were used for the spectrometer and for the step motor. PC programs specifically developed for the Minispec and the controller drive the scanner. The main program is a modified CPMG pulse sequence program. It works in the following way:

- The number of scanning points is determined by the drill core length and the distance between the points. These values are user inputs.

- When the measurements are finished, the Minispec generates and sends a pulse to the controller. It activates the step motor program and the Halbach scanner moves a chosen distance.
- There is a time delay between the CPMG measurements and the Halbach scanner movement. The time delay is long enough to change a position of the Halbach scanner to the next measurement point.
- The maximum available number of pulses in the existing CPMG program is extended to from 3000 to 7000. It allows to record a full CPMG decay without changing the echo time which is 0.1 ms.
- When a core scan is finished, the Minispec generates a pulse for the controller to move the Halbach scanner back to the initial position.
- The measurement results are saved in an external file.

The program for the motor waits until the controller is activated by the Minispec and starts the motor that moves the Halbach sensor a chosen distance and then stops it.

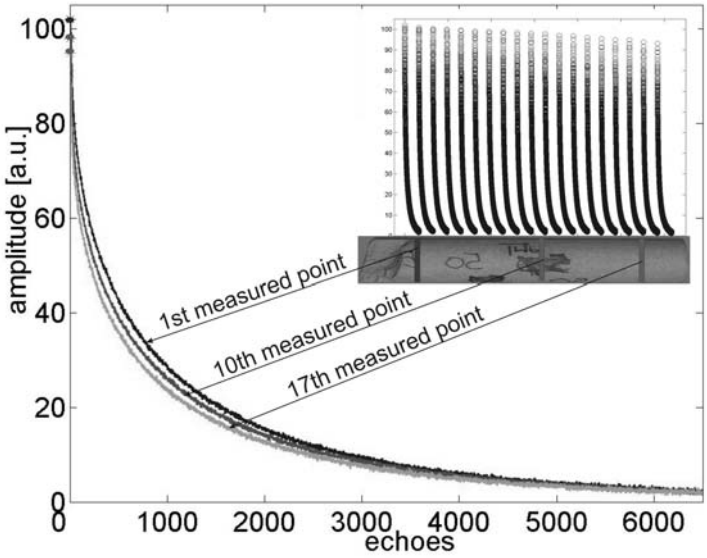

Fig. 3.7 *CPMG relaxation echo envelopes, which are received during scanning of the core. The main graph shows three decays measured at the one edge of the core, its middle part and another edge with marked initial amplitudes for each decay. All three decays are different. The inserted small graph shows all measured echo envelopes along the sample and the amplitudes of the decays are decreasing from the left to the right side*.

Experiment

In one measurement, the Halbach sensor moves along a plastic tube in which a drill core is placed and scans it at different positions. To automate measurements, a simple CPMG pulse program was modified in such way that the spectrometer sends a pulse to the motor via the step motor controller after finishing measurements at one point. The motor moves the Halbach magnet by a chosen distance, stops and waits a few seconds while the spectrometer provides a measurement. For example, a core is measured at 19 different points if it has 21 cm length and the scanning step is 1cm (with 1 cm distance from both edges of the core) using a CPMG pulse sequence. Figure 3.7 shows the CPMG relaxation echo envelopes measured at 19 different points along a core of 21 cm length. The experimental time (with 8 scans) includes a measuring time of each point (around 15 - 20 s) and a time for moving the Halbach magnet. The whole measurement time of a core with 20-30 cm length is about 15 minutes depending on the speed of stepping.

The selected decays are from the one edge of the core, the central part and from another edge of the core. The measured signal at the first point decays slower with longer T_2 times than that at last measured point. The results presented in Fig. 5.4 show clearly that the sample is heterogeneous. The presented echo envelopes have decaying amplitudes from point to point along the core.

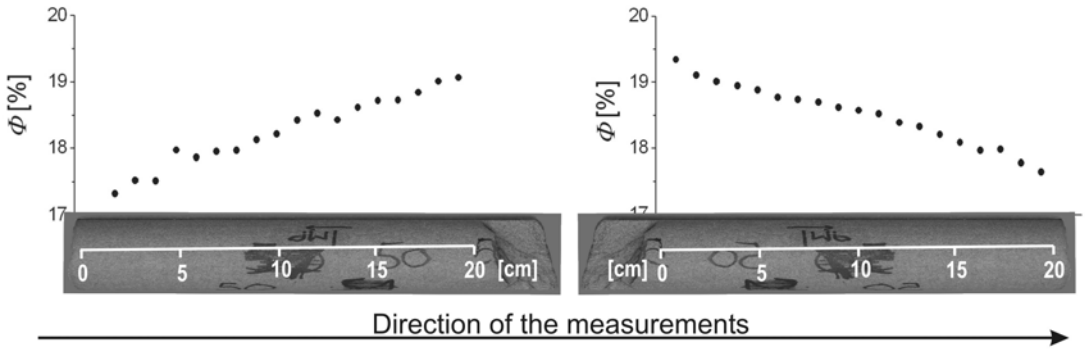

Fig. 3.8 *The porosity distribution in the same drill core mapped on-line. The experiments were done in different days. For comparison with the first experiment, the drill core was scanned in reverse direction showing good reproducibility and accuracy of the results.*

The reproducibility of the results was checked by scanning the same drill core in opposite direction (Fig. 3.8). In both cases, the results were comparable and show the same behavior. The porosity change is 3 % for this core and the variance is less than 1 %. Other sandstone cores measured with the core scanner also exhibit an inhomogeneous porosity distribution. Therefore, 1D images of the porosity distribution over different, long drill cores were measured non-destructively with the *on-line* NMR core scanner (Fig. 3.9).

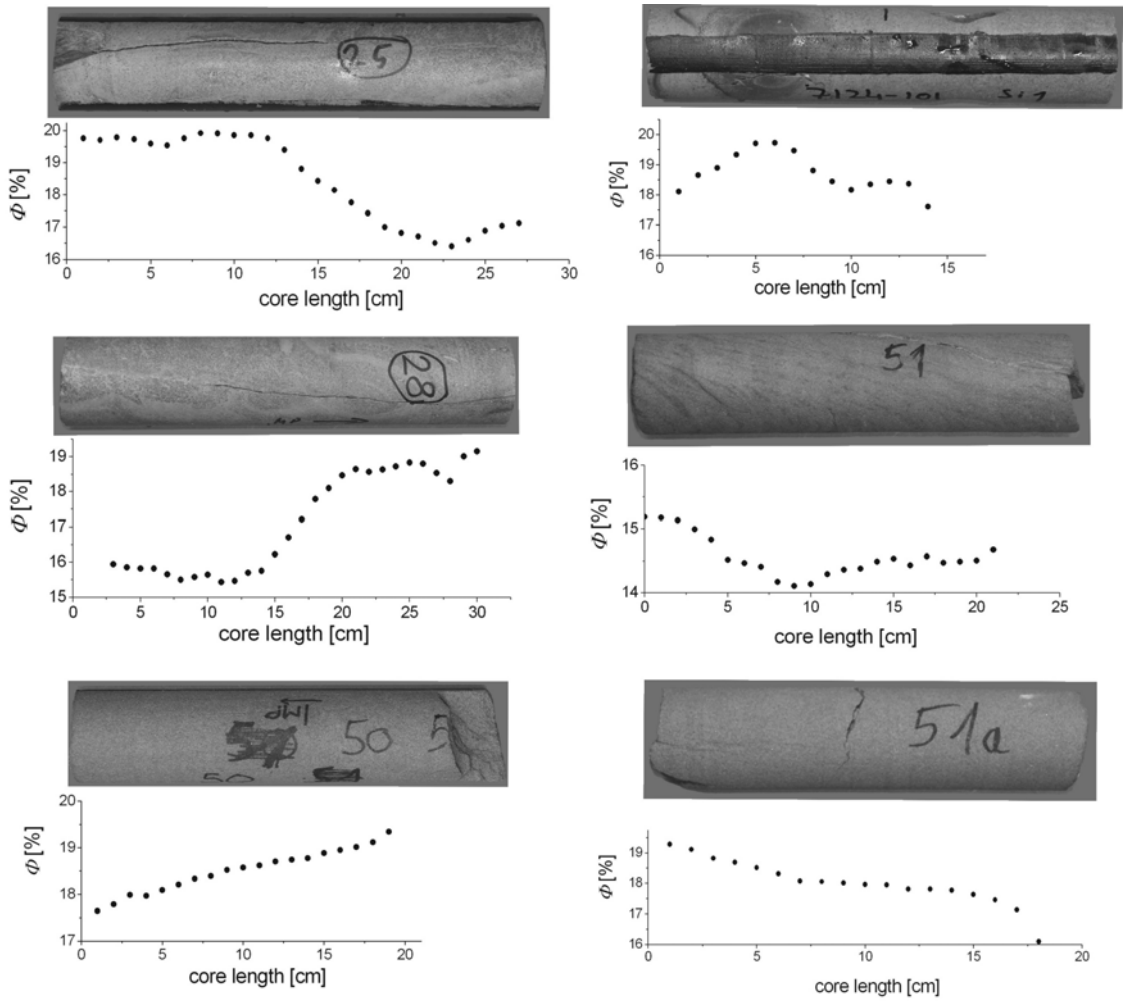

Fig. 3.9 *1D porosity distribution images. Porosity of six different drill cores.*

3.3. Conclusions

The study of CPMG relaxation echo envelopes can provide information on structural parameters of porous media. We have shown that a Halbach sensor can be used for measurements of porosity in cylindrical samples with different diameters of up to

60 cm. In measurements of porosity of big samples (8 cm, 10 cm diameter) using another Halbach magnet we faced the problem of incomplete saturation. Thus, we could calculate the effective porosity but not the total porosity. Therefore, it is advised to measure such samples directly after recovery.

Nevertheless, as our study shows, the NMR porosity in cylindrical samples with different diameters can be calculated with high accuracy and is comparable to that measured by independent methods. The Halbach sensor is equipped with the rf coils of different diameters. These coils are easy to exchange.

Porosity is determined by NMR with good accuracy. The method is simple and fast. There is no need for a special sample treatment. This method can be applied not only for sandstones. The porosities measured by NMR are reliable and have been checked on many different core plugs and cores using the exchangeable rf coils.

The new experimental device with a Halbach scanner for on-line measurements of porosity was developed in our laboratory. Measurements can be made at porosities as low as 1 %. The new NMR on-line core scanner allows non-destructive *on-line* analysis of water saturated (or proton containing fluids) cores to determine porosity, 1D porosity images, and pore size distributions. Moreover, the diameter of the tube where a sample is placed allows measuring samples with diameters smaller than 6 cm. In this case the different coefficient of normalization with respect to bulk water in a corresponding sensitive volume should be used.

The results were recorded using different programs: one is a modified CPMG pulse program of the Minispec spectrometer that also leads the Motoware program of the stepping motor; the second one is a program to compute the T_2 distribution function. Future work can be the integration of these programs into one, with a convenient interface for users. The designed instrumentation can also be used for a homogeneity control of cylindrical objects or the study of liquid explosives inside bottles and containers.

4. Quantifying diffusion in the presence of internal gradients

Important attributes of fluid saturated porous media are internal gradients due to a difference in magnetic susceptibility between the solid matrix and the pore fluid. Diffusion of the water protons in the internal inhomogeneous magnetic field controls the decay rate of the transverse NMR signal. Indeed, since the samples are heterogeneous porous media, it is difficult to evaluate this process in detail as the internal field inhomogeneities depend on the pore geometry and the petrophysical characteristics of the samples. It is important to remember that the most homogenous region of the magnetic field of the Halbach magnet in the central cylindrical volume with 2 cm diameter is used in the following experiments. This avoids difficulties associated with the external magnetic field gradient at sufficiently short echo time. In all experiments, the magnetic field of the Halbach scanner is considered to be homogeneous while the diffusion of spins in the internal gradients leads to extra transverse relaxation.

This chapter attempts to quantify effect of the diffusion influence in internal gradients in sandstones by applying 1D and 2D relaxation experiments. First, the diffusion effect on the T_2 distributions from conventional CPMG experiments is discussed. Second, the diffusion effect is estimated qualitatively and quantitatively by 2D $T_1 - T_2$ correlation experiments. Then permeability estimations based on NMR data are presented which clarify the role of diffusion. The correlation of the estimated permeability values k_{NMR} with permeability values k_{GAS} measured independently by gas flow experiments is analyzed and a methodology to improve the permeability values from NMR data in the presence of strong internal gradients is proposed.

4.1. Diffusion in 1D experiments with the CPMG sequence and its influence on T_2 distributions

The following discussion focuses on transverse relaxation because it can be measured much faster than longitudinal relaxation and yields equally valuable information. But transverse relaxation processes in fluid-saturated porous media are difficult to interpret

because many factors need to be taken into account such as size and shape of the pore space and the surface properties of the solid grains. Nevertheless, the NMR relaxation yields petrophysical information about reservoir rock and fluid properties: porosity, permeability (a measure of the ability of a rock to transmit fluids), pore size distribution, etc. For example, in a study conducted by our partners from Applied Geophysics (AG), pore sizes obtained by mercury porosimetry were experimentally correlated with T_2 distributions measured by an improved Halbach scanner, Fig. 4.1 [Arn2]. It was shown that T_2 distributions determined with the Halbach scanner can be related to pore size distribution and, thus, permeability can be estimated.

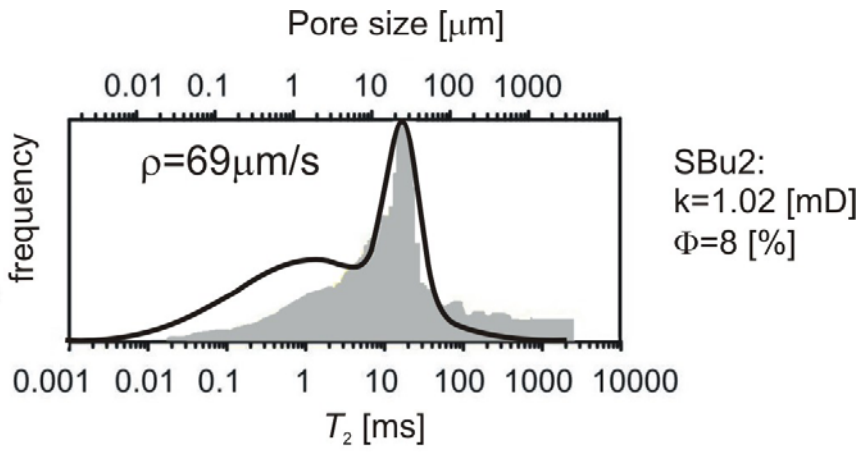

Fig. 4.1 *Pore size distribution of a limestone by mercury porosimetry (gray area) and by NMR (T_2 distribution, black line) measured with the improved Halbach scanner [Arn1].*

A relatively simple way to analyze the porous media is by means of the T_2 distribution function $P(T_2)$. One just needs to measure the NMR echo envelope with the CPMG pulse sequence and process it by any 1D inverse Laplace program (different programs are reviewed in Appendix C). In water-saturated rocks, the T_2 values typically span several decades from microseconds to several seconds because of the broad distribution of pore sizes. Figure 4.2a shows the observed CPMG decay measured with the Halbach scanner and the corresponding T_2 distribution function for a sandstone (VESF: porosity-20 %, permeability-735 mD). The transverse relaxation times of this sandstone vary from 3 ms up to 500 ms. The inserted T_2 distribution of the VESF core plug reveals both producible and irreducible water. The main contribution is from the producible water as expected from high values of porosity and permeability. An

estimation of the producible water or, so called, free water (or free fluid index - FFI) is important for the oil industry since it can be replaced by oil. Producible fluids reside in large pores whereas the bound fluids reside in small pores. The term "bound water' (bulk volume irreducible - BVI) describes the part of the water that is kept in the pores under a certain capillary pressure and is therefore, not producible or movable. A cutoff time ($T_{2,cutoff}$) determined empirically is normally used to discriminate between free water and bound water. The part of distribution function below the cutoff corresponds to the irreducible water which may be clay-bound and capillary-bound water. The producible water corresponds to values above the cutoff. The cutoff is different for different types of rocks and depends on the capillary pressure, lithology, and pore characteristics. For example, $T_{2,cutoff}$ values of 33 ms and 92 ms are recommended for sandstones and carbonates, respectively. In some particular cases it has been reported in the literature that the cutoff for sandstones can be as low as 15 ms and as high as 200 ms [Dar]. In the calculations below for sandstones, a cutoff of 33 ms was used as for the general case. The shape of the transverse relaxation distribution in Fig. 4.2b indicates that there is a high probability that producible water in pores can be replaced by oil. The amounts of free and bound water are estimated as ~ 98 % and ~ 2 %, respectively. The amount of free water is shown by the ratio of the area under the part of the distribution curve to the respect of the cutoff normalized to the total area under the T_2 distribution curve. BVI is calculated similarly but the BVI part of the distribution curve is taken from the left T_2 value up to the $T_{2,cutoff}$ value.

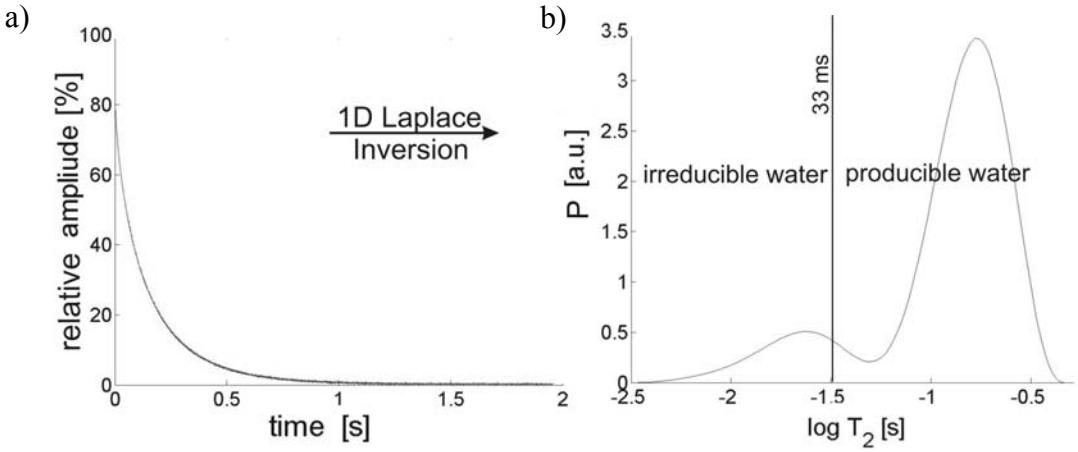

Fig. 4.2 *a) The CPMG echo envelope. b) Corresponding T_2 distribution function $P(T_2)$ measured on sandstone plug VESF.*

If different kinds of samples could be measured just by simply replacing them in the magnet without changing the experimental parameters there would be no need for any additional calculations. However, having measured pure water it is not possible to use the same experimental parameters for water-saturated sandstones due to the huge difference in the amount of protons in the same sensitive volume of the Halbach scanner and different mechanisms of relaxation. Therefore, the difference in the receiver gain of the NMR instrument must be taken into account. All results were calibrated to those for bulk water obtained at 55 dB amplification while the receiver gain to measure a signal from protons in porous media was much higher. For example, the sandstone plug of VESF has been measured at 77 dB amplification. To compare both distribution functions of water and of the sandstone, the measured data were scaled to the same receiver gain (55 dB). Afterwards, porosity was calculated by dividing the area under the T_2 distribution curve for VESF (0.125 s) by the area under the T_2 distribution of water (0.541 s). The porosity value of the VESF sandstone found from NMR data is 23 % and is in good agreement with independent measurements (24 %). It should be noted that the VESF sandstone has high porosity and permeability which facilitates the NMR measurements. Many other sandstones have critically low porosity and permeability which give rise to difference in diffusion in the internal gradients of the porous media and change the shape of the T_2 distributions.

As the mentioned before, the data interpretation and detailed analysis of the diffusion influence on the transverse relaxation are complicated due to differences of the sediment structures and their characteristics, influences of experimental parameters and a delicate way of using the mathematical software. To minimize the signal attenuation from diffusion by molecular diffusion in the internal gradients, it is important to apply closely spaced pulses in the CPMG sequence. A short echo spacing is essential for accurate and reproducible measurements of NMR porosity, pore-size distribution, and permeability especially in formations containing clay-bound and capillary-bound water in small pores. Different contributions of diffusion in internal gradients are demonstrated below on core plugs of various structures and low magnetic susceptibility measured at different echo times. CPMG decays and corresponding T_2 distributions of three selected plugs from different formations are presented in next three figures (Fig. 4.3, Fig. 4.4, Fig. 4.5). The samples are COF (Cottaer sandstone: 25 %, 59.2 mD), SASF (Sander Schilfsandstein: 21 %, 1.75 mD), and IBSF (Ibbenbürener sandstone: 11 %, 0.2 mD). COF and SASF have comparable values of porosity but differ

significantly in permeability values that yield different distributions of the same amount of water. In the case of the COF sandstone with a bigger amount of large pores and higher permeability, the internal gradients are expected to be smaller than for the SASF sandstone. The third sandstone (IBSF) has a twice smaller value of porosity than the two above mentioned plugs and very low permeability. The measurements were done at different receiver gain amplification of 77 dB, 76 dB and 80 dB for COF, SASF, and IBSF, respectively.

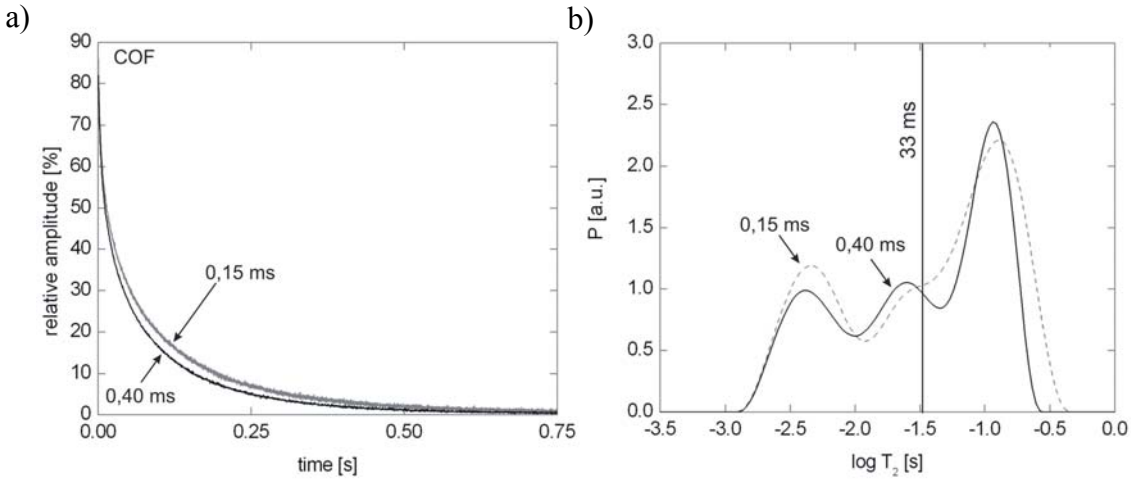

Fig. 4.3 *COF: porosity - 21 %, permeability – 59.2 mD. a) The CPMG decays. b) Corresponding distribution functions are obtained at an echo time 0.15 ms (gray curves) and 0.40 ms (black curves).*

Like the two others, the COF sandstone was measured with the CPMG sequence at echo times of 0.15 ms and 0.40 ms, and the corresponding T_2 distribution functions were calculated, (Fig. 4.3). The obtained signals decay with different relaxation rates when measured at different echo times and the corresponding distribution functions are different even for the *relatively good* characteristics of COF (high porosity and permeability compared to the two other plugs). The distribution function at 0.40 ms demonstrates that long spin-spin relaxation times are shortened by diffusion and therefore the occurrence frequency of short relaxation times increases. The occurrence frequency of long relaxation times decreases compared to the distribution function measured at 0.15 ms. The distribution function at 0.15 ms is wider and shifted to the right towards long relaxation times.

The diffusion effect on the T_2 distribution of the second sandstone SASF with lower permeability (Fig 4.4) is clearly seen too, but its influence is different from that of

the sandstone COF. The signal at short spin-spin relaxation times is lost at a long echo time of 0.40 ms by relaxation. The distribution function at 0.15 ms is wider from the side of the short relaxation times. The different influence of the diffusion in COF and in SASF can be explained by their structural differences. According to their distribution functions both samples have pores in the same range of sizes but their permeability values are very different ($k_{GAS,\ COF} >> k_{GAS,\ SASF}$) and so are their tortuosities.

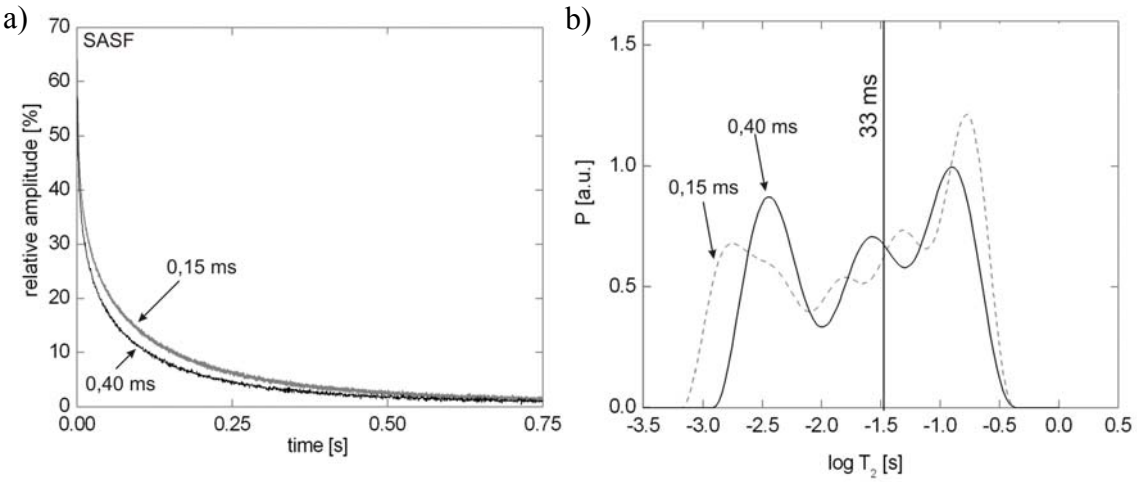

Fig. 4.4 *SASF: porosity - 18 %, permeability –1.75 mD, measured at t_E=0.15 ms (grey curves) and at t_E=0.40 ms (black curves).*

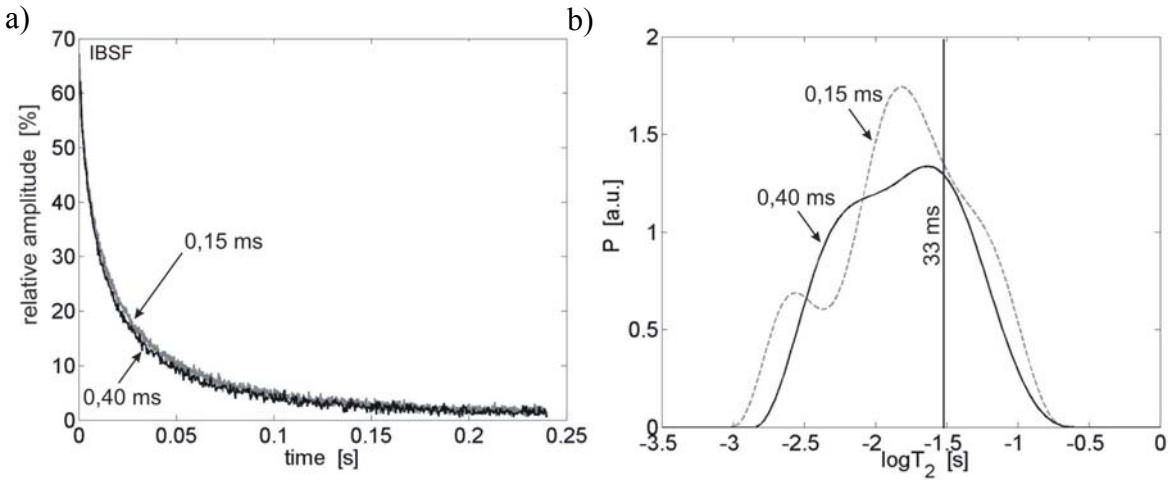

Fig. 4.5 *IBSF: porosity - 11%, permeability - 0.2 mD. a) CPMG decays measured at different echo times are slightly different. b) Corresponding T_2 distributions. The main contribution arises from bound water that corresponds to the low permeability of IBSF.*

In Fig. 4.5 results for the IBSF sandstone (11 %, 0.2 mD) are presented. The decays are not so much different as in the previous two cases but nearly twice as short

because IBSF is characterized by much lower permeability. The diffusion effect is similar to the SASF sandstone when the transverse relaxation is shortened in small pores or fast relaxation decays are lost at long echo time. The main contribution to the T_2 distribution comes from the dominant surface relaxation in micro pores associated with bound water.

The shortest possible echo spacing in the study is 0.06 ms. The corresponding T_2 distributions cover a wide range with fine details. The presented results show that already the CPMG decays reveal some properties of rocks. If a sediment has low porosity and permeability with small amount of bulk water inside, the decay is fast with low amplitude. The study of such sediments requires a CPMG pulse sequence with a few hundred echoes (300-400) at short echo time (0.06 ms). While the samples that contain a high quantity of bulk water are measured either with many echoes and the same short echo time if it is possible or with many echoes (~7000) and longer echo times. Therefore, samples with similar characteristics were measured with the same optimum experimental parameters.

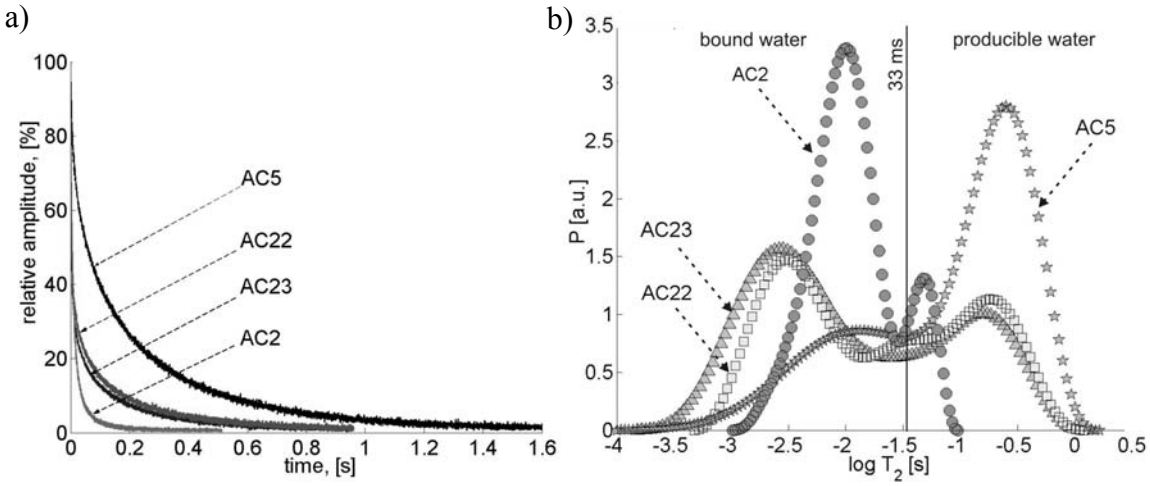

Fig. 4.6 *a) CPMG decays and b) corresponding bimodal T_2 distribution functions of the Allermöhe sandstones with low permeability values (AC2, AC22, AC23) and relatively high permeability (AC5). The cutoff at 33 ms, common for sandstones, separates free and bound waters. Free water relates to the large pores of a rock while the peak of bound water indicates micro pores.*

The influence of diffusion was checked also with 25 Allermöhe sandstones from one formation. The Allermöhe sandstones [Arn1] with low magnetic susceptibility of 0 SI -10^{-4} SI are characterized by low porosity from 2 % up to 13 % and fairly low

permeability values 0.05 mD – 20.7 mD. The pore-sizes in these sandstones vary between 0.01 μm and 100 μm. Figure 4.6 demonstrates decays (on the left) and T_2 distributions (on the right) of some selected Allermöhe sandstones: AC2 (12%, 0.05 mD), AC22 (8%, 0.394 mD) and AC23 (8%, 0.398 mD), AC5 (11%, 9.34 mD). 6400 echoes and the shortest possible echo time of 0.06 μs were used in these experiments. The measured CPMG decays of sandstones with almost the same characteristics AC22 and AC23 are identical and decay within the same average time. Their T_2 distribution functions are very similar and demonstrate comparable contributions from bound and free water. Two other sandstones AC2 and AC5 are examples of very short and very long decays, respectively. The corresponding T_2 distributions have main contributions from bound water for the sandstone AC2 and from bulk water for the sandstone AC5. The presented T_2 distributions show various ranges of pore sizes of these sandstones as well as different percentages of small and large pores.

The T_2 distributions of the Allermöhe sandstones show clearly different contributions from producible and irreducible water depending on the micro porous structure and on the permeability values. Most of the T_2 distributions are bimodal and can be partitioned into capillary- and clay-bound water in small pores with fast relaxation and free, producible water in large pores with slow relaxation. According to the T_2 distributions, the Allermöhe sandstones are divided into two groups. The first group of sandstone samples with fairly low permeability of less than 1 mD exhibits large frequencies of occurrence in the range of short relaxation times (3 ms – 40 ms) indicating the presence of micro porosity. The second group of sandstones with higher permeability has higher frequencies of occurrence at long relaxation times (200 ms – 400 ms) corresponding to large pores. The amount of irreducible bound water decreases with increasing permeability and macro porosity of the rock.

Therefore, the CPMG measurements with the same echo time conducted on sandstones from different formations demonstrate the different influence of diffusion on transverse relaxation. The study with different echo times helps to manipulate the diffusion effect which is weaker at short echo time. Nevertheless, 1D experiments with the CPMG sequence at different echo times cannot predict the effect of diffusion in internal gradients on transverse relaxation in rocks with various structures. It is advantageous to study the influence of diffusion in internal gradients with 2D correlation relaxation-relaxation experiments.

4.2. Two-dimensional $T_1 - T_2$ correlation experiments

To quantify the influence of diffusion on the shape of the T_2 distribution function, 2D T_1-T_2 correlation experiments were performed with the Halbach scanner on the same water saturated sandstones.

Relaxation properties, such as T_1 and T_2, are commonly used to identify mixed fluids in rocks by distinct T_1/T_2 ratios or to study their dynamics in porous media. Both of these quantities can be measured simultaneously in T_1 - T_2 correlation experiments. The T_1/T_2 ratio can be extracted from the 2D T_1-T_2 spectrum, and its value identifies the influence of diffusion on transverse relaxation. To acquire a T_1-T_2 correlation spectrum, the NMR data are measured using a conventional CPMG pulse train encoded by a saturation recovery experiment. The sequence for 2D T_1-T_2 experiments is presented in Fig. 4.7. This sequence consists of the two distinct parts mentioned above. Originally, it was proposed to use an inversion recovery in the first part of the sequence while we changed it to a saturation recovery. The advantage of using saturation recovery over inversion recovery is the fact that saturation is a well defined state that may be rapidly imposed on the sample whereas thermal equilibrium as needed in the inversion recovery experiments, only occurs after a very long relaxation period. On the other hand, it is much easier to destroy magnetization as in saturation recovery experiments than to invert it as in inversion recovery experiments. In a saturation recovery experiment, the initial magnetization M_0 is destroyed at the beginning by an aperiodic series of 90° pulses. In an inversion recovery experiments, the initial magnetization M_0 at the start of the experiment is inverted by a 180° pulse, so that the range of recovery during the subsequent build-up of M_0 is extended to $2M_0$.

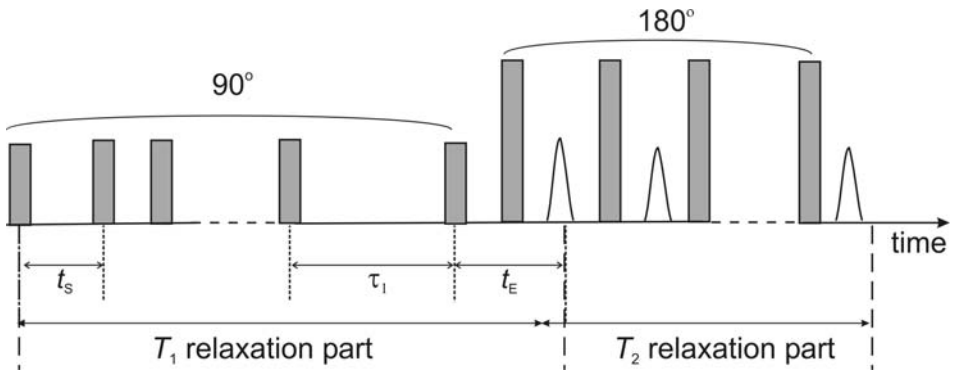

Fig. 4.7 *Pulse sequence for measuring T_1-T_2 relaxation correlation. t_S is the saturation delay time which decreases from pulse to pulse as $t_S/(n-1)$. τ_1 is the saturation recovery time, t_E is the echo time.*

The initial part of the saturation-recovery sequence (Fig 4.7) is used to detect T_1 relaxation. The initial magnetization is demolished by applying nine 90° pulses and it recovers with τ_1. The second part is used to detect T_2 relaxation by a CPMG sequence. The correlation of T_1 - T_2 is reached by variation of τ_1 with subsequent CPMG detection. t_E has to be short enough to minimize the diffusion influence on the transverse relaxation.

The general settings of the measurements are chosen in such way that realistic information can be obtained within a short measurement time. The average measurement time of 2D experiments on cylindrical water-saturated plugs of 2 cm diameter is 30 min. The main settings are the following: τ_1 (1st dimension) varies from 0.5 ms up to 6 s in 35 steps; the number of echoes (2nd dimension) is varied from 400 up to 5000; t_E equals either 0.06 ms, 0.15 ms, or 0.4 ms, the number of scans is either 8, or 16, or 32. Figure 4.8 shows the raw NMR T_1-T_2 data recorded from a plug of sandstone s4 with high permeability of 540 mD and porosity of 13 %. Sandstone s4 has big quartz grains and relatively well-connected pores that provide a good quality signal with high signal-to-noise ratio. Saturation recovery is clearly seen along the τ_1 axis as well as CPMG decays along the $n_j t_E$ axis.

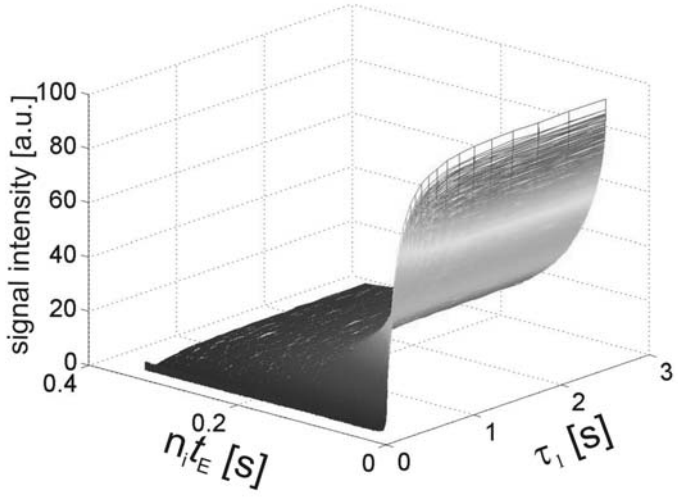

Fig. 4.8 *The measured magnetization as a function of* τ_1 *(response to the saturation recovery) and* $n_j t_E$ *(response to the CPMG decay) from the sandstone s4 characterized by high porosity and permeability.*

From the T_1 - T_2 correlation experiment, the measured magnetization $M(\tau_1, n_j t_E)$ of the water protons in the saturated rock depends on the longitudinal relaxation time T_1 and the transverse time T_2. It is described by [Son3]

$$M(\tau_1, n_j t_E) = \iint dT_1 dT_2 f(T_1, T_2) k_1(T_1, \tau_1) k_2(T_2, n_j t_E), \tag{4.2.1}$$

where n_j is the echo number and t_E is the echo time. The quantities

$$k_2(T_2, n_j t_E) = \exp\left\{-\frac{n_j t_E}{T_2}\right\} \quad \text{and} \quad k_1(T_1, \tau_1) = 1 - \exp\left\{-\frac{\tau_1}{T_1}\right\}$$

are matrices known from the experiment. The 2D distribution function $f(T_1, T_2)$ follows from Eq. (4.2.1) after 2D inverse Laplace transformation using the two-dimensional inversion routine [God1]

$$M(\tau_1, n_j t_E) \overset{\substack{2D \\ ILT}}{\longrightarrow} f(T_1, T_2). \tag{4.2.2}$$

The '2D Laplace Inversion software' requires special input data presented in matrix form. For this purpose, special programs were developed to transform the experimental data file into three matrixes for further processing and analysis (Appendix C).

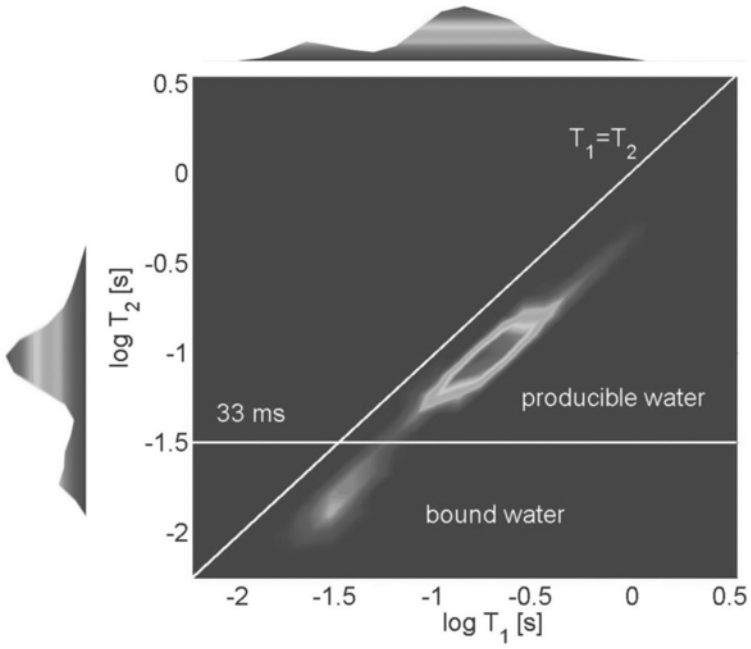

Fig. 4.9 *T_1-T_2 correlation spectrum of the s4 sandstone (porosity 13 % and permeability 540 mD) measured with the Halbach scanner at 9.6 MHz and the shortest possible echo time of 0.06 ms. On the top and on the left-hand side, projections along the longitudinal and transverse relaxation dimension are shown.*

An example of a 2D spectrum of water in the sandstone sample s4 processed from the data shown in Fig. 4.8 is presented in Fig. 4.9. The two-dimensional T_1-T_2 map covers a wide range of T_1 and T_2 values from a few mille- seconds to seconds, owing to a wide range of pore sizes. The T_1/T_2 ratio in the 2D distribution is nearly constant and equals to 1.77. Projections along the longitudinal and the transverse relaxation dimensions have components with short T_1 and T_2 from clay-bound and capillary-bound water with relaxation dominated by surface mechanisms in small pores. The major peak at long T_1 and T_2 values with a maximum at T_1 = 0.18 s and T_2= 0.10 s corresponds to free water in big pores. The T_2 cutoff at 33 ms common for sandstones divides producible from bound water. The ratio of T_1/T_2 =1.77 indicates attenuation of transverse magnetization by diffusion in the internal gradients. At t_E = 0.06 ms the shortening of T_2 by signal attenuation from diffusion at the Larmor frequency of 9.6 MHz of the Halbach scanner is sufficiently suppressed. Then, obtained by integrating the 2D spectrum, the T_1 and T_2 distributions of sandstones appear to be similar to each other but shifted as for sandstone s4 with high permeability. This can be

clearly observed when the T_1 distribution is plotted together with the T_2 distribution shifted by the T_1/T_2 ratio (Fig 4.11a).

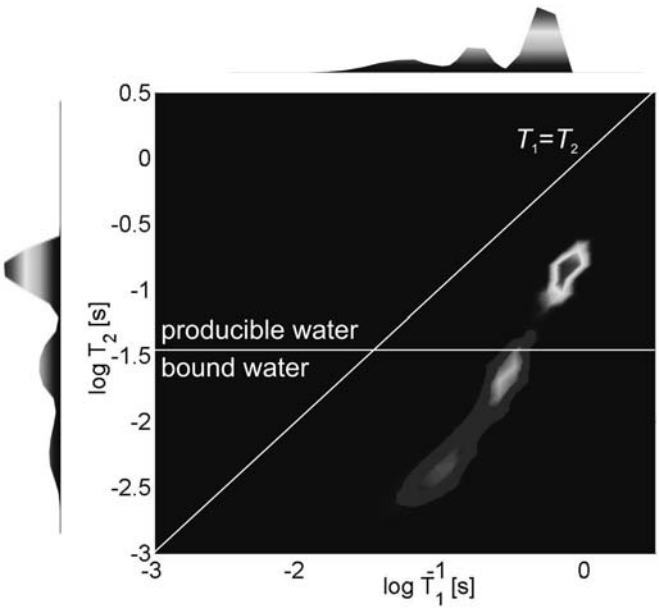

Fig. 4.10 *Correlation spectrum of the sandstone AC19 (porosity 8 % and permeability 13.9 mD). The T_1/T_2 ratio increases from large pores to small pores indicating stronger internal gradients in small pores.*

To compare with that of the s4, 2D correlation spectrum of the sandstone AC19 with low permeability is presented in Fig. 4.10. The main difference between the AC19 and the s4 spectra is that the T_1/T_2 ratio increases from large pores to small pores. This shows that the influence of diffusion in the internal gradients of the small pores increases, the transverse relaxation times become much shorter than longitudial relaxation times. This leads to a significant variation of the T_1/T_2 ratio from 5 up to 25, and the T_2 distribution of a plug AC19 does not look similar to the T_1 distribution. Since the T_1/T_2 ratio is not constant, T_1 and T_2 distributions of AC19 are aligned relatively to each other using T_1/T_2 =5 for the peak of free water on 2D map (Fig 4.11b). Despite the fact that the distribution functions of s4 are shifted to shorter times compared to AC19, i.e. s4 has a more pronounced structure than AC19, the diffusion influence of s4 is much weaker than of AC19. Thus an estimation of the T_1/T_2 ratio, its value and alteration can probe the diffusion effect depending on the structure and amount of paramagnetic impurities in the porous medium.

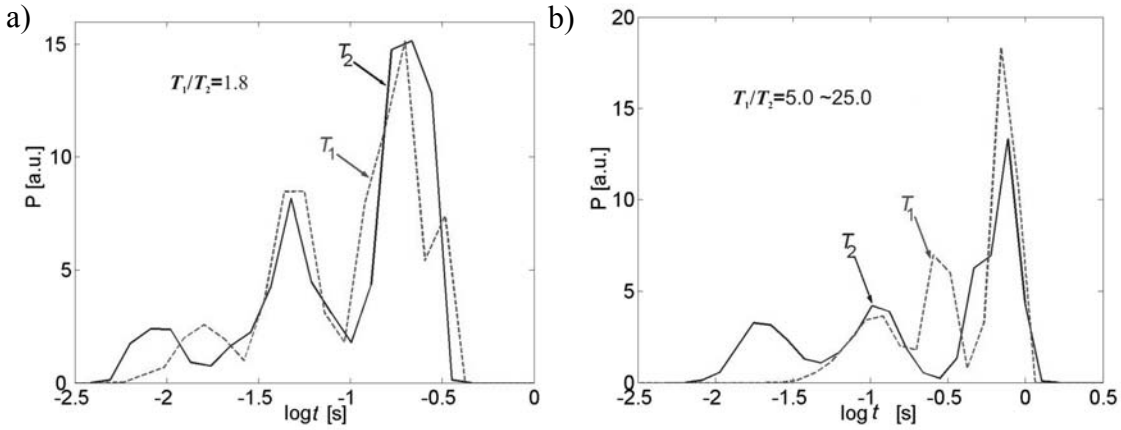

Fig. 4.11 *Integrated 1D T_1 and T_2 distributions obtained from 2D correlation experiments for a) sandstone s4 with high permeability with nearly constant T_1/T_2 ratio and b) sandstone AC19 with low permeability with strongly varied T_1/T_2 ratio.*

2D relaxation-relaxation experiments with the Halbach scanner were used to study the diffusion influence on the transverse relaxation in water-saturated sandstones from different formations. Three selected 2D T_1-T_2 correlation spectra of sandstone plugs from different formations (VESF from Velpe, BASF from Baumberg, and BHSF from Barkhausen in Germany) are presented in Fig 4.12. Sandstone VESF has high porosity and permeability that gives a strong peak of free water. BASF has the same porosity as VESF but lower permeability. Therefore, the 2D map of BASF demonstrates mainly bound water in small pores and a bit of free water in large pores. Moreover, the range of T_1-T_2 maps of VESF and BASF is absolutely different. The sandstone BHSF has the lowest porosity and permeability values among all analyzed sediments, and only bound water is detected. The unusual location of its 2D signal away from the diagonal can be explained by low signal-to-noise ratio. The signals in these 2D T_1-T_2 maps correlate with properties of porous media and are used to develop a new pore model ([Pap1], in preparation).

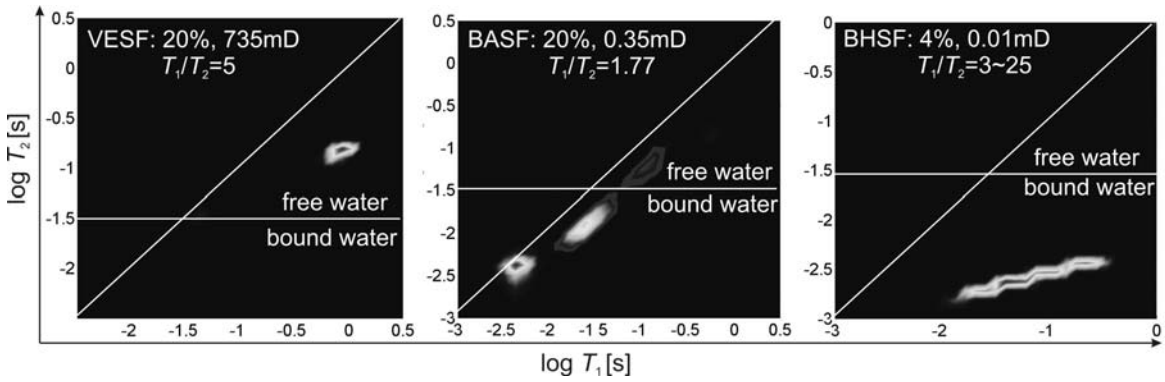

Fig. 4.12 *The 2D T_1-T_2 correlation spectrum for plugs VESF, BASF and BHSF from different formations. The diagonal with T_1=T_2 is drawn for a reference. t_E=0.15 ms.*

For comparison with 1D CPMG data, T_1-T_2 correlation experiments were provided on the same group of samples from Allermöhe borehole. The 2D maps of the Allermöhe core plugs vary very much from one to another and indicate different mechanisms of relaxation. An enhancement of the T_1/T_2 ratio from large pores to smaller pores from 4 to 10 (and in some cases up to 30) is noticed for all Allermöhe sandstones even at the shortest possible echo spacing of 0.06 ms. The influence of internal gradients is particularly high in the samples with high micro porosity. A good illustration of this fact is the 2D map of sandstone AC23 with a permeability of 0.398 mD (Fig 4.13a). Most 2D T_1-T_2 maps display a bimodal behavior, which is consistent with the T_2 distributions of Allermöhe sandstones from 1D CPMG measurements (Fig. 4.6).

The three Allermöhe sandstones AC1, AC2, AC3, with the lowest values of permeability less than 0.5 mD are unique. The 2D T_1-T_2 experiments on AC1 and AC3 with porosity less than 3% and very rapid relaxation failed because of the low signal-to-noise ratio. The 2D map of AC2 (Fig 4.13b) (with 8 % porosity and the lowest permeability of 0.048 mD among the Allermöhe sandstones) contains mainly bound water. It has clearly two shoulders: first the one at high T_1 is parallel to the diagonal with T_1/T_2=2.6 and the second one is with nearly constant T_1 whereas the T_1/T_2 ratio increases up to 10. Probably the second shoulder is an experimental artifact due to the low signal-to- noise ratio. Nevertheless, AC2 can be characterized as a sample with strong internal gradients that give rise to diffusion attenuation of the magnetization. The NMR measurements of the sandstone AC2 can be declared as unique because of its lowest permeability. There is a strong mismatch in the correlations of the T_1 and T_2 distributions of AC23 (Fig. 4.14a) and of AC2 (Fig. 4.14b).

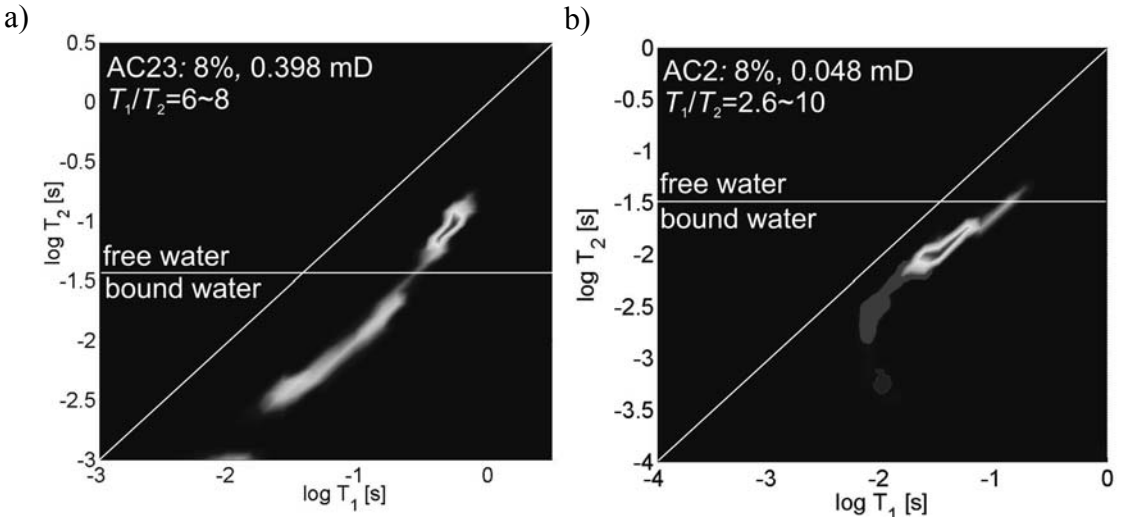

Fig. 4.13 *a) 2D spectrum of AC23, typical for Allermöhe sandstones, where bulk and bound water are clearly resolved. b) Unique 2D spectrum of AC2 with lowest permeability, where mainly bound water is determined.*

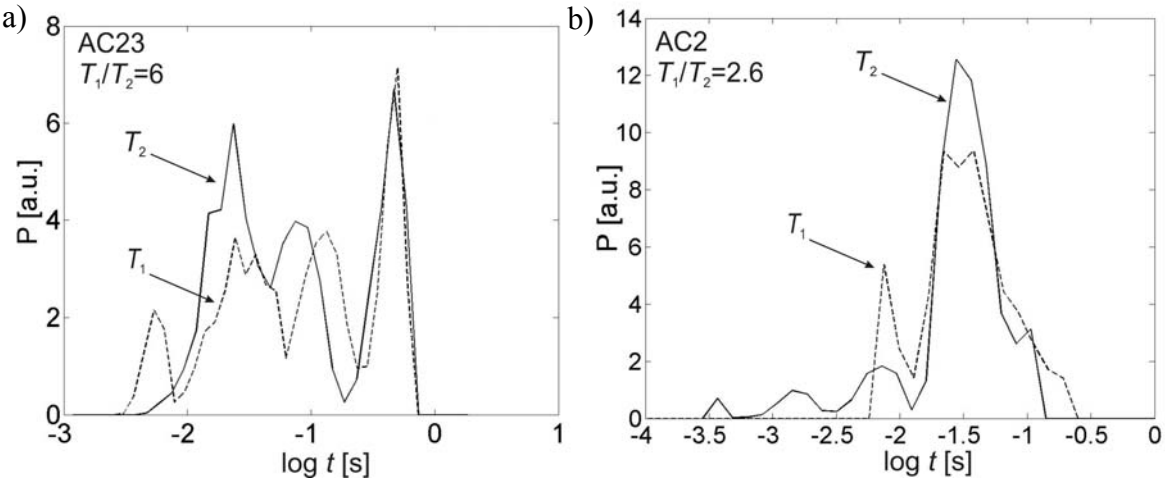

Fig. 4.14 *The T_1 and T_2 projections are aligned together to monitor the diffusion influence in different pores.*

As in the case of 1D CPMG, it is important to apply rf pulses in short intervals to reduce the diffusion effect in the final maps. For example, Fig 4.15 shows the two-dimensional T_1-T_2 map of the sandstone sample AC6 (Φ = 6 %, k_{GAS} = 1.85 mD) measured at t_E = 0.06 ms (Fig. 4.15a) and at t_E = 0.15 ms (Fig. 4.15b). The T_1/T_2 ratio varies less when measured at shorter t_E.

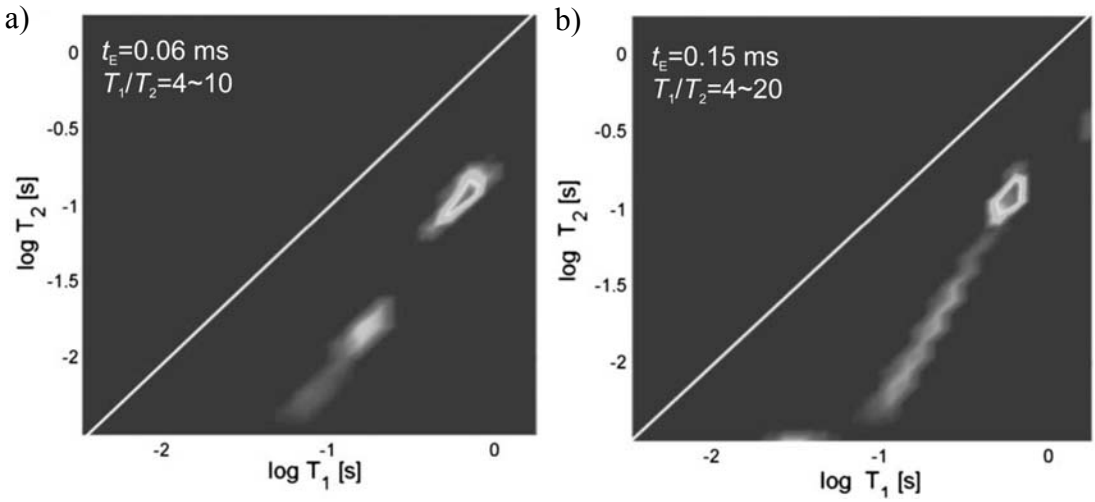

Fig. 4.15 *The T_1-T_2 correlation spectrum of sandstone AC6 with small quartz grains obtained from the experiments at different echo time t_E. The diagonal is the line at T_1=T_2. The T_1/T_2 ratio is higher for smaller than for bigger pores. This indicates an enhancement of the diffusion effect for large echo times t_E.*

As a result, the influence of the local gradients on the transverse relaxation of the Allermöhe sandstone samples with high micro-porosity is evident even at the shortest possible echo time of 0.06 ms. This means that the chosen echo time is not short enough for sediments with high micro porosity. The lower T_1/T_2 ratio for the larger pores is the result of the bulk contribution to the relaxation which is in general much slower than surface relaxation. The micro-pores inside the grains are apparently of very small sizes, thus there is a high surface contribution to the relaxation. Another reason for an enhanced T_1/T_2 ratio is the stronger influence of diffusion in the internal gradients in the small pores compared to that in the larger pores. Hence, permeability values of Allermöhe sandstones obtained from NMR transverse relaxation data tend to be underestimated.

2D T_1-T_2 experiments were also performed with the on-line NMR core scanner on long drill cores of sandstones with 6 cm diameter (used for on-line measurements of porosity in chapter 3). As mentioned above, all plugs analyzed in the 2D experiments are of 2 cm diameter while the cores are much bigger (6 cm diameter). In all studied samples, T_1 is nearly twice as large as T_2 according to the corresponding 2D maps in Fig. 4.16. Moreover, the results appear faithful in spite of the large volume of the magnetic field with the consequently higher inhomogeneity. The presence of two distinct pore environments is evident for all cores where both bulk and bound water

contribute to relaxation. According to these 2D maps all these drill cores have high porosity and permeability. At the same time, these maps have artifacts such as additional separated peaks from the main ridge and a shape of a tail deviating from the line of constant T_1/T_2 ratio which arise from the diffusion influence. These first experiments showed that 2D experiments can be performed in on-line mode if appropriate software is designed. To minimize the influence of diffusion in on-line 2D experiments, the rf pulses can be shortened and the distance between them reduced by using a higher power amplification of the receiver and a lower quality factor of the rf circuit.

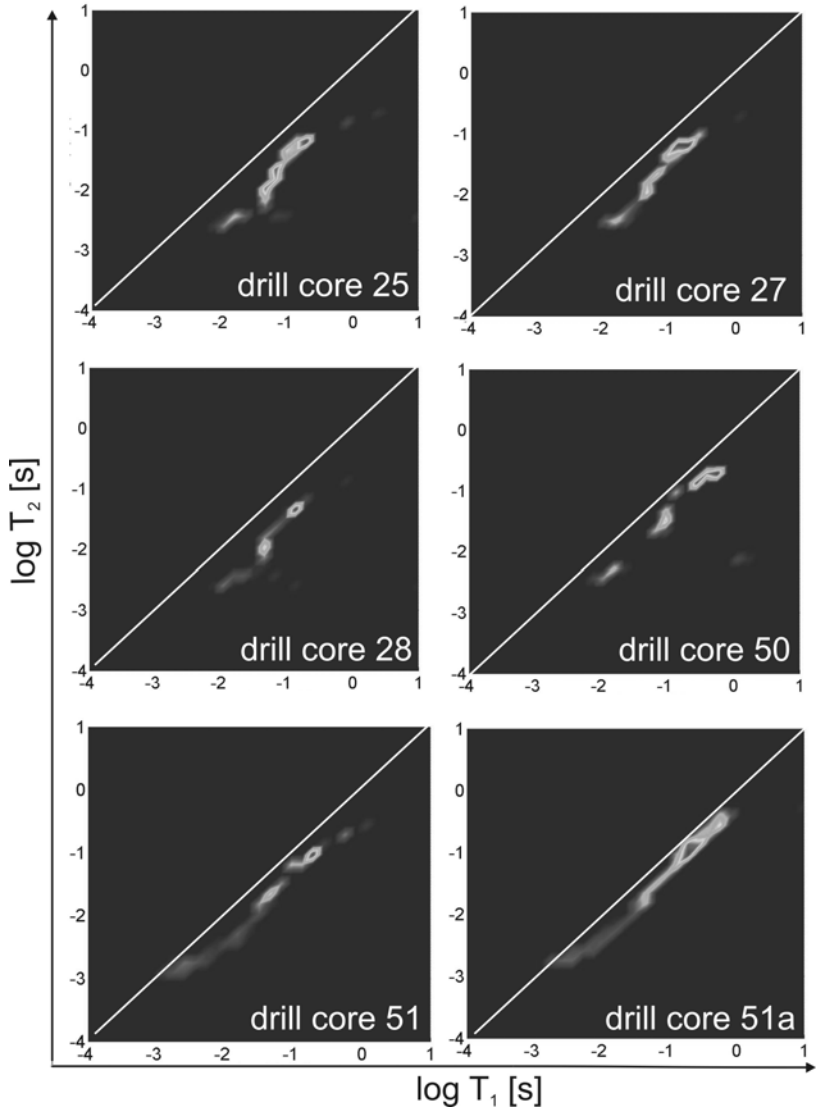

Fig. 4.16 *2D T_1-T_2 spectra of long drill cores with 6 cm diameter. The T_1 and T_2 distributions are similar to each other for each core. The T_1/T_2 ratio is nearly constant and changes from 1 up to 2 depending on a core. All maps show a slight influence of diffusion on the transverse relaxation.*

2D relaxation correlation experiments with the Halbach scanner were used to discriminate mixed fluids - water and Norwegian light crude oil in commercial sand. Three different mixtures were prepared for these experiments. The first one is sand mixed with water, the second is sand mixed with the oil, and the third mixture is sand with added water and oil. The order in which the fluids were supplied to the sand is an important because water and oil are not miscible and their uptake depends on the wetting properties of the whole system.

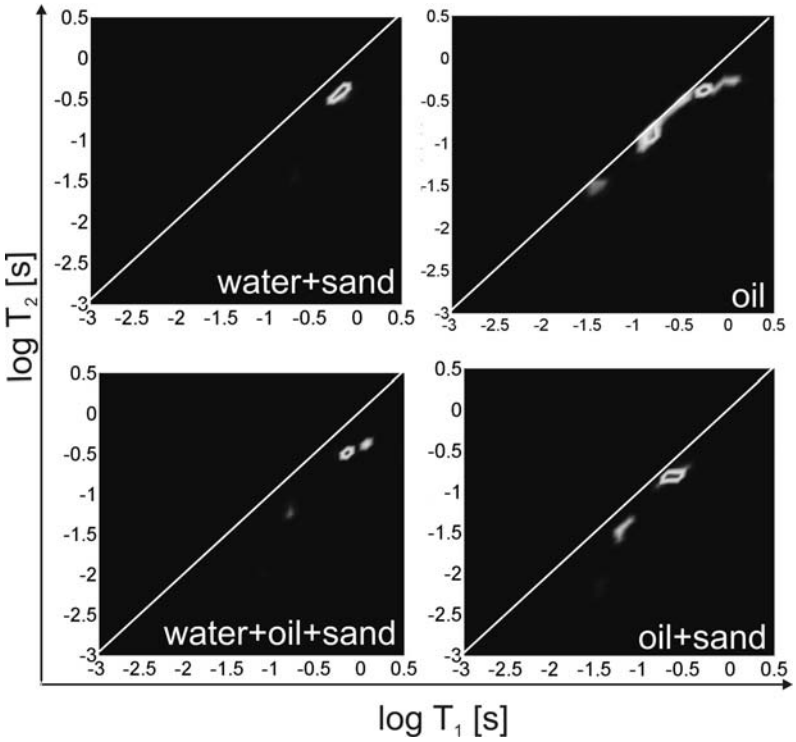

Fig. 4.17 *The T_1-T_2 correlation spectra of sand mixed with water and oil, and for the bulk oil.*

2D spectra for each particular case are presented in Fig 4.17. The spectrum of water mixed with sand shows one peak shifted to shorter relaxation times with T_1=0.7 s and T_2=0.5 s while both these times are about 2 s for bulk water. The spectrum of the bulk oil is wide spread corresponding to different hydrocarbon components. It includes the time range of water in the sand. The spectrum of the sand mixed with oil is discrete with shorter relaxation times. The similar behavior is observed when sand is mixed with both fluids. It is difficult to distinguish between water and oil in the sand comparing these 2D maps because the relaxation times of both fluids are overlapping. It is clear,

however, that 2D diffusion-relaxation correlation experiments have potential to discriminate fluids with distinct effective diffusion coefficients.

4.3. Permeability estimation in the presence of internal gradients from NMR data

The permeability of a porous material depends on the pore volume (porosity), pore shape and topology (tortuosity). It characterizes flow of hydrocarbons in oil and gas reservoirs, and groundwater in aquifers. The NMR estimation of permeability is based on a combination of experimental and theoretical models and relationships. The unit of permeability - the Darcy - has dimensions of area, and from practical considerations in petrophysical applications, permeability can be considered as being proportional to the square of some geometrical size. There are two empirically developed models to predict permeability from porosity most frequently used in well logging: the Coates/Timur model [Coates2, Tim1] and the Mean T_2 model [Kenyon1].

In the Coates (or Free Fluid) model, the size parameter enters implicitly via the $T_{2,\text{cutoff}}$, which determines the ratio of *FFI* to *BVI*, where $FFI = \phi - BVI$. This equation is based on the fact that permeability in clastic reservoirs is related to the irreducible fluid saturation (S_w). Thus, based on numerous core measurements, Coates developed an equation:

$$k_{\text{NMR}} = ((\phi/10)^2(FFI/BVI))^2, \tag{4.3.1}$$

BVI and FFI correlate with the irreducible fluid saturation (ϕS_w) and ($\phi(1 - S_w)$), respectively. This model requires estimation of the proportion of free and bound water that is usually done by means of a centrifuge.

In the Mean T_2 (or SDR, Schlumberger Dall Reaserch) model, the size parameter enters through the geometrical mean of the transverse relaxation spectra. This model is based on the fact that the relaxation times depend on the surface-to-volume ratio of the rock and is related to permeability. The Mean T_2 model describes an empirical relationship between NMR porosity and the logarithmic mean value of the T_2 relaxation time distribution, which was checked for hundreds of different core samples. Kenyon described this relationship as

$$k_{\text{NMR}} = a\, T^2_{2,\text{LM}} \phi^4, \tag{4.3.2}$$

where $T_{2,\mathrm{LM}}$ is the logarithmic mean value of the transverse relaxation time distribution, ϕ is porosity (we used porosity calculated from NMR data), and a is the factor which depends on the surface relaxivity. The constant a is an empirical value that depends not only on the lithology but also on paramagnetic and ferromagnetic impurities. This quantity differs very much from one formation to another. $T_{2,\mathrm{LM}}$ is calculated according to:

$$\log\{T_{2,\mathrm{LM}}\} = \frac{\sum_i f_i \log\{T_{2i}\}}{\sum_i f_i}, \tag{4.3.2a}$$

where the T_2 distribution consists of several components with amplitudes f_i and relaxation times T_{2i}.

The analysis presented in this study is based on the Mean T_2 Model because it is relatively simple, does not require any discrimination between free and bound water and works better than the Coats model for rocks with low permeability. The permeability values are calculated according Eq. (4.3.2) with the constant a equal to 4.6 as it is recommended for the sandstones and verified with independently measured permeability values by the gas flow method. A correlation is presented in Fig 4.18. As expected, the permeability values of Allermöhe sandstones (white circles) are underestimated except for one (AC2) with very low permeability. The other data points (black circles) which belong to sandstones from different formations lie along the diagonal $k_{\mathrm{NMR}} = k_{\mathrm{GAS}}$.

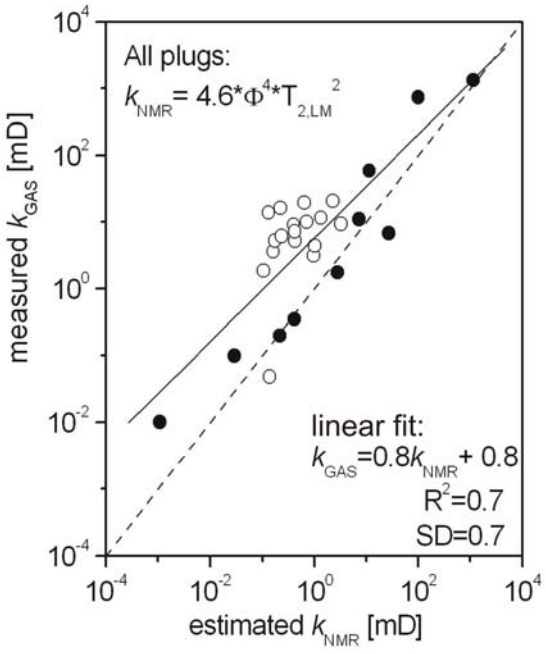

Fig. 4.18 *Correlation of the permeability values (k_{NMR}) found from NMR measurements with (k_{GAS}) measured by the gas flow method, where white circles are Allermöhe sandstones and black ones are plugs from different formations. The diagonal (dashed line) corresponds to k_{NMR}= k_{GAS} plotted for reference. The solid line is a linear fit of the all data points.*

It is obvious that the main error in the calculation of permeability values from NMR data comes from the logarithmic mean value of the transverse relaxation time. It was shown already that NMR determines porosity values with high accuracy. This study used the fact that the effect of the diffusion in internal gradients on T_2 distribution can be quantified by T_1/T_2 ratio estimated from the 2D $T_1 - T_2$ correlation experiments. To overcome the influence of diffusion and to minimize its effect on the permeability estimation of sandstones with high micro porosity and a T_1/T_2 ratio higher than 3, it is proposed in this work to calculate the $T_{2LM,B}$ value from the part of the transverse relaxation distribution above the cutoff of 33 ms appropriate for producible water. Therefore, permeability is calculated as

$$k_{NMR} = 4.6 T_{2LM,B}^2 \phi^4, \tag{4.3.3}$$

where the $T_{2LM,B}$ is the logarithmic mean value corresponding to the bulk water:

$$\log\{T_{2LMIB}\} = \frac{\sum_i f_i \log\{T_{2i}\}}{\sum_i f_i} \qquad \text{for all } T_{2i} > 33 \text{ ms.} \qquad (4.3.3a)$$

Figure 4.19 presents the permeability values of Allermöhe sandstones (white points) and plugs from different formations (black points) with the *free water* correction applied if T_1/T_2 is higher than 3 and according to the standard $T_{2,LM}$ value if T_1/T_2 is less than 3 (Table 1, Appendix B). After correction, all data points of the Allermöhe sandstones are shifted to the diagonal. A noticeable shift of the data points is observed for the samples with the main contribution from bound water into the relaxation process, i.e. for the sandstones with low permeability and high micro porosity, a large amount of small pores, and a high T_1/T_2 ratio (Fig. 4.19). An example is AC9 with a 9.4% porosity, $T_{2,LM}$ = 35 ms, and $T_{2LM,B}$ = 119 ms that yields permeability values k_{NMR} = 0.4 mD and the corrected value of 5 mD, respectively, while the k_{GAS} = 5.26 mD and its T_1/T_2 ratio varies from 6 up to 24. For example, AC7 has k_{GAS}=3.59 mD and k_{NMR}=0.2 mD, which was found according to the Kenyon equation and a corrected value is 3.4 mD with varied T_1/T_2 (Fig. 4.20). The VESF plug from another formation has k_{GAS}=735 mD, k_{NMR}=99 mD and a corrected value of 170 mD, its 2D T_1-T_2 map gives a high constant T_1/T_2 ratio.

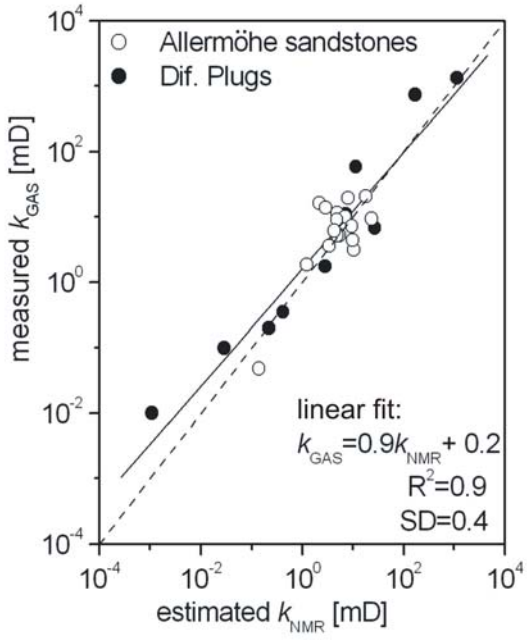

Fig. 4.19 *Obtained final correlation of the permeability value for different sandstones. If the sandstone is characterized by a high T_1/T_2 ratio, the 'free water' correction improves the permeability estimation, which is very obvious for Allermöhe core plugs.*

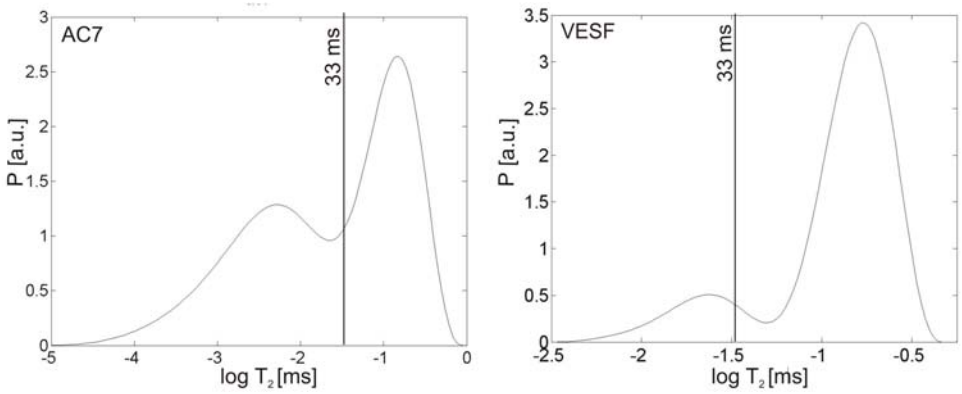

Fig. 4.20 *T_2 distribution for AC7 (T_1/T_2 varies from 3 up to 16, k_{GAS}=3.59 mD) and for VESF (T_1/T_2 is constant and equals 5, k_{GAS}=735 mD)*

A limit of the Kenyon equation has been found in the study. This equation does not work for sandstones either with permeability values less than 1 mD or when low permeability is combined with a high and strongly varying T_1/T_2 ratio. Examples of such T_2 distributions are presented in (Fig 4.21) indicating mainly only bound water. Therefore, the *free water* correction cannot be applied for such distributions.

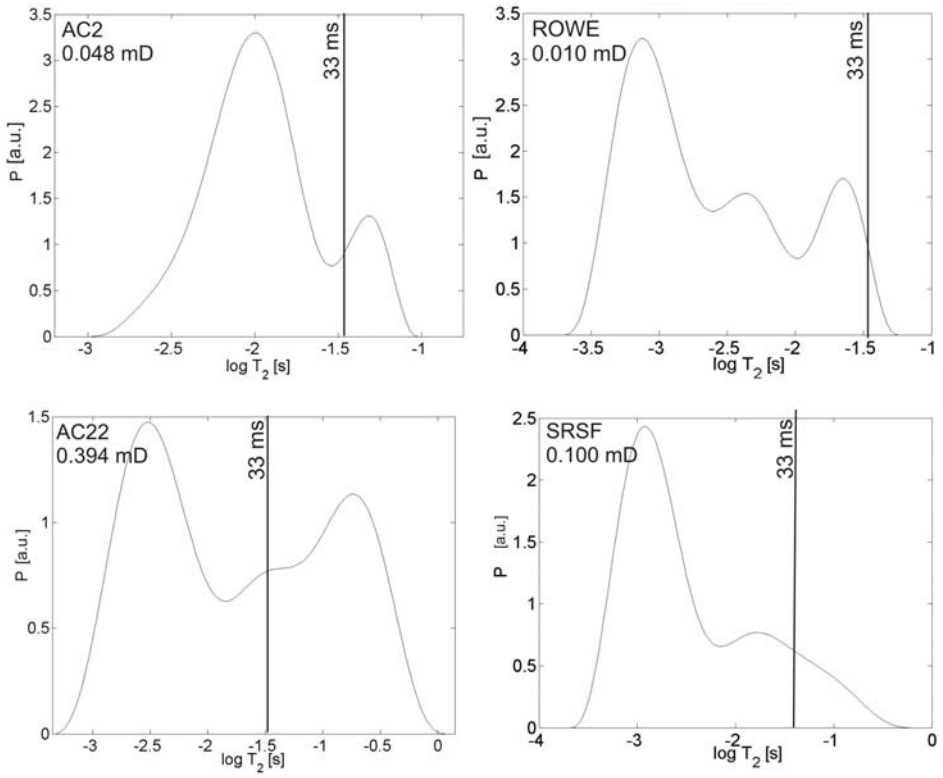

Fig. 4.21 *T_2 distributions of sandstones with permeability less than 1 mD. The Kenyon equation does not work.*

The study conducted on different cylindrical sandstone plugs with 2 cm diameter proves that 1D relaxation measurements with the Halbach scanner at 9.6 MHz can be used for estimation of permeability based on the Kenyon equation involving the *free water* correction with respect to the diffusion influence, which can be quantified by 2D relaxation-relaxation experiments.

4.4. Accuracy of 1D and 2D experiments

2D data maps provide intrinsically more information than the 1D data maps because more experimental parameters are included [Son3, Hür3]. In this study, 1D spectra of T_1 and T_2 are obtained from 2D map by integrating along the appropriate dimensions and comparing with corresponding 1D T_2 distributions from conventional CPMG data measured at the same echo time. An example of such a comparison is presented for AC7 in Fig 4.22. Although the overall T_2 distributions are similar, the peaks obtained from the 2D spectra have more details.

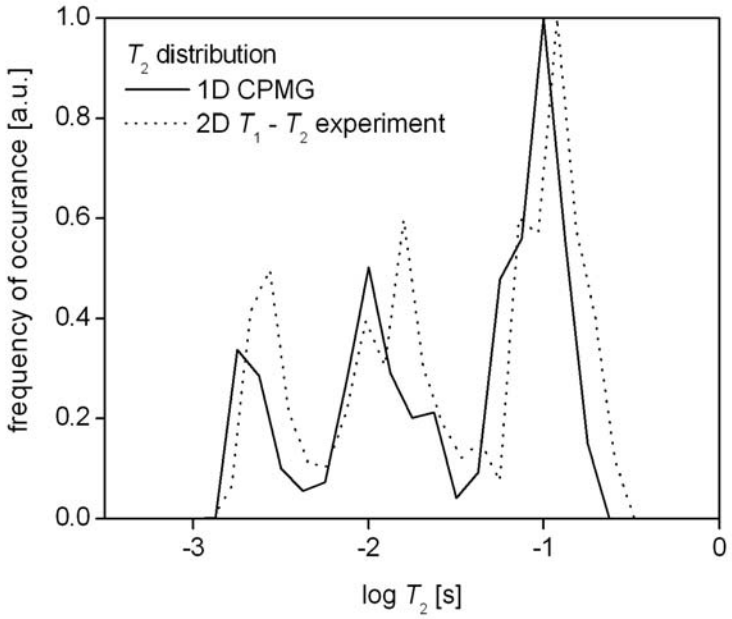

Fig. 4.22. *Comparison of T_2 spectra of AC7 obtained from conventional CPMG and from 2D T_1-T_2 experiments measured at the same echo time of 0.15 ms.*

Thus, if T_2 distributions from conventional CPMG and from 2D T_1-T_2 experiments are used for permeability prediction, results of different accuracy are obtained (Table 2 in Appendix B). At the same time, the accuracy of the permeability values from transverse relaxation can be compared with permeability values calculated from T_1 distributions from 2D spectra since T_1 does not depend on diffusion. Permeability values are calculated with the 'free water' correction from transverse relaxation time distributions of 1D and 2D experiments for the same formation of Allermöhe sandstones. The transverse relaxation measurements on the sandstones of this formation are strongly influenced by diffusion. The 'free water' correction decreases the influence of diffusion on transverse relaxation as it is much stronger in smaller pores than in larger ones.

The permeability values of the Allermöhe sandstones were calculated from 1D and 2D experiments using Eq. 4.3.3, and the factors *a* were estimated from the cross plot of k_{gas} versus $\Phi^4 T^2_{2LM,B}$ instead of using the recommended value of 4.6. Figure 4.23a shows the dependence of gas permeability k_{GAS} on $\Phi^4 T^2_{2LM,B}$ where $T_{2LM,B}$ is estimated from conventional CPMG experiments. The gray point indicates the sandstone AC5 which is excluded from the calculation as an outlier (and which requires a further geophysical analysis). A linear fit of these data gives a constant *a* of 5.1 instead of 4.6.

The same coefficient is much higher (about 50) when the logarithmic mean T_2 value is calculated from the complete distribution. Indeed, it has been reported in the literature that this coefficient can vary to up to 100 for different formations [Dar1]. Therefore, the high values of the coefficient *a* identify the presence of strong internal gradients.

Nevertheless, the permeability values of the Allermöhe sandstones estimated from conventional CPMG data cover the same range as k_{GAS} and differ from it by less than a factor of 3 (Fig. 4.23b).

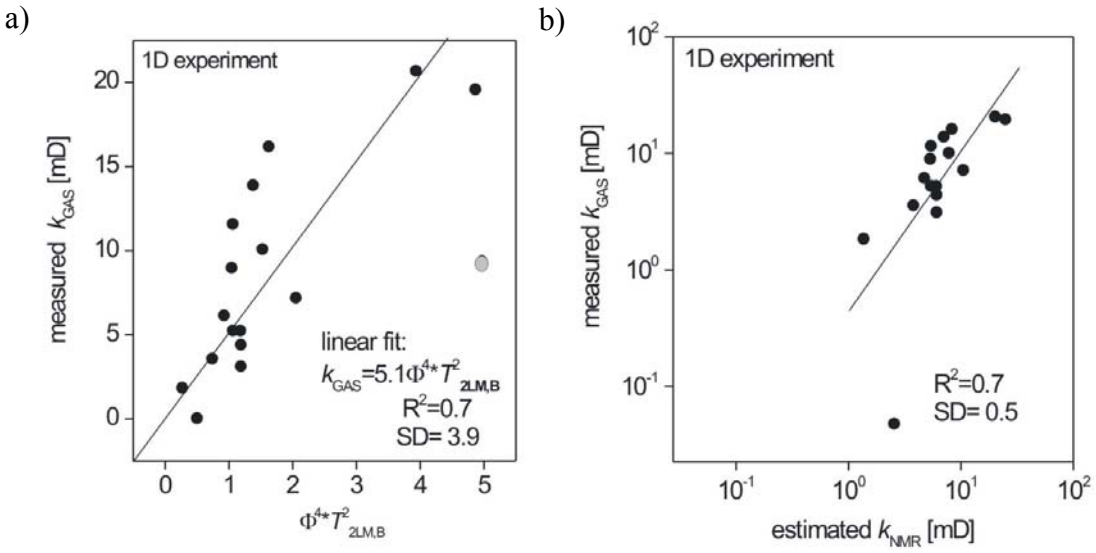

Fig 4.23**.** *a) Estimation of the factor a of the Kenyon equation with the 'free water' correction (Eq. 4.3.3) for the Allermöhe sandstones from 1D CPMG experiments. b) Correlation of permeability values for the Allermöhe sandstones from 1D CPMG and gas flow data. The solid line is a linear fit.*

The same calculations were performed for transverse relaxation time distributions obtained from 2D T_1-T_2 correlation experiments. The cutoff for free water was used to estimate $T_{2LM,B\ INT}$ and, afterwards, the factor *a* was found from the plot of permeability k_{GAS} versus $\Phi^4 T^2_{2LM,B\ INT}$. The results are presented in Fig. 4.24. The scatter is slightly less compared to 1D experiments (Fig. 4.23a). The permeability values obtained from the integrated transverse relaxation distributions correlate better with permeability values from the gas flow method with R^2=0.8 (Fig. 4.24b).

The permeability values estimated from the longitudinal relaxation time distributions from the same 2D T_1-T_2 correlation experiments which are not influenced by diffusion demonstrate the best correlation with gas flow method with R^2=0.9 (Fig. 4.25).

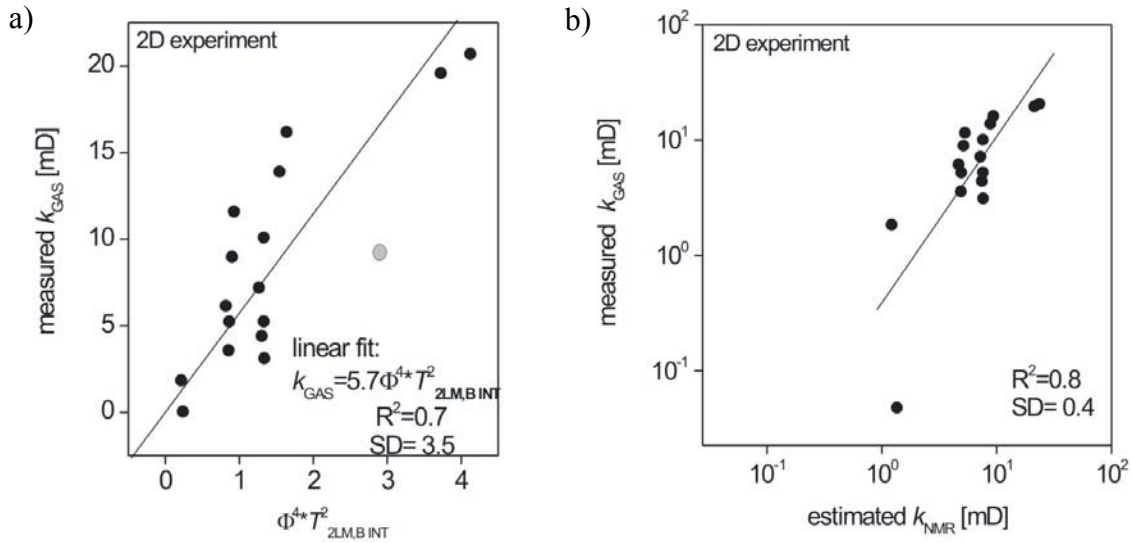

Fig. 4.24 *a) Estimation of the constant a for the Allermöhe sandstones from 2D transverse relaxation using the logarithmic mean values $T_{2LM,B\,INT}$. b) Corresponding permeability values obtained from 2D T_1-T_2 correlation experiments.*

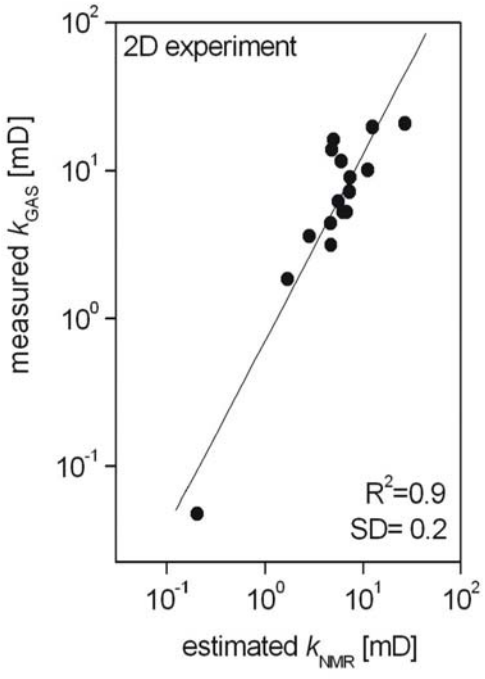

Fig. 4.25 *Correlation of permeability values for Allermöhe sandstones received from the longitudinal relaxation time distribution in 2D $T_1 - T_2$ correlation experiments. The solid line is a linear fit of the data.*

In conclusion, the coefficients *a* obtained from 2D experiments (5.7) and conventional CPMG data (5.1) provided with the Halbach scanner are comparable to the recommended value (4.6). The correlation coefficient R^2 (ideally R^2=1) increases from 0.7 to 0.9 and the standard deviation SD (ideally SD=0) of the fit changes from 0.5 to 0.2 for conventional CPMG and for longitudinal relaxation, respectively. An obvious improvement in the permeability prediction has been demonstrated, when cutoff for free water was applied to transverse relaxation time distributions. The accuracy of 2D relaxation correlation experiments is higher than the accuracy of conventional CPMG data and after a 'free water' correction it is comparable to that of longitudinal relaxation experiments. This is explained by the fact that more experiments are involved and the transverse relaxation distribution is obtained by averaging over a number of T_2 experiments.

Therefore, mobile NMR can be used to estimate permeability without involving any other independent methods even in the presence of internal gradients if the T_1/T_2 ratio is known. Thus, the procedure to estimate permeability can be the following. During drilling a few samples should be checked for their T_1/T_2 ratios, and permeability can be estimated according to the Kenyon equation with or without correction of $T_{2,LM}$ for the whole formation.

4.5. Conclusions

The transverse relaxation process in the presence of diffusion in internal gradients in sediments with high micro porosity and low permeability was studied with the mobile NMR core scanner. When water-saturated sediments with low magnetic susceptibility are placed in the homogeneous part of the magnetic field of the Halbach scanner, a spatially varying field with its associated gradients appears naturally inside the porous medium. The influence of internal gradients is associated with the properties of a sample such as permeability, pore size distribution, and porosity. To study the influence of diffusion in internal gradients, cylindrical plugs of different sandstones with 2 cm diameter were tested by conventional CPMG and 2D correlation relaxation experiments with the Halbach scanner.

The T_2 distributions obtained from CPMG and from 2D T_1-T_2 correlation experiments are comparable but the 2D spectra and the integrated transverse and

longitudinal relaxation time distributions provide more details and higher accuracy. In both 1D and 2D experiments, free and bound water are graphically resolved corresponding to porosity and permeability of a sample. The diffusion influence in internal gradients in water-saturated sediments with particular structures can be estimated by 2D T_1 –T_2 correlation experiments according to the T_1/T_2 ratio. Measurements with the conventional CPMG sequence at different echo times are characterized by different magnitudes of the diffusion effect on transverse relaxation but cannot quantify it for a particular structure.

The obtained 2D T_1-T_2 correlation spectra were used to calculate distinct T_1/T_2 ratios for monitoring the diffusion effect and for the identification of different fluids. The analysis confirmed that the lower T_1/T_2 ratio for the long T_1 and T_2 components is the result of the free water contribution. The reason for a high and in some cases not constant T_1/T_2 ratio is due to a combination of the fast surface relaxation and the diffusion in the internal gradients of small pores. The amount of micro porosity of sandstones with low permeability (< 20 mD) determines the influence of diffusion in internal gradients on the T_2 distribution, for example, for Allermöhe sandstones.

Two-dimensional T_1-T_2 correlation experiments conducted on sandstones with low magnetic susceptibility, high permeability (>500 mD) and macro porosity at a short echo time of 0.06 ms showed that the influence of diffusion is negligible and the corresponding 2D spectra show signal closely parallel to the diagonal with T_1=T_2, meaning that all water molecules in the rock essentially have an identical T_1/T_2 ratio. Hence, there is a single surface relaxation for all the variation of local surface-to-volume ratios, or pore sizes.

At the same, it has been shown that the Halbach core scanner is a lightweight mobile NMR tool suitable for nondestructive geophysical applications [Anf2, Blü4], i.e. measurements of porosity, pore-size distributions and permeability in water-saturated cylindrical drill cores and plugs with different diameters. The Halbach core scanner is calibrated for permeability prediction using the Mean T_2 model. The *free water* correction has to be introduced for sandstones if the T_1/T_2 ratio is higher than 3. The permeability values from NMR data differ by a factor of 4 or less when compared to values derived by the gas flow method.

Some limits of the Halbach scanner were found in this study. The 2D experiments failed on the sandstones with fairly low permeability less than 0.5 mD and porosity less

than 3 %. Moreover, the Mean T_2 model does not work for permeabilities lower than 1 mD.

The methodology of the 2D T_1-T_2 correlation experiments with the Halbach sensor was established with all steps from the beginning: improvement of the rf circuit for measurements at shorter echo time, development of the pulse sequence and identification of optimal experimental parameters, data processing, and analysis of the correlation spectra. The 2D maps were obtained by commercial '2D Laplace Inversion' software (Magritek Ltd, New Zealand, 2004). Sample characteristics such as porosity, permeability, and integrated longitudinal and transverse distributions, and their logarithmic mean values were calculated by software developed in this work.

5. Restricted diffusion in water-saturated core plugs

Diffusion and self-diffusion are basic mass transport mechanisms which determine the motion, redistribution, accumulations and release of fluids in soils, sediment layers, and rocks. Measurements of the diffusion of water absorbed in the pores are strongly affected by the presence of the solid matrix of the porous medium. Therefore the apparent self-diffusion coefficient $D(\Delta)$ in the pore space depend on the observation time (Δ) due to a restriction of the diffusion path at the pore/grain interface.

This chapter introduces pulsed field gradient (PFG) experiments with the improved Halbach scanner on water-saturated plugs of sediments. The 13-interval pulse sequence with the multi echo detection scheme was implemented to compensate the influence of internal gradients. First the diffusion experiments were performed on bulk water to calibrate the gradients. Then the time-dependence of the diffusion coefficients of water diffusing in the pore space of rocks was measured. First results are presented below.

5.1. PFG experiments with the Halbach scanner

The study was conducted on water-saturated core plugs from natural sedimentary rocks which are characterized by complex micro-geometries and broad distributions of pore sizes. For water molecules in the pore space of a rock, the mean-square displacement is often expressed as an effective diffusion coefficient $D(t)$ [Hür7]:

$$D(t) \equiv \frac{1}{2t}\left\langle [z(t) - z(0)]^2 \right\rangle, \tag{5.1.1}$$

where $(z(t)\text{-}z(0))$ is a displacement of water molecules during the diffusion time t. At short times, the diffusion coefficient D(t) is determined by the surface-to-volume ratio of the pore space, Eq. 5.1.2 [Lat3, Mit1].

$$\frac{D(t)}{D_0} = 1 - \frac{4}{9\sqrt{\pi}}\frac{S}{V}\sqrt{D_0 t} + O(D_0 t). \tag{5.1.2}$$

For long times, $D(t)$ is determined by the tortuosity $\mathcal{T}$ which characterizes the connectivity of the pore space, Eq. 5.1.3.

$$\lim_{t\to\infty}\frac{D(t)}{D_0}=\frac{1}{\mathcal{T}}. \tag{5.1.3}$$

Diffusion measurements by PFG NMR in heterogeneous porous media may contain significant sources of error, for example, the influence by the coupling between applied and internal magnetic field gradients on the attenuation of the NMR signal. The measured diffusivity therefore may not correspond to the actual diffusion coefficient of the probing molecules within the heterogeneous sample [Zho1]. Several pulse sequences applying bipolar magnetic field gradients for diffusion measurements in heterogeneous porous media have been proposed in order to suppress the cross terms between the applied and the internal magnetic field gradients [Lat2, Hür7, Sør1].

In this study, the 13-interval PFG NMR sequence proposed by Cotts [Cot1] was used for the self-diffusion measurements on sandstones. This pulse sequence eliminates, to first order, the effects of internal gradients by applying bipolar gradient pulses separated by 180° pulses. Furthermore, a multi-echo acquisition scheme was implemented to improve the signal-to-noise ratio by adding the echo train generated during the acquisition period [Cas1, Per1, Per2, Rat1] (Fig. 5.1).

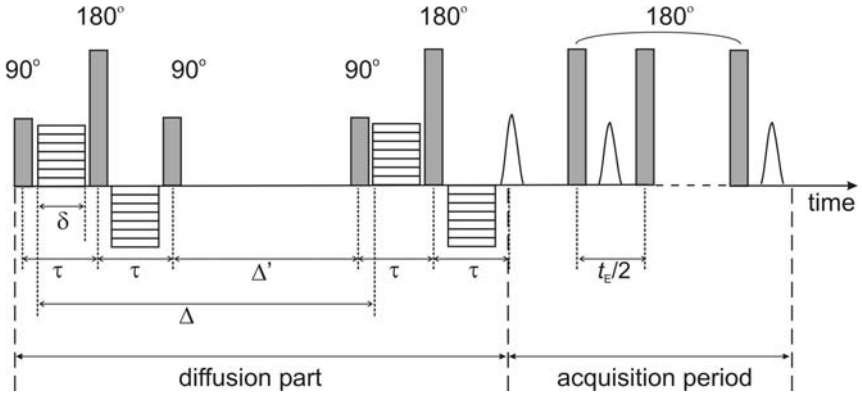

Fig. 5.1 *The 13-interval pulse sequence with a multi-echo detection to improve signal-to-noise ratio*

In the diffusion measurements with the Halbach scanner, the time between the 90° and 180° rf pulses was always set to τ=140 μs, the duration of the bipolar gradient pulses was δ = 100 μs. The measurements were performed at a temperature of T=23° C, where diffusion coefficient of water is $D_0=2.26\cdot10^{-9}$ m^2/s. In these experiments, the dependence of the NMR signal amplitude on the gradient pulse strength G_i was

observed. The attenuation of the NMR signal M(G_i, Δ')/ M_0(G=0, Δ') was calculated according the equation [Vog1]

$$\ln\left(\frac{M(G_i,\Delta')}{M_0(G=0,\Delta')}\right) = -(\gamma 2\delta G_i)^2 D(\Delta')\left(\Delta'+\frac{3}{2}\tau-\frac{1}{6}\delta\right). \qquad (5.1.4)$$

Equation (5.1.3) is valid when the short-gradient-pulse limit is fulfilled (2τ << Δ'). The time dependence of the self-diffusion was studied by changing the evolution time Δ' from 5 ms up to 600 ms on the several water-saturated plugs of sediments.

The calibration curve of the gradient system on bulk water with known diffusion coefficient at the given temperature is presented in Fig. 5.2. The gradient strength G_i varies from 0 up to 0.43 T/m. Furthermore measurements on bulk water were performed at different evolution times. As expected for bulk liquids, the obtained self-diffusion coefficient does not depend on the observation time.

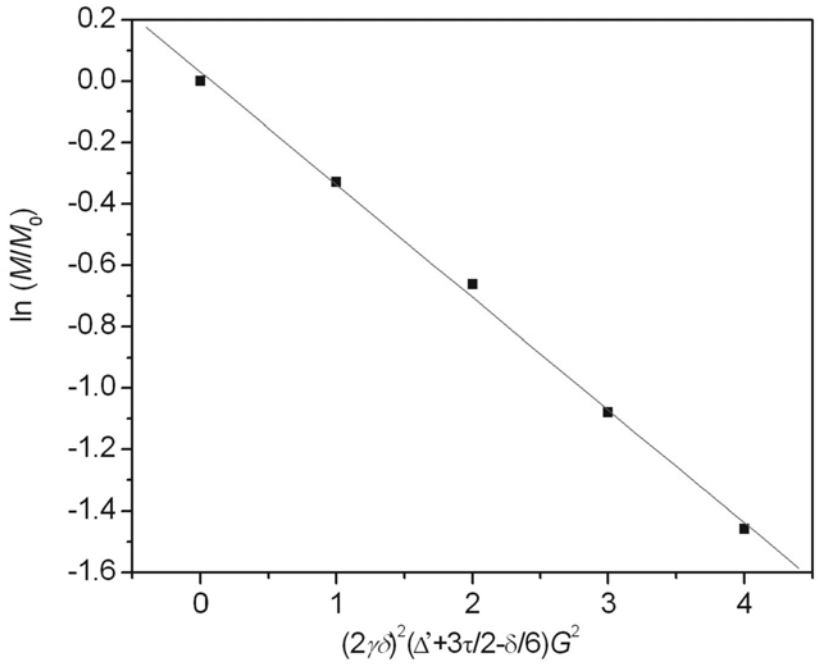

Fig. 5.2 *Calibration of the gradient strength according to the Eq. 5.1.3 with known time intervals and the diffusion coefficient of water.*

The measurements on the water-saturated sediments were performed in the same way as on bulk water, although the samples were characterised by a distribution of longitudinal relaxation times. The exploratory experiments were done on sandstones

with a wide range of T_1 distribution with the main contribution of the relaxation process from the bulk water. T_1 distributions were obtained from 2D T_1- T_2 correlation experiments. For example, the Allermöhe sandstone AC5 has three T_1 maxima ranging from 100 ms up to 1 s (Fig. 5.3). Figure 5.4 shows raw PFG data for this sandstone at different observation times which lead to varying $D(\Delta')/D_0$ ratios depending on the diffusion time Δ'. $D(\Delta')/D_0$ ratios were estimated with the help of linear fits of Eq.5.1.4 for bulk water and for sandstone AC5 measured with the same experimental parameters. The resultant $D(\Delta')/D_0$ values are 0.53, 0.05, and 0.04 for Δ' equal to 50 ms, 100 ms, and 200 ms, respectively.

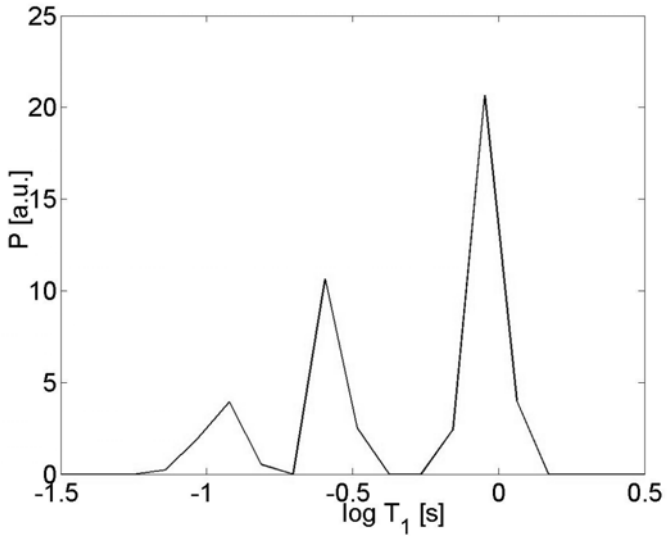

Fig. 5.3 *T_1 distribution of the sandstone AC5*

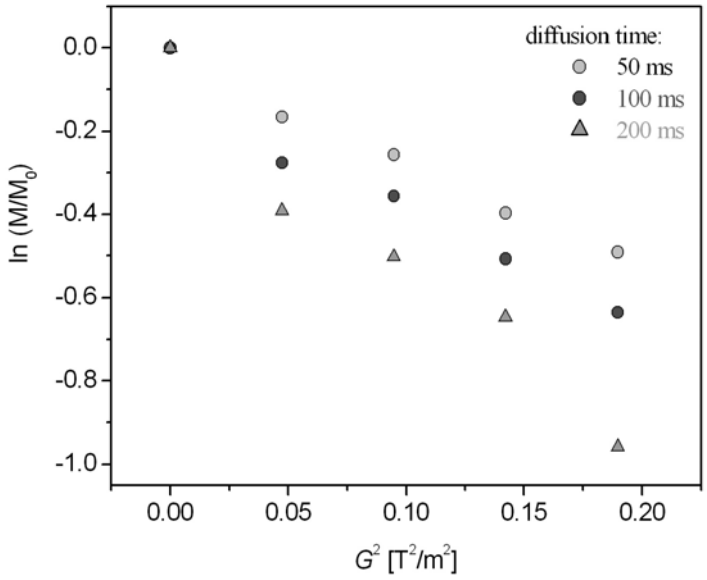

Fig. 5.4 *Typical raw PFG data obtained for a water-saturated plug of sandstone. The diffusion coefficient at each observation time is determined from the slope.*

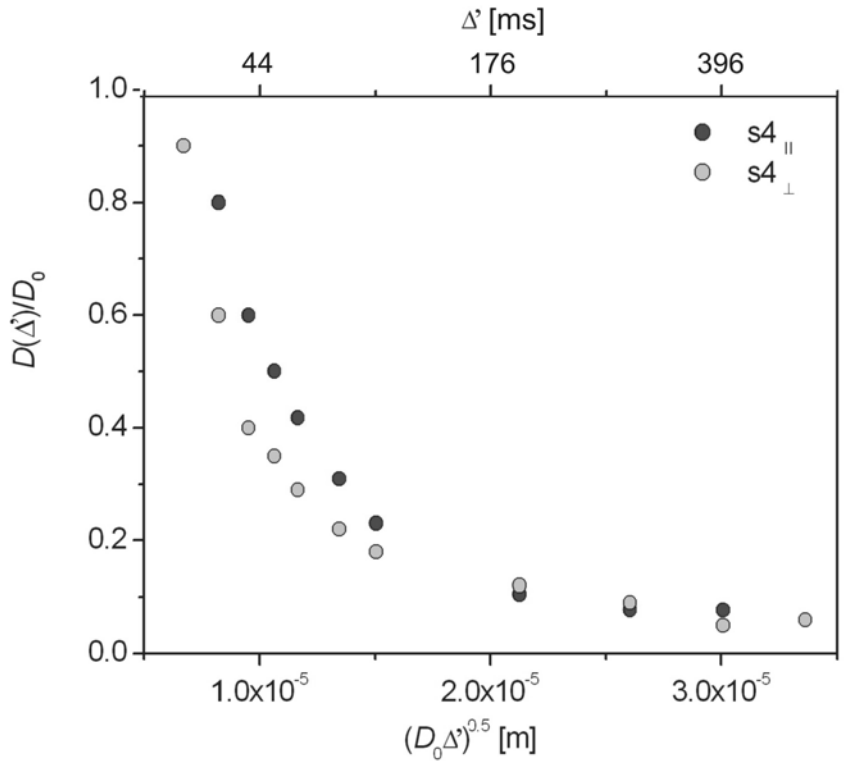

Fig. 5.5 *Normalized diffusion coefficient D(Δ')/D*$_0$ *versus diffusion length* $\sqrt{D_0\,\Delta'}$. *Both plugs belong to the same drill core and are cut in perpendicular and parallel directions to the strata.*

Selected water-saturated plugs cut in perpendicular directions to the strata of the drill core were analyzed to study their anisotropy. For example, Figure 5.5 shows diffusion curves for a pair of plugs $s4_{\perp}$ and $s4_{\parallel}$ which are cut in vertical and parallel direction to the strata of the same drill core, respectively. Sandstone s4 has T_1 relaxation times in the range of 30 ms - 400 ms (Fig. 4.11a). Thus, PFG experiments were performed over a wide range of diffusion times from 20 ms up to 400 ms. It's clearly seen that the water molecules diffuse over longer distance in $s4_{\parallel}$ than in $s4_{\perp}$ at the same evolution time when it is shorter than 200 ms. A significant loss of signal is observed at diffusion times longer than 200 ms. The diffusion curves become identical at about 20 μm of the diffusion length that corresponds to 180 ms of the evolution time and can be explained by a significant influence of T_1 relaxation. Nevertheless, Figure 5.5 shows a different behavior of the diffusion curves of sandstone plugs cut in perpendicular and parallel directions which quantifies some inhomogeneity or anisotropy. Probably this difference in behavior may lead to different values of tortuosity that should be checked on longer diffusion length scales. The distances that can be probed by PFG NMR are limited by $\sqrt{D_0 T_1}$. According to these results, tortuosity that is associated with long diffusion times cannot be estimated realistically for the majority of sediments provided by AG because these samples are characterized by short T_1. It is emphasized that for a successful application of the PFG method for the analysis of sediments the samples should be saturated with another liquid or gas (for example, xenon) with longer T_1. It was proved that usually it is not possible to reach the tortuosity limit using water as a saturating fluid of rocks [Lat2, Lat3, Hür].

To check the properties of the $s4_{\perp}$ and $s4_{\parallel}$ plugs, the 3D proton density images were measured with a high field Bruker DMX 300 spectrometer. In this experiment, the images were recorded with a resolution of 180 μm and a field of view 25 mm × 25 mm. The recording time of one image was several hours. 2D cross-sections of plugs are presented in Fig. 5.6. The regions with less proton density appear darker than those with higher density. Plug $s4_{\perp}$ has a region with low proton density (dark area) while there is roughly equal distribution of the water protons in plug $s4_{\parallel}$. This can explain the difference in diffusion curves probably due to inhomogeneity or anisotropy of the plugs. Unfortunately, the same experiments on the SCD plugs provided by Applied Geophysics for PFG experiments failed because of extremely short values of T_1.

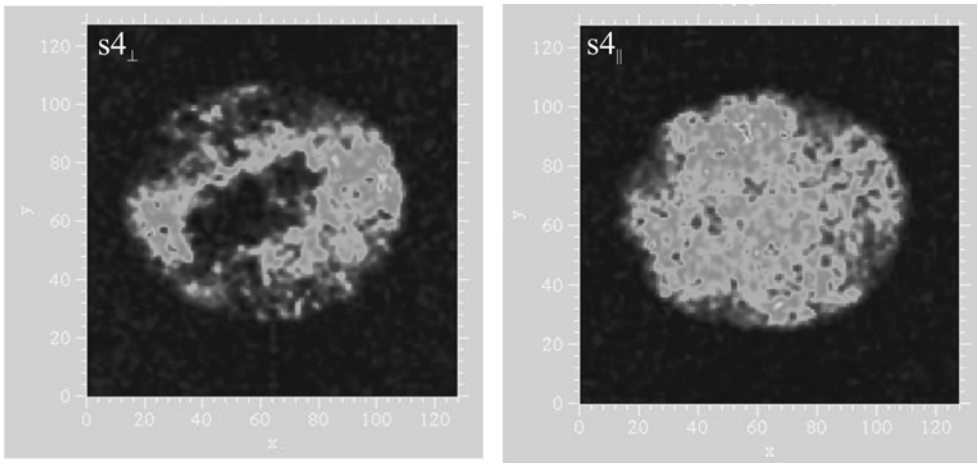

Fig. 5.6 *Images of the* $s4_{\perp}$ *and* $s4_{\parallel}$ *obtained with a high field Bruker DMX* 300 *spectrometer. Probably the difference in the signal distribution comes either from higher inhomogeneity of* $s4_{\perp}$ *compared to* $s4_{\parallel}$ *or from anisotropy.*

5.2. Conclusions

The main intention was to equip the Halbach scanner with the set of gradient coils to provide PFG experiments with mobile NMR. The developed hardware was successfully tested using the 13-interval pulse sequence on bulk water and several water-saturated plugs. The PFG experiment on bulk water showed that the set of gradient coils generates the linear gradient in the region of the rf coil with 24 mm diameter and 12 mm length. PFG experiments with the Halbach scanner on water-saturated plugs are limited by short T_1 values of water molecules in sediments.

6. Summary and Outlook

A lightweight mobile Halbach scanner with sophisticated hardware requirements (larger sensitive volume and higher homogeneity of the magnetic field, different diameters of rf coils and a set of gradient coils) has been developed. The Halbach scanner was successfully tested for different geophysical applications: for fast and non-destructive measurements of porosity in drill cores with diameters up to 60 mm and estimation of permeability in core plugs of 20 mm diameters. Currently it is used by Macromolecular Chemistry Department and Applied Geophysics Institute of RWTH Aachen University in different projects.

A new experimental machine - the NMR on-line core scanner with a sliding Halbach magnet was built and corresponding software was developed. The NMR on-line core scanner can be used for on-line operation on a vessel or drilling platform to measure porosity and pore-size distribution of large-size cylindrical and semi-cylindrical water-saturated drill cores with minimal human interaction and without prior preparation. At this time, our results showed that there is a great potential to develop the NMR on-line core scanner for measurements not only of porosity but also of permeability in long, large-sized IODP drill cores directly after the recovery. Figure 6.1 shows first results of relaxation data processing measured on-line along a core of 6 cm diameter (Fig. 6.1a). The core porosity values corresponding to the marked points were calculated automatically using a modified CPMG program (Fig. 6.1b) while permeability values (Fig. 6.1c), T_2 distributions (Fig. 6.1d) were computed in a standard way. When large-size cores are studied compared to 2 cm diameter plugs the influence of diffusion increases, as the magnetic field of the Halbach scanner becomes more inhomogeneous. Hence, permeability values are underestimated and T_2 distributions are shifted to the shorter relaxation. Nevertheless, bound and free water are clearly resolved. To overcome the influence of diffusion in external gradients of the magnetic field, the time intervals in the pulse sequence for measurements of the transverse magnetization have to be shortened. Since the large cores require larger diameter of the rf coil, the pulse lengths increases requiring higher power. For this purpose, an additional power amplifier can be used.

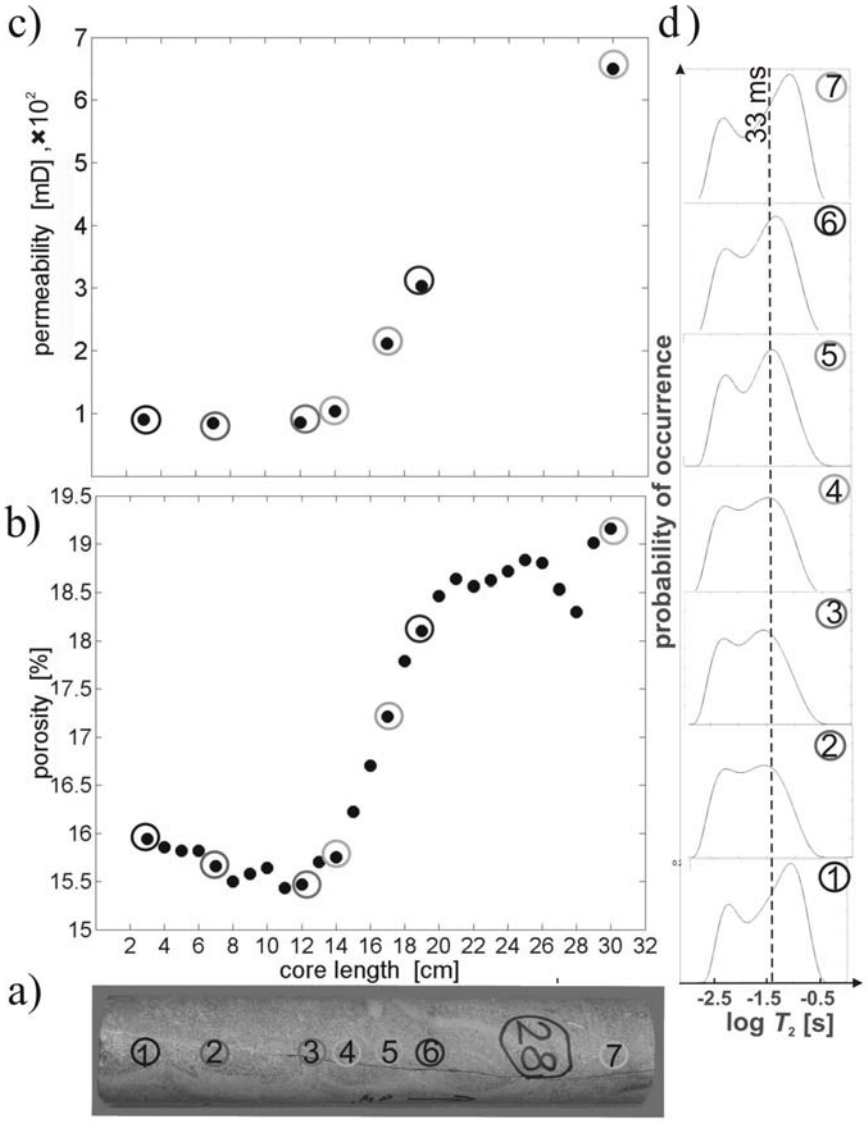

Fig. 6.1 *Example of structural data analysis from NMR measurements of a sandstone. a) Sandstone core, 6 cm in diameter and 32 cm long, mapped automatically with the NMR scanner at 28 points within 20 minutes. b) 1D profile of porosity along the core. c) Permeability estimated from the NMR data at the points marked along the core. d) Relaxation time distributions.*

The standard NMR techniques such as relaxation and diffusion as well as novel 2D correlation studies with the Halbach scanner were successfully performed on fully water-saturated core plugs of different sizes. The most homogeneous part of the static magnetic field of the Halbach scanner was used in the analysis of diffusion. It was shown that diffusion of spins in the internal gradients of porous media leads to an extra attenuation of the transverse magnetization decay especially if the samples are characterized by high micro porosity. The T_1/T_2 ratio obtained from 2D T_1-T_2

correlation experiments was used to quantify the diffusion influence in the internal gradients. It was demonstrated that the internal gradients of porous media strongly affect the relaxation measurements if the T_1/T_2 ratio is high and/or not constant. Additionally, the T_1/T_2 ratio is used in the prediction of the permeability of water-saturated core plugs. It is proposed to use a *free water* correction in the Kenyon equation if the T_1/T_2 ratio is higher than 3. With the *free water* correction, the permeability values have higher accuracy.

Short T_1 relaxation of water molecules in porous media limits the PFG experiments on water-saturated sediments. It is preferable to perform a PFG analysis of diffusion on xenon-saturated sediments to reach the tortuosity limit and to study anisotropy [Mai1, Mai2]. Meanwhile, a further model of the Halbach core scanner was developed suited for drill cores with diameters up to 100 mm or relaxation measurements of different cylindrical objects (Fig. 6.2).

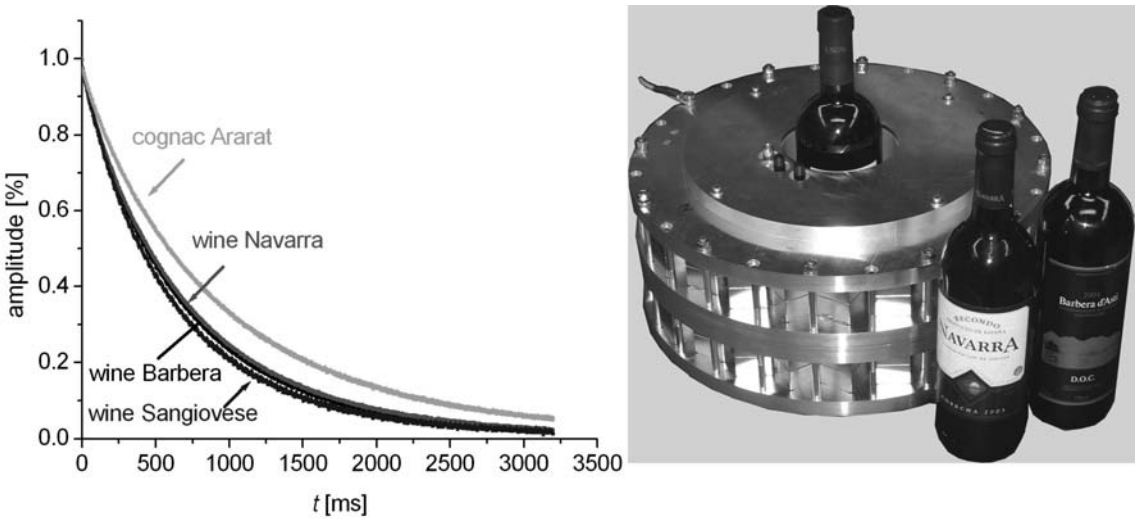

Fig. 6.2 *The CPMG echo envelops measured on bottles of different wines using the Halbach core scanner for drill cores of cylindrical objects with diameters up to 100 mm.*

Appendix A

```
-----------------------------------------------------------------------------------------
        modified CPMG Sequence for a Bruker minispec
-----------------------------------------------------------------------------------------
program setup();
par;
  dbw   (1000.000000);
  abw   ("narrow");
  off_comp("on");
  det_mode("complex");
  dig_res("fast");
endpar;
return(TRUE);
program measure();

#Definition of variables#
real pl,att1,att2,acq,frq, tau0,pts,length, step,a,b,c,total_step;
int ph90[20],ph18[20],phrc[20],ns;
int count,count2,echoes,sample_points,i, count_step, RG;
char text[256], name[64], name0[64];
real x_array[65536],y_array[65536],z_array[65536];
real m_array[65536],t_array[65536];
real points,result[5],error[5],mean1;
int n,order,show,time,korr,l1,maxj;
int l,j,k;
real amp,amp_old,save_amp[65536];
int save_time[65536];
real Mh20,RG_h2o,porosity[16384],d_h2o, d_core, k_por;

Mh20=82.7;    RG_h2o=55;   d_h2o=64;

#Definition of pulse phases#
```

```
ph90[ 0]      =   0;   ph18[ 0]      =  90;  phrc[ 0]      =   0;
ph90[ 1]      =  90;   ph18[ 1]      = 180;  phrc[ 1]      =  90;
ph90[ 2]      = 180;   ph18[ 2]      = 270;  phrc[ 2]      = 180;
ph90[ 3]      = 270;   ph18[ 3]      =   0;  phrc[ 3]      = 270;
ph90[ 4]      =   0;   ph18[ 4]      = 270;  phrc[ 4]      =   0;
ph90[ 5]      =  90;   ph18[ 5]      =   0;  phrc[ 5]      =  90;
ph90[ 6]      = 180;   ph18[ 6]      =  90;  phrc[ 6]      = 180;
ph90[ 7]      = 270;   ph18[ 7]      = 180;  phrc[ 7]      = 270;
ph90[8]=REDO;       ph18[8]=REDO;       phrc[8]=REDO;

# Input Routine #
set_input("Recycling delay [s] (real)",get_rd);
set_input("Larmor frequency [MHz] (real)",get_nmr_freq);
set_input("Receiver Gain (integer)",get_gain);
set_input("Scans (integer), x*8",get_scans);
get_input("Experiment Settings");
if( ESC or CANCEL) goto ende; endif;

par;
 rd(ator(tst_input(0)));
 nmr_freq(ator(tst_input(1)));
 gain(atoi(tst_input(2)));
 scans(atoi(tst_input(3)));
endpar;

ns=atoi(tst_input(3));
RG=atoi(tst_input(2))
scans (ns);
goto check1; label back1;    # check for scans = x * 8 for complete phase-cycling #

set_input("Pulse length [us] (real)",6);
set_input("Pulse attenuation [dB] (real)",5);
set_input("Echo time TE [ms] (real)",0.1);
set_input("No. of echoes (integer)",7000);
```

```
get_input("Experiment Settings");
if( ESC or CANCEL) goto ende; endif;

pl=ator(tst_input(0));
att1=ator(tst_input(1));                    # Pulse attenuation for preparation pulse #
att2=att1-5;                                # Pulse attenuation for refocusing pulse #
tau0=0.5*ator(tst_input(2));                        # Echo time /2 = Pulse distance   #
echoes=ator(tst_input(3));

set_input("core length [cm] (real)",12.0);
set_input("step [cm] (real)",3.0);
set_input("diameter of a core [mm] (real)",64.0);
get_input("Core's parameters");
if( ESC or CANCEL) goto ende; endif;

length=ator(tst_input(0));
step=ator(tst_input(1));
d_core=ator(tst_input(2));

k_por=Mh20*d_core*d_core*pow(10.0 , 0.05*(RG-RG_h2o))/pow(d_h2o,2);
k_por=1/k_por;

if ( tau0 - get("RDT") <= 0.0 )
  print_line(RESULTBOX," ");
  print_line(RESULTBOX,"---- Echo time < RDT ----");
  print_line(RESULTBOX," ");
  goto ende;
endif;

pointer fnameP;
fnameP = input_text( "File Name for Output", "C:\core1\core1_1.dat" );
if( ESC or CANCEL) goto ende; endif;
strcpy( name, fnameP );
file_name( ASCII_FILE, name );
```

```
acq= 0.003;              # acquisition time, change this depending on echo broadness#
pts   = 1.0;                        # Factor for acquisiton, 1.0 means 1 point per 1 µs #
 goto parameterausgabe; label back0;

if (echoes*acq*pts*1000>61840.)
        print_line(RESULTBOX,"");
        print_line(RESULTBOX,"Too much digital points!");
        print_line(RESULTBOX,"Reduce no. of echoes or");
        print_line(RESULTBOX,"acq-Time or pts/echo !!!");
        print_line(RESULTBOX,"");
        goto ende;
endif;
 signal_display_type("LINES");

# number of scans#
a=length/step;
b=round(a);
c=abs(a-b);

if (c==0)
total_step=b;
else
total_step=b+1;
endif;

count_step=0;

while (count_step<total_step);
 par; scans (ns);endpar;

pulses;
 ssp(pl,ph90,att1);
 sd(tau0-pl/1000);
```

```
 ploop (echoes)
  ssp(pl,ph18,att2);
  sd(tau0-acq/2-pl/2000+0.0032);
  adi(acq,acq*pts*1000,phrc);
  sd(tau0-acq/2-pl/2000-0.0032);
 endploop;
sd(0.06);
endpulses;

measure;
if        ( ERROR or ESC or CANCEL ) return( TRUE ); endif;

  sig_abscissa(-1,-1,x_array); # time axis #
  sig_ordinate(-1,-1,y_array); # REAL data #
  sig_swap;
  sig_ordinate(-1,-1,z_array);  # IMAGINARY data #
  points = sig_points(-1,-1);
   i=0;
   while(i<points)
     m_array[i]   =   ((y_array[i]*y_array[i])   +   (z_array[i]*z_array[i]))^0.5;   #   build
magnitude #
     i=i+1;
   endwhile;
replace_signal(x_array,m_array,points);
  sample_points=round(points/echoes);
  print_line(RESULTBOX,sample_points);
   k=0;

while(k<echoes)
  mean1=0;
  j=0 ;
   while(j<sample_points)
    mean1=mean1+m_array[j+k*(sample_points-1)];
    j=j+1;
```

```
  endwhile;
  save_amp[k]=round(100*mean1/3.0)/100;
  t_array[k] = round(x_array[k*sample_points+1]*100)/100;
  print_line(ASCII_FILE,t_array[k],"    ",save_amp[k]);
 k=k+1;
endwhile;
 print_line (RESULTBOX, "porosity in <##.#> point",count_step+1,"=
<##.#>%",100*round(k_por*save_amp[2]));
signal_display_type("CIRCLES");
 replace_signal(t_array,save_amp,k);

korr = 0;
l=0;
while(l < k-korr)
 t_array[l] = t_array[l+korr];
 save_amp[l] = save_amp[l+korr];
 l= l +1;
endwhile;

# Activating the Motoware program#
label motoware;
par;  scans (1); endpar;
pulses;
sd(500)
st ( TRIGGER_ON, 6 );
st(5,0);
st ( TRIGGER_OFF, 6);
sd(7000);
count_step=count_step+1;

if (count_step=total_step)
sd (7000);
st ( TRIGGER_ON, 5 );
st(5,0);
```

```
st ( TRIGGER_OFF, 5);
endif;

endpulses;
measure;
endwhile;

print_line(MESSAGEBOX);
print_line(CONFIRMBOX,"Measure Again ?");
if ( ESC or CANCEL) goto ende; endif;
print_line( MESSAGEBOX, "CPMG Sequence (complex, 8 phases)    measuring...");

label ende;
return( TRUE );

# MAIN PROGRAM FINISHED #
label parameterausgabe;
print_line(RESULTBOX_TITLE,"CPMG, complex, 8 phases ");
print_line(RESULTBOX,"recycle delay:     ",get_rd," s");
print_line(RESULTBOX,"scans:             ",get_scans);
print_line(RESULTBOX,"frequency:         ",get_nmr_freq," MHz");
print_line(RESULTBOX,"receiver gain:     ",get_gain," dB");
print_line(RESULTBOX,"primary pulse:     ",pl," us (",att1," dB)");
print_line(RESULTBOX,"refocusing pulse:  ",pl," us (",att2," dB)");
print_line(RESULTBOX,"echo time (TE):    ",2*tau0," ms");
print_line(RESULTBOX,"no. of echoes:     ",echoes);
print_line(RESULTBOX,"acq-time per echo: ",acq*1000," us");
print_line(RESULTBOX,"points per echo:   ",acq*1000*pts);
print_line(RESULTBOX,"total dig. pts:    ",acq*1000*pts*echoes);
print_line(RESULTBOX,"File: ", name );
print_line(MESSAGEBOX,"CPMG Sequence (complex, 8 phases)");
print_line(ASCII_FILE,"CPMG, complex, 8 phases ");
print_line(ASCII_FILE,"recycle delay:     ",get_rd," s");
print_line(ASCII_FILE,"scans:             ",get_scans);
```

```
print_line(ASCII_FILE,"frequency:         ",get_nmr_freq," MHz");
print_line(ASCII_FILE,"receiver gain:     ",get_gain," dB");
print_line(ASCII_FILE,"primary pulse:     ",pl," us (",att1," dB)");
print_line(ASCII_FILE,"refocusing pulse:  ",pl," us (",att2," dB)");
print_line(ASCII_FILE,"echo time (TE):    ",2*tau0," ms");
print_line(ASCII_FILE,"no. of echoes:     ",echoes);
print_line(ASCII_FILE,"acq-time per echo: ",acq*1000," us");
print_line(ASCII_FILE,"points per echo:   ",acq*1000*pts);
print_line(ASCII_FILE,"total dig. pts:    ",acq*1000*pts*echoes);
print_line(ASCII_FILE,"TE/ms    Int/%");
goto back0;

label check1;         # check for correct number of scans for a complete phase cycling #
# print_line(RESULTBOX,get_scans,"  ",round(get_scans/8)*8);#
if (get_scans <> round(get_scans/8)*8 )
        print_line(CONFIRMBOX,"Please enter a scan number x*8.");
        return( TRUE );
endif;
goto back1;
```

```
---------------------------------------------
        Motoware program
---------------------------------------------

son=1          % enable the servo driver
vm=100         % maximum velocity
ac=50          % accelaration
vs=10          % start rate
pr=1600        % pulses per revollution
con=6400       % specifies the number of pulses per well-known unit - length, volume
NSTART=7       % Set input 7 as start input; command enables an interrupt feature that
will detect a start signal at the same moment it occurs
ap=0           % actual position

   IF IN1=1
   :LOOP sr=1                  % Move relative 1000 pulses forward
     wait rs=0                 % wait for motor to stop
     J:LOOP

   IF IN2=1;
   sr=-total_step*1            % move motor to the initial position
   wait rs=0                   % wait for motor to stop
```

Appendix B

Table 1. Estimation of permeability according to the Kenyon equation ($\boldsymbol{k_{NMR}}$) with the *free water correction* (k_{NMR} corrected).

Core plug	T_1/T_2	k_{NMR}, [mD] $4.6 \cdot \Phi^4 \cdot T_{2,LM}^2$	k_{NMR} corrected, [mD] $4.6 \cdot \Phi^4 \cdot T_{2LM,B}^2$	k_{GAS}, [mD]
BASF	1.2 ~ 2	0.3		0.35
BBSF	2	1129.00		1324
BHSF	3 ~ 25	$4.00 \cdot 10^{-6}$		0.01
COF	3	12		59.2
IBSF	2 ~ 4	0.2		0.2
OBKI	3	7		11
ROWE	3 ~ 10	0.001		0.01
SASF	3	3		1.75
SRSF	4 ~ 10	0.03		0.1
VESF	5	99	170	735
ZUSF	1.3 ~ 2	27		6.78
AC2	4.5 ~ 48	0.14	-	0.048
AC4	3.6 ~ 37	1.3	5	11.6
AC5	4.7 ~ 16	4	23	9.34
AC6	6 ~ 15	0.1	1	1.85
AC7	3 ~ 16	0.2	3.4	3.59
AC8	6 ~ 30	0.2	5	5.25
AC9	5.9 ~ 24	0.4	5	5.26
AC10	4.6 ~ 29	2.0	18	20.7
AC12	4 ~ 9	0.9	10	3.13
AC13	4 ~ 24	1.0	10	4.42
AC14	5 ~ 30	1	7	10.1
AC15	5 ~ 7	1	8	19.6
AC16	6.5 ~25.5	0.4	5	8.99
AC17	5.5 ~ 43	0.2	2	16.2
AC18	6 ~ 33	0.2	4	6.16
AC19	5 ~ 25.5	0.13	3	13.9
AC20	5.5 ~ 21	0.3	9	7.2

Table 2. Comparison of permeability values of Allermöhe sandstones obtained from transverse relaxation time distribution from conventional CPMG and from 2D T_1-T_2 experiments after a *free water* correction and from longitudinal relaxation time distribution from 2D T_1-T_2 experiments.

Core plug	CPMG	2D T_1-T_2 experiment		k_{GAS}, [mD]
	k_{NMR} via $5.1 \cdot \Phi^4 \cdot T^2_{2LM,B}$, [mD]	k_{NMR} via $5.7 \cdot \Phi^4 \cdot T^2_{2LM,B\,INT}$, [mD]	k_{NMR} via $1.2 \cdot \Phi^4 \cdot T^2_{1LM,INT}$, [mD]	
AC4	5.4	5.3	8	11.6
AC6	1.4	1.2	1.4	1.85
AC7	3.7	4.8	2	3.59
AC8	6.0	4.9	9	5.25
AC9	5.4	7.5	8	5.26
AC10	20.0	23	22	20.7
AC12	6.0	7	3.5	3.13
AC13	6.0	7	7	4.42
AC14	7.7	8	11	10.1
AC15	25	21	21	19.6
AC16	5	5	10	8.99
AC17	8	9	14	16.2
AC18	5	5	6	6.16
AC19	7	9	9	13.9
AC20	11	7	8	7.2

Appendix C

General theory.

The main mathematical tool used in our study is the inverse Laplace transformation. It is used to derive a distribution of relaxation times from a multi-exponential decay. This algorithm is widely accepted to describe the NMR decay in heterogeneous systems. The NMR decay can be described as

$$s(t) = \sum_{j=1}^{M} g_j \cdot e^{-W_j t} \qquad \text{(B.1)},$$

where M is the number of microdomains with a spin density g_j and the relaxation constant W_j. For example, it can be the decay in PFG experiments with $t = q^2 = (\gamma\delta G)^2$, where γ is the nucleus gyromagnetic ratio, δ is the gradient duration, G is the gradient intensity. $W=D\Delta$, where D is a diffusion coefficient and Δ is time. On the other hand, the NMR decay can be represented as a Laplace transform:

$$s(t) = \int_0^{\infty} P(a) \cdot e^{-at} da\,, \qquad \text{(B.2)}$$

which is a particular case of a broad class of Fredholm integrals of first kind:

$$s(t) = \int_{a_{\min}}^{a_{\max}} P(a) \cdot f(t,a) da\,, \qquad \text{(B.3)}$$

where $P(a)$ is a distribution function and $f(t, a)$ is a known kernel. The kernel is defined by the type of measurements (either relaxation or diffusion exponent for 1D experiments). The goal is to determine the function $P(a)$ given the NMR data $s(t)$. This problem is mathematically ill-posed. This means that their solution is extremely sensitive to small changes or error in the inputs. It may lead to a large number of solutions, all satisfying Eq. (B.3) within the experimental error. For this reason, it is necessary to use special numerical approaches to obtain a stable solution of the Laplace (Fredholm) problem. Thus inversion algorithms are required that lead to a quadrature method, which summarize the value of the integrand on a sequence of abscissas within the range of integration. In this case, the approximation of the Eq. (B.3) is

$$s(t) = \int_{a_{\min}}^{a_{\max}} P(a) \cdot f(t,a) da = \sum_{j=1}^{N} w_j P(a_j) f(t,a_j)\,, \qquad \text{(B.4)}$$

where w_j are the weights of the quadrature rule. Since the NMR signal is a series of discrete experimental noisy points $s_j = s(t_j)$ equations (B.4) can be written in the matrix form:

$$s = Kp + \varepsilon\,, \tag{B.5}$$

where s is the vector of experimental values, p is the discrete approximation of $P(a)$, K is a kernel that represents the matrix $w_j\, f(t_j,a_j)$, and ε is unknown noise component. Usually the least-square algorithm is used to find the solution of Eq. (B.5)

$$p^* = \arg\min_{p\geq 0} \left\| s - Kp \right\|^2 \tag{B.6}.$$

The non-negative (NN) condition $p\geq 0$ comes from the physical meaning of p, i.e. the spin density. This condition is used to stabilize the solution. Typically, the number of experimental data is larger than the number of points to sample the P function. This will not lead to a unique solution. To solve this problem, regularization methods are used together with the NN condition to stabilize the solution of Eq. (B.6). In this case, Eq. (B.6) is changed into:

$$p^* = \arg\min_{p\geq 0} \left[\left\| s - Kp \right\|^2 + \lambda \Phi(p) \right] \tag{B.7},$$

where λ is a regularization parameter and $\Phi(p)$ is a regularization function. It helps to reintroduce part of the correlation, lost during the discretization process. The first term shows the difference between the data and the fit. The regularization term is responsible for the desired smoothness of the discretized density function.

There are several ways to solve Eq. (B.7). Usually the regularization operator can be considered as a function of first or higher derivatives of the solution p. Different programs exist for the Laplace transform such as 'UPEN' (uniform penalty of multiexponential decays data) developed in Italy [Bor1, Bor2] and the '2D Laplace Inversion' program written in New Zealand [God1, Son3].

UPEN

UPEN is one of the first programs available for the NMR data processing. The program is written in True Basic and works as a full window MS DOS application. It is a one-dimensional multi-exponential inverse Laplace transformation. The UPEN algorithm solves Eq. (B.7) using the uniform penalty algorithm within an iteractive procedure [Bor1, Bor2].

2D Laplace Inversion

The second program is the Two-Dimensional Laplace Inversion that can process one dimensional data as well as two dimensional data. The program has the interface written in Matlab ® with the code section for the computation in C. The program requires at least Matlab 6 ® to run. In this program to solve Eq. (B.7), the one-dimensional Laplace inversion comprises a non-negative least square fit with the addition of a smoothing term. Additionally, it can be used to obtain a 2D Laplace transformation. This program transforms the two-dimensional problem into a one-dimensional one by using the singular value decomposition (SVD) algorithm.

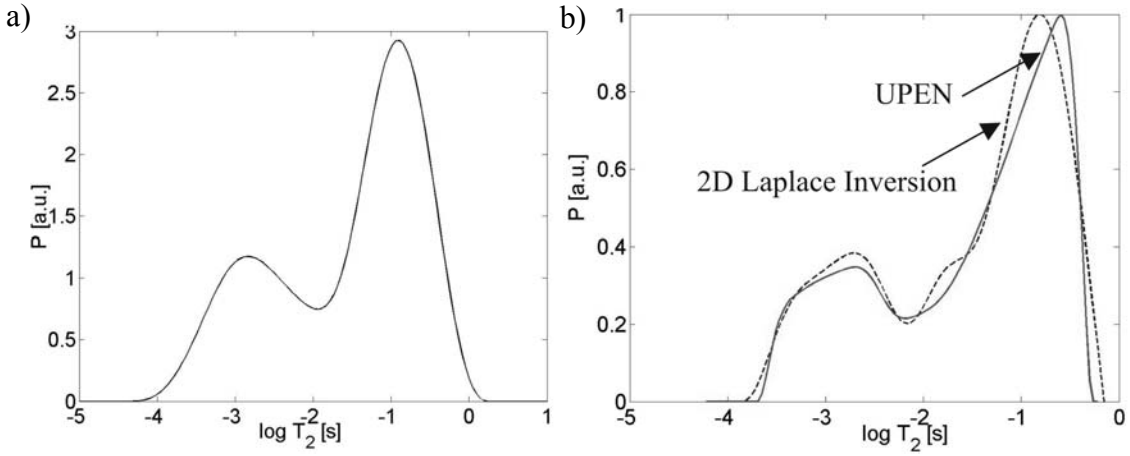

Fig. B.1 *T_2 distribution function calculated for the same sandstone using different available software. a) The real T_2 distribution function. b) T_2 distribution functions obtained by the UPEN software (the solid line) and by the 2D Laplace Inversion (the dashed line) for the same data but with a higher smoothing parameter than that used for the real distribution function in a).*

Using of the programs

In this study, the 2D Laplace Inversion was used for both types of experiments: for one-dimensional and two-dimensional ones. It was found that a distribution function obtained via 2D Laplace Inversion corresponds better to our expectations about the samples according to its characteristics than the distribution calculated with UPEN. In some cases the T_2 distribution function obtained with the UPEN program appeared to be with less features and extended. Especially it is sensitive to the signal-to-noise ratio. It was discussed in the literature that the output of the UPEN program can have different meaning, which is related to the *real distribution function* via a special coefficient [Lav1]. Figure B.1a shows the real T_2 distribution obtained by the 2D Laplace Inversion

software. Figure B.1b demonstrates T_2 distributions for the same data set calculated by the UPEN program and by the 2D Laplace Inversion program with a wrong smoothing parameter. Thus the UPEN output can be considered to deliver a general description of a sample rather than a correct T_2 distribution. In the study all T_2 distributions and 2D maps were obtained by the 2D Laplace Inversion program but firstly this program was tested with simple data set and some simulations.

Simulations

First, the 2D Laplace Inversion was tested with the bulk water which has only one relaxation time. Processing 2D T_1-T_2 data for bulk water doped with $CuSO_4$ with different discretization leads to the distribution maps presented in Fig B.2. The 2D map obtained with less discretization points of 15×15 is broader while the same 2D map indicates a narrow peak when higher discretization of 35×35 points is used.

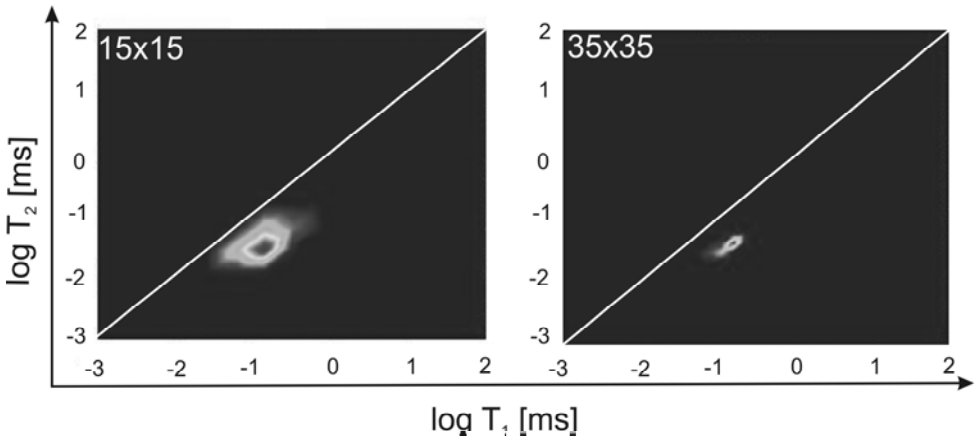

Fig. B.2 *2D distribution maps for the bulk water doped with $CuSO_4$ obtained by 2D Laplace Inversion with different discretizations of 15×15 and 35×35 points.*

Since the main goal was to estimate diffusion qualitatively with less time expense, a discretization grid of 32×32 points was used for the 2D data processing. Indeed, the highest discretization for 2D experiments can be 64×64 but it takes much time for calculation and the result shows the same main features as for a 32×32 point discretization (this limitations comes from the technical characteristics of a PC and software). At the same time, the discretization cannot be higher than the resolution of the experimental data itself. Thus, the saturation recovery time τ_1 should be changed (n+1) times during the experiment as well as the number of echoes should be chosen equal (n+1) in order to obtain final maps with n×n. discretization The change in

numbers of echoes does not influence the time of measurements much while changes in the number of points in the dimension associated with longitudinal relaxation increases the experimental time dramatically.

The simulations of the NMR experiment show that the chosen parameters are reasonable. The 2D T_1-T_2 decay signal was simulated for the water-saturated sample as

$$M(t) = M_0 \cdot (1 - \exp\{-\tau_1/T_1\}) \cdot \exp\{-nt_E/T_2\} + \text{noise}\ , \qquad \text{(B.8)}$$

where τ_1 and nt_E were changed according an experiment setup: τ_1 from 0.003 s up to 1.7 s linearly on a logarithmic scale, the number of echoes was chosen n=5400 with an echo time t_E=0.08 ms. Noise was introduced into the signal as a random gaussian function with respect to the initial magnitude of the signal M_0. The simulation was simplified by considering a bimodal T_1 and T_2 distribution with the main contribution from the bulk water. Afterwards the data was processed by 2D Laplace Inversion (Fig. B.3). The 2D maps obtained from experimental data (Fig. B.3a) and from the simulated data (Fig. B.3b) are in good agreement with each other. This shows that the chosen parameters are reasonable.

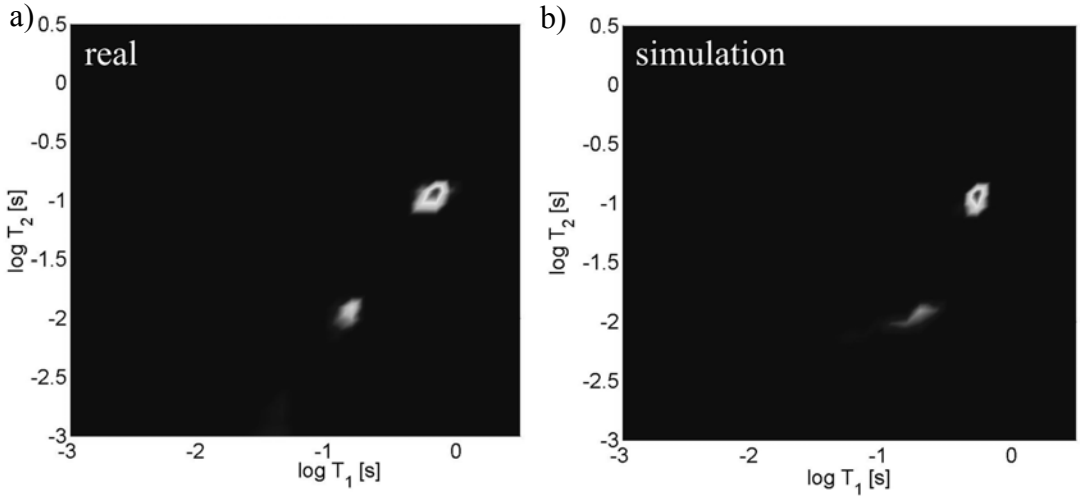

Fig B.3 *2D distribution maps obtained by 2D Laplace Inversion on a 32×32 point grid. a) 2D map obtained from the real experimental data.* b) *2D map obtained from the data simulated according to the experimental parameters.*

Additional programs

In this study several programs were written in MatLab ® for the analysis of experimental data, adopting them for further processing by 2D Laplace Inversion and for the analysis of 2D maps as well as programs which simulate simplified experimental

data. For example, the data analysis includes reorganizing raw data into 3 matrices with respect to experimental dimensions that are required by the 2D Laplace Inversion software. Additionally, both projections are calculated for the raw data to monitor the experiment and for the 2D map to compare T_1 relaxation with T_2 and for the calculation of corresponding T_1/T_2 ratios. Also properties of the samples such as permeability, porosity, amount free and bound water, all other additional information have been calculated.

References.

[Abr1] Abragam, *The Principles of Nuclear Magnetism*, Clarendon Press, Oxford, 1961

[Anf1] S.Anferova, V.Anferov, M.Adams, P.Blümler, N.Routley, K.Hailu, K. Kupferschläger, M.Mallet, G.Schroeder, S.Sharma, B.Blümich, *Construction of a NMR-MOUSE with Short Dead Time,* Concepts in Magnetic Resonance (B), **15**(1), 15 (2002)

[Anf2] S.Anferova, V.Anferov, D.G.Rata, B.Blümich, J. Arnold, C.Clauser, P.Blümler, H. Raich, *A Mobile NMR Device for Measurements of Porosity and Pore Size Distributions of Drilled Core Samples,* Concepts in Magnetic Resonance (B), **23**(1), 26, 2004

[Anf3] S. Anferova, V. Anferov, J. Arnold, E. Talnishnikh, M. Voda, K. Kupferschläger, P.Blümler, C.Clauser, B.Blümich, *Improved Halbach sensor for NMR scanning of drill cores,* MRI, **25**, 547 (2007)

[Anf4] S. Anferova, E. Talnishnikh, V. Anferov, B.Blümich,J. Arnold, M. Voda, K. Kupferschläger, P.Blümler, C.Clauser, *Determination of porosity and novel 2D relaxation and diffusion experiments with mobile NMR Halbach scanner,* MRI, **25**, 474 (2007)

[App1] S. Appelt, F. W.Häsing, H. Kühn, J. Perlo, B.Blümich, *Mobile High Resolution Xenon Nuclear Magnetic Resonance in the Earth's Magnetic Field,* Phys. Rev. Lett., **94**, 197602 (2005)

[Arn1] J. Arnold, Doctoral Dissertation, RWTH Aachen University (2007, in preparation)

[Arn2] J. Arnold, C. Clauser, C. Pechnig, S. Anferova, V. Anferov, B. Blümich, *Porosity and Permeability from Mobile NMR Core-Scanning*, Petrophysics, **47**, 306 (2006)

[Blo1] F. Bloch, *Nuclear Induction,* Phys. Rev., **70**, 460 (1946)

[Blü1] B. Blümich, NMR Imaging of Materials, Clarendon Press, Oxford, 2000

[Blü2] B. Blümich, S. Anferova, S. Sharma, A.L. Segre, C. Federici, *Degradation of Historical Paper: Nondestructive Analysis by the NMR-MOUSE®*, JMR, **161**, 204(2003)

[Blü3] B. Blümich, V. Anferov, S. Anferova, M. Klein, R. Fechete, M. Admas, F. Casanova, *A Simple NMR-MOUSE® with a Bar Magnet,* Magn. Reson. Eng., **15**(4), 255 (2002)

[Blü4] B. Blümich, S. Anferova, R. Pechnig, H. Pape, J. Arnold, C. Clauser, *Mobile NMR for porosity analysis of drill core sections,* Journal of Geophysics and Engineering, **1**(3), 177(2004)

[Bor1] G. C. Borgia, R.J.S. Brown, P. Fantazzini, *Uniform-penalty inversion of multiexponential decay data*, JMR, **132,** 65 (1998)

[Bor2] G. C. Borgia, R.J.S. Brown, P. Fantazzini, *Uniform-penalty inversion of multiexponential decay data II: data spacing, T2 data, systematic data errors, and diagnostics JMR*, **147,** 273 (2000)

[Brow1] K.R. Brownstein and C.E. Tarr, *Importance of classical diffusion in NMR studies of water in biological cells***,** Phys. Rev. A, **19**, 2446 (1979)

[Brown1] R.J. S. Brown, Bull. American Phys. Society (III), 1, 126(1956)

[Cal1] P. T. Callaghan, *Principles of Nuclear Magnetic Resonance Microscopy*, Clarendon Press, Oxford, 1991

[Cal2] P.T. Callaghan, D. MacGowan, K.J. Parker, F.O. Zelaya, *Influence of field gradient strength in NMR studies of diffusion in porous media,* MRI, **9**, 663 (1991)

[Cal3] P.T. Callaghan, A. Coy, T.P.J. Halpin, D. MacGowan, K.J. Parker, F.O. Zelaya, *Diffusion in Porous Systems and the Influence of Pore Morphology in Pulsed Gradient Spin-Echo Nuclear Magnetic Resonance Studies,* J. Chem. Phys., **97**, 651 (1992)

[Cal4] P.T. Callaghan, S. Godefroy, B.N. Ryland, *Diffusion-Relaxation Correlation in Simple Pore Structures,* JMR, **162,** 320 (2003)

[Cal5] P.T. Callaghan, I.Furó, *Diffusion-Diffusion Correlation and Exchange as a Signature for Local Order and Dynamics,* Chem. Physics, **120(8)**, 4032 (2004)

[Car1] H.Y. Carr, E.M. Purcell, *Effects of Diffusion on Free Precession in Nuclear Magnetic Resonance Experiments,* Phys. Rev., **94**, 630 (1954)

[Cas1] F. Casanova, J. Perlo, B. Blümich, *Velocity distributions remotely measured with a single-sided sensor*, JMR, **171**, 124(2004)

[Che1] Z. Chen, J. Zhong, *Unconventional Diffusion Behaviors of Intermolecular Multiple-Quantum Coherences in Nuclear Magnetic Resonance,* J. Chem. Physics, **114**, 5642 (2001)

[Che2] Q. Chen, A.E. Marble, B. G. Colpitts, B.J. Balcom, *The Internal Magnetic Field Distribution, and Single Exponential Magnetic Resonance Free Induction Decay, in Rocks,* JMR, **175**, 300(2005)

[Coa1] G.R. Coates, L. Xiao, M.G. Prammer, NMR Logging Principles and Applications, Halliburton Energy Services, Houston, 1999

[Coa2] G.R. Coates, J.L. Dumanoir, *A New Approach to Improved Log-Derived Permeability,* The Log Analyst, **15** (1), (1974)

[Cot1] R.M. Cotts, M.J. R.Hoch, T. Sun, J.T. Markert, *Pulsed Field Gradient Stimulated Echo Methods for Improved NMR Diffusion Measurements in Heterogeneous Systems,* JMR, **83**, 252 (1989)

[Dar1] T. Darling, "Well Logging and Formation Evaluation", Gulf Professional Publishing, An Imprint of Elsevier Science, 2005

[Dun1] K.-J. Dunn, D.J. Bergman and G.A. Latorraca, "Nuclear Magnetic Resonance Petrophysical and Loggining Applications", Pergamon, Oxford, 2002

[Ehl] M. Ehlers, J. Bluhm, Porous Media, Springer, Berlin,2002

[Eid1] G. Eidmann, R. Salvelsberg, P. Blümler, B. Blümich, *The NMR MOUSE, a Mobile Universal Surface Explorer,* JMR, **A122**, 104(1996)

[Ern1] Richard R. Ernst, Geoffrey Bodenhausen and Alexander Wolkaun, Principles of Nuclear Magnetic Resonance in One and Two Dimensions, Clarendon Press, Oxford, 1987

[Fre1] R. Freedman, N. Heaton, *Fluid Characterization Using Nuclear Magnetic Resonance Logging,* Petrophysics, **45**, 241(2004)

[Fuk1] E. Fukushima, S.B.W.Roeder, Experimental pulse NMR.A Nuts and Bolts Approach, Westview Press, 1981

[God1] S. Godefroy, P.T. Callaghan, *2D relaxation/diffusion Correlation in porous Media,* MRI, **21**, 381(2003)

[Hal1] K. Halbach, *Strong Rare Earth Cobalt Quadrupoles,* IEEE Tran. NS-26, 3882, (1979)

[HNMR] "History of NMR Well Logging", Concepts in Magnetic Resonance, **13**, 335-413, 2001

[Hür1] M. D. Hürlimann, *Effective Gradients in Porous Media Due to Susceptibility Differences,* JMR, **131**, 232(1998)

[Hür2] M. D. Hürlimann and L. Venkataramanan, *Quantitative Measurements of Two-Dimensional Distribution Functions of Diffusion and Relaxation in Grossly Inhomogeneous Fields*, JMR, **157,** 31 (2002)

[Hür3] M. D. Hürlimann, L. Venkataramanan, C. Flaum, *The Diffusion-Spin Relaxation Time Distribution Function as an Experimental Probe to Characterize Fluid Mixtures in Porous Media,* J. Chem. Physics, **117**, 10223 (2002)

[Hür4] M. D. Hürlimann, M. Flaum, L. Venkataramanan, C. Flaum, R. Freedman, G.J. Hirasaki, *Diffusion-Relaxation Distribution Functions of Sedimentary Rocks in Different Saturation States,* MRI, **21**, 305(2002)

[Hür5] M. D. Hürlimann, D.D. Griffin, *Spin Dynamics of Carr-Purcell-Meiboom-Gill-like Sequences in Grossly Inhomogeneous B_0 and B_1 Fields and Application to NMR Well Logging,* JMR, **143**, 120 (2000)

[Hür6] M. D. Hürlimann, *Diffusion and Relaxation effects in General Stray Field NMR Experiments,* JMR, **148**, 367(2001)

[Hür7] M. D. Hürlimann, K.G. Helmer, L.L. Latour, C.H. Sotak, *Restricted Diffusion in Sedimentary Rocks. Determination of Surface-Area-to-Volume Ratio and Surface Relaxivity,* JMR, **111A**, 169 (1994)

[Hür8] M. D. Hürlimann, L. Burcaw, Y.-Q. Song, *Quantitative Characterization of Food Products by Two-Dimensional D-T_2 and T_1-T_2 Distribution Function in a Static Gradient,* J. Colloid and Interface Science, **297**, 303 (2006)

[Ken1] W.E. Kenyon, P. Day, C. Starley, J.F. Willemsen , *A Three - Part Study of NMR Longitudinal Relaxation Properties of Water Saturated Sandstones*. SPE Form Eval 1988;3:622-636.

[Kle1] R. L. Kleinberg, M. A. Horsfield, *Transverse Relaxation Processes in Porous Sedimentary Rock,* JMR, **88**, 9(1990)

[Kle2] R.L. Kleinberg, W.E.Kenyon, P.P.Mitra, *Mechanism of NMR Relaxation of Fluids in Rock,* JMR (A), 108, 206(1994)

[Kle3] R. L. Kleinberg, *Well Logging*, Schlumberger-Doll Research, Ridgefield, CT, USA, 1996

[Kle4] R. L. Kleinberg, C. Straley, W. E. Kenyon, R. Akkurt, and S. A. Farooqui, 68 Annual Technical Conference and Exhibition, SPE 26470, 1993.

[Kle5] R. L. Kleinberg, *Pore Size Distribution, Pore Coupling, and Transverse Relaxation Spectra of Porous Rocks,* MRI, **12**, 271 (1994)

[Kle6] R. L. Kleinberg, *Utility of NMR T_2 Distributions, Connection with Capillary Pressure, Clay Effect, and Determination of the Surface Relaxivity Parameter ρ_2,* MRI, **14**, 761(1996)

[Kor1] J.-P. Korb, *Surface Dynamics of Liquids in Porous Media,* MRI, **19**, 363 (2001)

[Lam1] R. Lamanna, *On the Inversion of Multicomponent NMR Relaxation and Diffusion Decays in Heterogeneous Systems*, Concepts in Magnetic Resonance Part A, **26A(2)**, 78(2005)

[Lat1] L.L. Latour, R.L. Kleinberg, A.J. Sezginer, *Nuclear-Magnetic-Resonance Properties of Rocks at Elevated-Temperatures,* J. Colloid and Interface Sci., **150,** 535 (1992)

[Lat1] L.L. Latour, R.L. Kleinberg, P.P. Mitra, C.H. Sotak, *Pore-Size Distribution and Tortuosity in Heterogeneous Porous Media,* JMR, **112A**, 83 (1995)

[Lat2] L.L. Latour, L. Li, C.H. Sotak, *Improved PFG Stimulated-Echo Method for the Measurement of Diffusion in Inhomogeneous Fields,* JMR, **101B**, 72 (1993)

[Lat3] L.L. Latour,P. P. Mitra, R.L. Kleinberg, C.H. Sotak, *Time-Dependent Diffusion Coefficient of Fluids in Porous Media as a Probe of Surface-to-Volume Ratio,* JMR, **101A**, 342 (1993)

[Mai1] R. W. Mair, M. D. Hürlimann, P. N. Sen, L. M. Schwartz, S. Patz, R. L. Walsworth, *Tortuosity Measurement and the Effects of Finite Pulse Widths on Xenon Gas Diffusion NMR Studies of Porous Media,* MRI, **19**, 345 (2001)

[Mai2] R. W. Mair, P. N. Sen, M. D. Hürlimann, S. Patz, D. G. Cory, R. L. Walsworth, *The Narrow Pulse Approximation and Long Length Scale Determination in Xenon Gas Diffusion NMR Studies of Model Porous Media,* JMR, **156**, 202 (2002)

[Mei1] S. Meiboom, D. Gill, *Modified Spin-Echo Method for Measuring Nuclear Relaxation Times,* Rev. Sci. Instrum., **29**, 668 (1958)

[Mit1] P.P. Mitra, P. N. Sen, L.M. Schwartz, P. Le Doussal, *Diffusion Propagator as a Probe of the Structure of Porous Media,* Phys. Rev. Lett., **68**, 3555(1992)

[Pap1] H. Pape, J. Arnold, R. Pechnig, C. Clauser, E. Talnishnikh, S. Anferova, B. Blümich, manuscript in preparation

[Par1] K. J. Parker, Mol. Physics, **17**, 355 (1969)

[Per1] J. Perlo, F. Casanova, B. Blümich, *3D Imaging with a Single-Sided Sensor: an Open Tomograph,* JMR, **166**, 228(2004)

[Per2] J. Perlo, Single-Sided NMR Tomography, PhD Thesis, Shaker Verlag, 2006

[Pur1] E. M. Purcell, *Spontaneous Transition Probabilities in Radio-Frequency Spectroscopy*, Phys. Rev., **69**, 681 (1946)

[Qia1] Y. Qiao, P. Galvosas, P. T. Callaghan, *Diffusion Correlation NMR Spectroscopic Study of Anisotropic Diffusion of Water in Plant Tissues*, Biophysical Journal, **89**, 2899 (2005)

[Rai1] H. Raich, P. Blümler, *Design and Construction of Dipolar Halbach Array with a Homogeneous Field from Identical Bar Magnets: NMR Mandhalas*, Concepts in Magnetic Resonance, **23B**, 16-25, (2004)

[Rat1] D.G.Rata, F. Casanova, J. Perlo, D.E. Demco, B. Blümich, *Self-Diffusion Measurements by a Mobile Single-Sided NMR Sensor with Improved Magnetic Field Gradient,* JMR, **180**, 229 (2006)

[Sel1] J.G. Seland, G.H. Sørland, K. Zick, B. Hafskjold, *Diffusion Measurements at Long Observation Times in the Presence of Spatially Variable Internal Magnetic Field Gradients,* JMR,**146**, 14 (2000)

[Sel2] J.G. Seland, K.E. Washburn, H. W. Anthonsen, J. Krane, *Correlations between Diffusion, Internal Magnetic Field Gradients, and Transverse Relaxation in Porous Systems Containing Oil and Water,* Phys. Rev. E, **70**, 051305 (2004)

[Sen1] P. Sen, *Time-Dependent Diffusion Coefficient as a Probe of Geometry*, Concepts in Magnetic Resonance, **23(A)1**, 1 (2004)

[Sli1] C. P. Slichter, *Principles of Magnetic Resonance*, 3d edition, Springer, Berlin, 1990

[Son1] Y.-Q. Song, *Novel NMR Techniques for Porous Media Research,* MRI, **21**, 207 (2003)

[Son2] Y.-Q, Song, M.D. Hürlimann, C. Flaum, *A Method for Rapid Characterization of Diffusion,* JMR, **161**, 222 (2003)

[Son3] Y.-Q, Song, L. Venkataramanan, M.D. Hürlimann, M. Flaum, P. Frulla, C.Starley, T_1-T_2 *Correlation Spectra Obtained Using a Fast Two-Dimensional Laplace Inversion,* JMR, **154**, 261 (2002)

[Son4] Y.-Q, Song, U. M. Scheven, *An NMR Technique for Rapid Measurement of Flow,* JMR**, 172**, 31(2005)

[Sør1] G.H. Sørland, , B. Hafskjold, O. Herstad, *A Stimulated-Echo Method for Diffusion Measurements in Heterogeneous Media Using Pulsed Field Gradients,* JMR,**124**, 172 (1997)

[Sta1] S. Stapf, S.-I Han, *NMR Imaging in Chemical Engineering*, Wiley-VCH, Weinheim, 2005

[Str1] J. H. Strange, J. Mitchell, J. B. W. Webber, *Pore surface exploration by NMR*, MRI, **21,** 221 (2003)

[Tan1] J. E. Tanner, *Use of the Stimulated Echo in NMR Diffusion Studies,* J. Chem. Phys.,**52,** 2523(1970)

[Tim1] A. Timur, *An Investigation of Permeability, Porosity, and Residual Water Saturation Relationships for Sandstone Reservoirs,* The Log Analyst, **9**(4), 8(1968)

[Vas1] S. Vasenkov, P. Galvosas, O. Geier, N. Nestle, F.Stallmach, J.Kärger, *Determination of Genuine Diffusion in Heterogeneous Media Using Stimulated Echo Pulsed Field Gradient NMR,* JMR, **149**, 228(2001)

[Ven1] L. Venkataramanan, Y.-Q. Song, M. D. Hürlimann, *Solving Fredholm Integrals of the First Kind With Tensor Product Structure in 2 and 2.5 Dimensions,* IEEE Trans., **50(5)**, 1017(2002)

[Vod1] M. A. Voda, *Advances in Studying Order and Dynamics in Condensed Matter by NMR,* PhD Thesis, http://darwin.bth.rwth aachen.de/opus3/volltexte/2007/1751

[Vog1] C. Vogt, P. Galvosas, N. Klitzsch, F. Stallmach, *Self-Diffusion Studies of Pore Fluids in Unconsolidated Sediments by PFG NMR,* Appl. Geophysics, **50**, 455 (2002)

[Was1] K.E. Washburn, P.T. Callaghan , *Tracking Pore to Pore Exchange Using Relaxation Exchange Spectroscopy,* Phys. Rev. Lett., **97**, 17552(2006)

[Zho1] J. Zhong, R.P. Kennan, J. C. Gore, *Effects of Susceptibility Variations on NMR Measurements of Diffusion,* JMR, **95**, 267(1991)

Acknowledgements

- ✓ First of all, I would like to acknowledge Prof. B. Blümich for giving me the opportunity to work in his group and to complete the study with this thesis, for his hospitality, invaluable support, helpful advices, and all his patience.
- ✓ I would like to thank Prof. C. Clauser for accepting to be the co-referent of my PhD thesis.
- ✓ I am grateful to Prof. D. Demco for the nice discussions and for his scientific assistance on my PhD thesis.
- ✓ I wish to thank Dr. S. Anferova, Prof. V. Anferov for their interesting way of being and their original ideas about NMR and life.
- ✓ A lot of thanks to the scientists of Applied Geophysics group, in particular Dr. H. Pape, Juliane Arnold, Lothar Ahrensmeier, and Annick Fehr.
- ✓ I should not forget Prof. S. Stapf for many hours of fruitful discussions, whatever a topic it was, as well as for being around even when there was no one in the Institute.
- ✓ Special thanks to Klaus Kupferschläger for building fine devices.
- ✓ I wish also to thank Dr. F. Casanova, Dr. J. Perlo, Jürgen Kolz for their time which we spend together in MOUSEoleum and for all their advices.
- ✓ I want to address my special thanks to Dr. A. Amar and Dr. K. Münnemann for teaching me imaging and for their tips in discovering Germany.
- ✓ I would like to acknowledge all my colleagues for the pleasant atmosphere at work and for being my friends. Thank to all of you: who are in the photo, who are not yet in it, and who are already not in this photo.

- ✓ Absolutely non scientific acknowledgements to my Friends and the Friend. All of them are very special people, who supported and help me during all these years, for whom no words can express my appreciation. Fortunately, this page has no place for a photo ☺
- ✓ Last but not least my sincere thanks to my family in Russia: my Mother, my sisters, especially, Dyushka, and my father. Thank you that you believe in me!

Curriculum Vitae

Personal information

Name	Elena Talnishnikh
Date of Birth	04.11.1978
Place of Birth	Saint-Petersburg, Russia
e-mail	telena@mc.rwth-aachen.de,
	elena_talnishnikh@hotmail.com

Education

21.08.2007	Date of doctoral examination
2004-2007	PhD Student at Macromolecular Chemistry, RWTH Aachen, Germany
2003-2004	PhD Student at Faculty of Physics, Saint–Petersburg State University, Russia
2000-2003	Master of Science in Physics, Faculty of Physics, Saint–Petersburg State University, Russia *Thesis:* "Quantum-mechanical calculation of vibrations of a molecule HONO"
1996-2000	Bachelor Degree in Physics, Faculty of Physics, Saint–Petersburg State University, Russia *Thesis:* "Quantum-mechanical analysis of an electron structure and vibrations of cis- and trans-isomers of a molecule HONO"
1986-1996	General secondary school, Saint-Petersburg, Russia

Publications

- Siegfried Stapf, Xiaohong Ren, Elena Talnishnikh, Bernhard Blümich, *Spatial distribution of coke residues in porous catalyst pellets analyzed by field-cycling relaxometry and parameter imaging*, MRI, **23,** 383(2005)
- Sophia Anferova, Vladimir Anferov, Juliane Arnold, Elena Talnishnikh, Mihai A. Voda, Klaus Kupferschläger, Peter Blümer, Christoph Clauser, Bernard Blümich, *Improved Halbach sensor for NMR scanning of drill cores,* MRI, **25** 474(2007)
- S. Anferova, E. Talnishnikh, V. Anferov, B. Blümich, J. Arnold, H. Pape, C. Clauser, *Determination of porosity and novel 2D relaxation and diffusion experiments with mobile NMR scanner,* MRI, **25** 547(2007)